Journal of Research of the National Institute of Standards and Technology

Volume 99 Number 5 September–October 1994

U.S. Department of Commerce—**Ronald H. Brown,** Secretary
Technology Administration—**Mary L. Good,** Under Secretary for Technology
National Institute of Standards and Technology—**Arati Prabhakar,** Director

The Journal of Research of the National Institute of Standards and Technology features advances in measurement methodology and analyses consistent with the NIST responsibility as the nation's measurement science laboratory. It includes reports on instrumentation for making accurate and precise measurements in fields of physical science and engineering, as well as the mathematical models of phenomena which enable the predictive determination of information in regions where measurements may be absent. Papers on critical data, calibration techniques, quality assurance programs, and well-characterized reference materials reflect NIST programs in these areas. Special issues of the Journal are devoted to invited papers in a particular field of measurement science. Occasional survey articles and conference reports appear on topics related to the Institute's technical and scientific programs.

ISSN 1044-677X **Coden: JRITEF** **Library of Congress Catalog Card No.: 89-656121**

United States Government Printing Office, Washington: 1994

Volume 99, Number 5, September–October 1994
Journal of Research of the National Institute of Standards and Technology

Contents

Articles

Conference Reports

News Briefs

GENERAL DEVELOPMENTS

Volume 99, Number 5, September–October 1994
Journal of Research of the National Institute of Standards and Technology

Volume 99, Number 5, September–October 1994
Journal of Research of the National Institute of Standards and Technology

Volume 99, Number 5, September–October 1994
Journal of Research of the National Institute of Standards and Technology

Volume 99, Number 5, September–October 1994
Journal of Research of the National Institute of Standards and Technology

[J. Res. Natl. Inst. Stand. Technol. 99, 593 (1994)]

Tilt Effects in Optical Angle Measurements

Volume 99 | Number 5 | September–October 1994

Yun H. Queen

National Institute of Standards and Technology,
Gaithersburg, MD 20899-0001

Vector analysis is used to determine the quantitative error in angle calibration using autocollimators. This error is caused by tilt in the mount upon which the artifact is placed. For tilt angles that are less than 1°, the error can be simplified to be the product of a coefficient and three terms. The three terms are: (1) the square of the tilt, (2) the sine of the artifact's nominal angle, and (3) the cosine of the artifact's nominal angle plus two times the artifact's position angle. It is shown that the error can be eliminated by placing the artifact at designated periodic positions.

Key words: AAMACS; angle blocks; angles; autocollimator; calibrations; polygons; tilt.

Accepted: June 13, 1994

1. Introduction

In 1990, the National Institute of Standards and Technology (NIST) acquired a new angle calibration instrument, the Advanced Automated Master Angle Calibration System (AAMACS), consisting of three stacked indexing tables. The AAMACS indexes to any angle position with a resolution of 0.003 arcsecond. Furthermore, the repeatability for each table is within ±0.03 arcsecond. Because of the acquisition of this highly repeatable and highly accurate instrument, the angle calibration service must redefine its procedures to minimize errors that were previously ignored. Six of these error sources are: (1) tilt in the mount, (2) seismic or acoustic vibration, (3) thermal drift and distortion, (4) air turbulence and refraction, (5) non-flatness of the artifact mirrors, and (6) autocollimator errors, including optical distortions, axis cross-talk, and calibration error. Of these error sources, only the tilt effect is discussed in this paper.

Errors due to the tilt effect in angle measurements have long been known. However, quantitative information about the tilt effect was unclear. Traditionally, the error in the measurement of angle blocks was averaged out with two measurements. The first measurement was done with the top of the artifact in an upward position and the second measurement was done with the bottom of the artifact in an upward position. This process did not reduce the error, but introduced more error if the top and bottom surfaces were not parallel.

The tilt effect was noted in the 1960's when Hume [1], using an autocollimator, measured an optical polygon placed on a tilted mount. By rotating the mount, the autocollimator's elevation or vertical reading changed direction. As a result, Hume recommended that the tilt must not be more than 2 arcminutes during a calibration. However, no quantitative indication of the error incurred was given. Therefore, the intention of this paper is to show how much the error of angle measurements results from tilt.

2. Instrumentation and Setup

An autocollimator was used to measure the angle position of a flat surface by directing a beam of light toward the surface. The light reflected back into the autocollimator was detected by a photocell, photomultiplier tube, or a CCD array. Inside the autocollimator, the angle of reflection was compared to a reference angle which was either single axis of dual axis [2]. The measuring axis was required to be squarely horizontal or vertical with respect to the axis of rotation.

For the analysis, an angle block was used as the artifact. The purpose of the calibration was to determine the corner angle formed between the two faces of the angle block. Although a nominal angle value, α, was provided by the manufacturer, this value may not be the true angle, thus requiring calibration. The following example shows a typical setup for an angle block calibration [3]. In Fig. 1, the angle block was wrung on top of a mount placed on an indexing table. One surface of the angle block was aligned with the autocollimator and its azimuth or horizontal position measured. The indexing table was then rotated to $(180° - \alpha)$ from the initial position where the other surface of the angle block was measured. Assuming the indexing table is perfect, the difference between the two angle measurements gives the true angle value from the nominal value. Figure 2 shows the same setup as Fig. 1 except that the mount is tilted with respect to the axis of rotation. Figure 2 measurements are different from those of Fig. 1 because of the presence of the tilt. This difference is the error in the angle measurement.

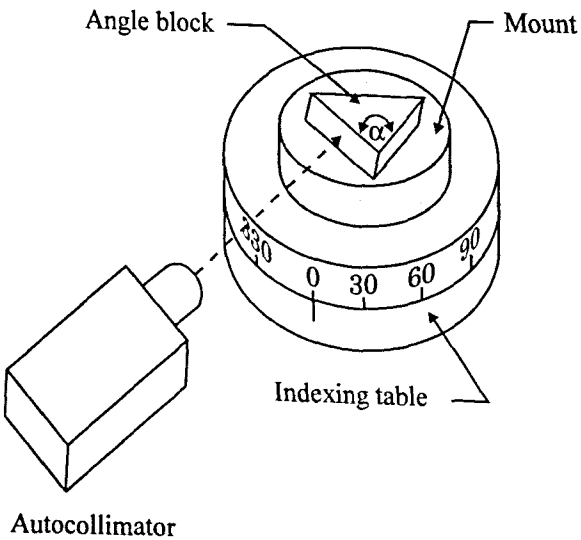

Fig. 1. Angle block calibration setup with no tilt in the mount.

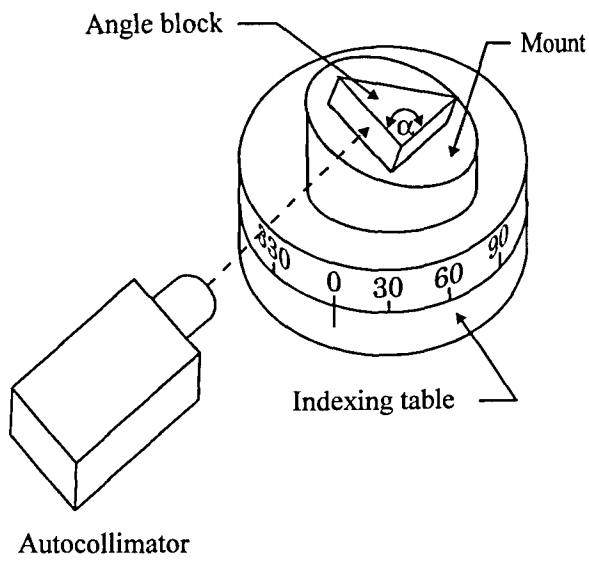

Fig. 2. Angle block calibration setup with tilt in the mount.

3. Theory

Figure 3 illustrates the setup of Fig. 2 with appropriate vectors. Three assumptions were made for the analysis: (1) the nominal angle was the true value, (2) the indexing table was perfect, and (3) the angle block was perpendicularly mounted on top of the mount. All three assumptions were justified because the actual values could be determined with a sufficiently small uncertainty.

3.1 Spatial Definitions

The coordinate space is defined by a right handed xyz-coordinate system. Its origin is in the center of the mount and the axis of rotation is in the z-axis. Four independent variables were considered: (1) the nominal angle, α, of the angle block, (2) the tilt angle, τ, of the mount, (3) the position angle, γ, of the angle block on the mount, and (4) the horizontal angle, ω, of the mount. The first independent variable was discussed above. The second variable, τ, is the smallest angle between M_{low} (vector from the origin to the lowest point of the mount) and the xy-plane. The third variable, γ, is the angle between the normal of the artifact's first surface, S_1, and M_{low}. The last variable, ω, is the angle between the $M_{low}z$-plane and the yz-plane.

Initially, the angle block was placed as close as possible to the center of the mount where surface S_1 was aligned with the autocollimator which was placed concentrically with the x-axis. The autocollimator light source was in the $-i$ direction.

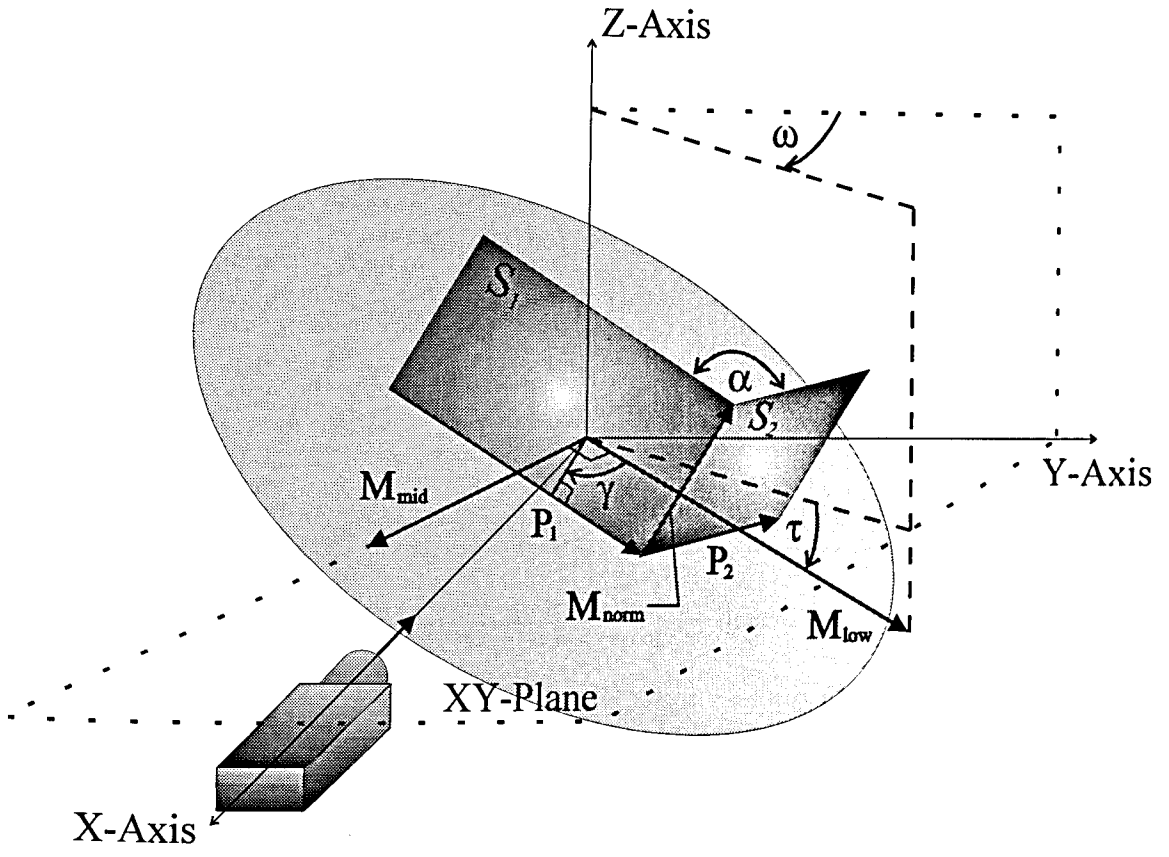

Fig. 3. Angle block calibration setup represented by vectors.

Consequently, the reflected light was in the i direction. The horizontal angle of the surface measured by the autocollimator was in the positive x-axis half of the xy-plane. This angle is measured positive in the clockwise direction from the x-axis as viewed from the positive z-axis.

3.2 Angle Definitions

There are 360 degrees (°) in a circle, 60 arcminutes (′) in a degree, and 60 arcseconds (″) in an arcminute. Therefore, there are 3600 arcseconds in a degree.

3.3 Analysis

Step 1. The normal vector of the mount, M_{norm}, is obtained by taking the cross product of M_{mid} and M_{low}. The vector M_{mid} is on the mount at 90° clockwise from M_{low}. These unit vectors are dependent on τ and ω as follows:

$$M_{norm} = M_{mid} \times M_{low} \tag{1}$$

$$M_{low} = \cos(\tau)\sin(\omega)i + \cos(\tau)\cos(\omega)j - \sin(\tau)k \tag{2}$$

$$M_{mid} = \cos(\omega)i - \sin(\omega)j \tag{3}$$

where τ is less than 90° and ω is between 0° and 360°, inclusive. These two angles are obtained experimentally.

Step 2. The vector, P_1, is related to the mount vectors by the following dot products:

$$P_1 \cdot M_{low} = \cos(\theta_1) \tag{4}$$

$$P_1 \cdot M_{mid} = \cos(\theta_2) \tag{5}$$

$$P_1 \cdot M_{norm} = \cos(\theta_3) \tag{6}$$

where

$$\theta_1 = \gamma - 90° \tag{7}$$

$$\theta_2 = \theta_1 - 90° \tag{8}$$

$$\theta_3 = 90°. \tag{9}$$

The three components of P_1 are determined by solving the above three simultaneous equations.

Step 3. The normal vector to surface S_1, N_1, is obtained by taking the cross product of P_1 and M_{norm} as follows:

$$N_1 = P_1 \times M_{norm}. \tag{10}$$

Step 4. The horizontal angle of surface S_1 measured by the autocollimator is the projection of N_1 onto the xy-plane:

$$\theta_{H:S_1} = \arcsin\left(-\frac{N_{1y}}{\sqrt{N_{1x}^2 + N_{1y}^2}}\right). \tag{11}$$

Step 5. The horizontal angle for surface S_2 is similarly obtained. First, the mount is rotated to a position such that surface S_2 is aligned with the autocollimator. Thus, the new mount angle becomes $(180° - \alpha) + \omega_{(old)}$. The tilt angle, the nominal angle, and the artifact's position angle remain unchanged. The angle between P_2 and M_{low} becomes $-(180° - \alpha) + \theta_{1(old)}$. The first four steps are repeated to solve for the horizontal angle of surface S_2. The differences in these horizontal angles, ϵ_H, is the error of angle measurement resulting from the tilt.

Step 6. The horizontal angle error, ϵ_H, is a function of τ, γ, α, and ω:

$$\epsilon_H = \theta_{H:S_2} - \theta_{H:S_1} \tag{12}$$

where

$$\theta_{H:S_1} = -\arctan\left(\frac{\cos(\tau)\cos(\gamma)\cos(\omega) - \sin(\gamma)\sin(\omega)}{\cos(\tau)\cos(\gamma)\sin(\omega) + \sin(\gamma)\cos(\omega)}\right) \tag{13}$$

$$\theta_{H:S_2} = -\arctan\left(\frac{\cos(\tau)\cos(\alpha+\gamma)\cos(\omega+180° - \alpha) - \sin(\alpha+\gamma)\sin(\omega+180° - \alpha)}{\cos(\tau)\cos(\alpha+\gamma)\sin(\omega+180° - \alpha) + \sin(\alpha+\gamma)\cos(\omega+180° - \alpha)}\right). \tag{14}$$

At this point, I would like to rectify an error in a previous paper [4] on the same topic. Equation (16), written as $\kappa = 1 + \sin^2(\tau)$, should be $\kappa = 1 + \tan^2(\tau)$. If the corrected equation is substituted into Eqs. (14) and (15) of the previous paper, these equations would be the same as the above Eqs. (13) and (14), respectively.

4. Theoretical Results

During calibration, it is customary to align the first surface of the artifact to the reference zero of the autocollimator as much as possible. Therefore, the mount angle, ω, during setup is determined by the position of the artifact (see Appendix A). As a result, the horizontal angle error is a function of just α, τ, and γ.

This error is plotted in Fig. 4 for a 90° angle block with respect to the tilt and block position. The tilt angle ranged from 0″ to 1200″ and the position angle ranged from 0° to 360°. As anticipated, the magnitude of the error increased with increased tilt. Note that despite an increase in tilt, when the artifact's position angle is 0°, 90°, 180°, or 270°, the error is zero.

Intuitively, this is expected. If surface S_1 is placed right at or right along the lowest tilt, surface S_2 by default is right along or right at the lowest tilt, respectively. Consequently, only the vertical angle is changed. However, when the position of the block is not placed at those locations, the error increases with an increase in tilt. This shows that by placing the artifact at strategic points, the error is eliminated.

Figure 5 shows the horizontal angle error for a 9′ tilt angle with respect to the nominal and block position. The nominal angle ranged from 0° to 180° and the position angle ranged from 0° to 360°. As anticipated, the horizontal angle error is bounded when the tilt angle is fixed.

5. Simplification of the Horizontal Angle Error

The horizontal angle error may be simplified, using a Taylor-series expansion:

$$\epsilon_H = (0.5)\tau^2\sin(\alpha)\cos(\alpha + 2\gamma) + O_1(\alpha,\gamma,\tau) \tag{15}$$

$$\epsilon_H = (2.424 \times 10^{-6})\tau^2\sin(\alpha)\cos(\alpha + 2\gamma) + O_2(\alpha,\gamma,\tau) \tag{16}$$

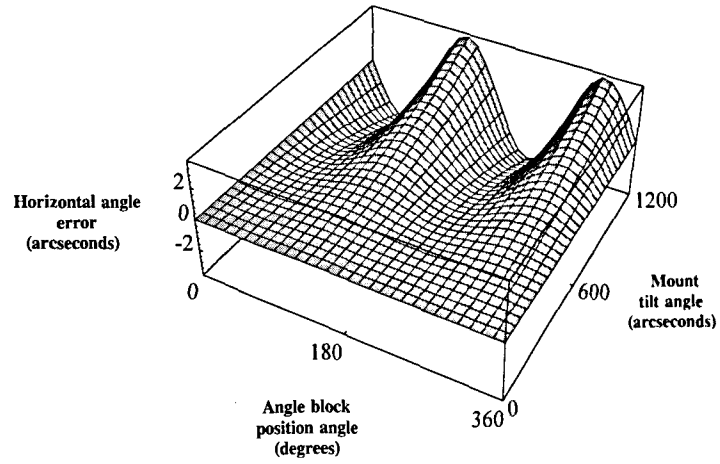

Fig. 4. Theoretical plot of the horizontal angle error for a 90° angle block with respect to the tilt angle and the artifact position angle.

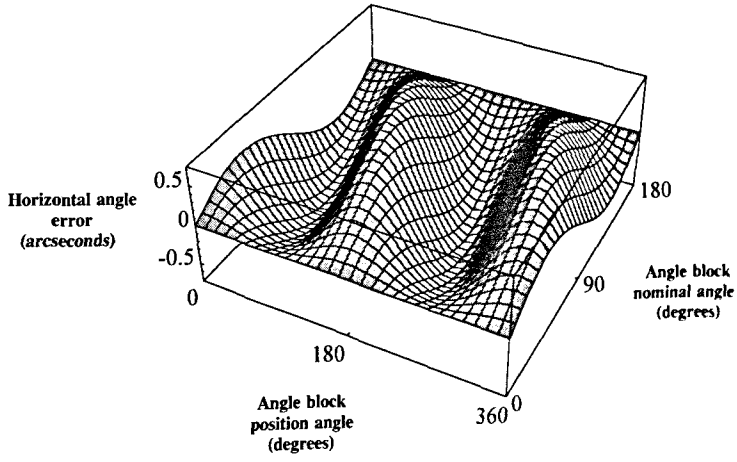

Fig. 5. Theoretical plot of the horizontal angle error for a tilt of 9′ with respect to the artifact nominal angle and position angle.

where ϵ_H and τ are expressed in radians in Eq. (15) and in arcseconds in Eq. (16). The terms $O_1(\alpha,\gamma,\tau)$ and $O_2(\alpha,\gamma,\tau)$ represent the sum of the remaining terms that are negligible for tilt angles less than 1° (see Appendix A).

The above equations show that the horizontal angle error is zero if the cosine term equals zero. This occurs when the artifact position, γ, is

$$\gamma = 45° - \frac{\alpha}{2} \pm 90°N \tag{17}$$

where N is a whole number from 0 to ∞. This means that if a 90° block is placed at 0°, 90°, 180°, or 270°, and so on at every 90° increment, the error is zero.

For constant tilt angles, the above equations show that the error is bounded by the maximum amplitude, A_{ϵ_H}:

$$A_{\epsilon_H} = (0.5)\tau^2 \tag{18}$$

$$A_{\epsilon_H} = (2.424 \times 10^{-6})\tau^2 \tag{19}$$

where A_{ϵ_H} and τ are expressed in radians in Eq. (18) and in arcseconds in Eq. (19).

6. Results

An experiment was performed which determined the horizontal angle error of a 90° angle block placed on mounts with tilt angles of 3′, 9′, and 20′. In all cases, the block was placed at the maximum tilt effect positions. For the 9′ case, the block was also placed at the zero tilt effect positions. Experimental results were compared with the theoretical results. The experimental results agreed very well with the predicted results with a difference of 0.04″ being the worst case. Note the similarity between Fig. 4 and Fig. 6.

A similar experiment was performed in which angle blocks of 30°, 60°, 90°, 120°, and 150° were placed on an approximately 9′ tilt mount. In this experiment, the angle blocks were placed at twenty-four evenly spaced positions from the lowest point of the tilt. Again, experimental results were compared with the predicted results, and again, they agreed well; the largest difference was only 0.17″. Note the similarity between Fig. 5 and Fig. 7.

For both experiments, each point was obtained by taking the average of two measurements. The first measurement was obtained by the conditions described. The second measurement was obtained by placing the angle block at 180° from its prescribed position. This was done for two reasons. First, in practical experience, there was a high probability of measurement error caused by the non-flatness of the measured surfaces and by the

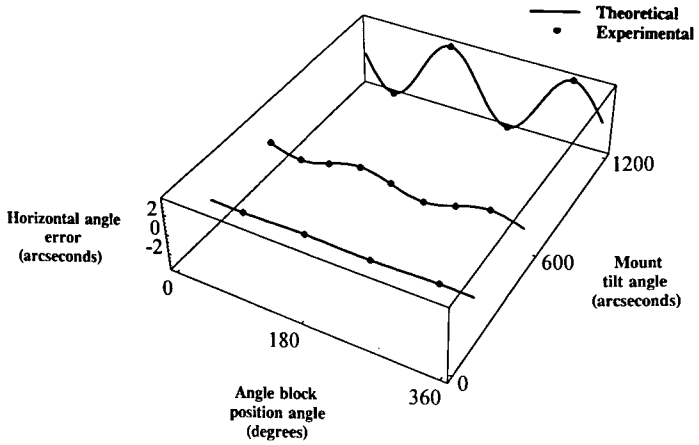

Fig. 6. Theoretical and experimental comparison of the horizontal angle error for a 90° angle block at tilt angles of 3′, 9′, and 20′ as a function of position angle.

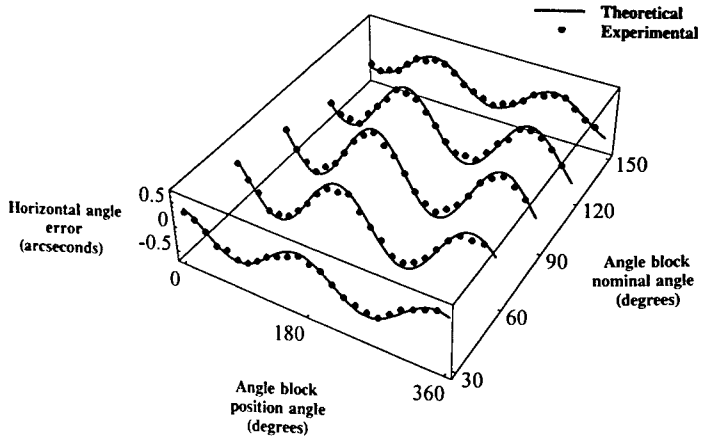

Fig. 7. Theoretical and experimental comparison of the horizontal angle error for 30°, 60°, 90°, 120°, 150° angle blocks, all at 9′ tilt as a function of position angle.

distortion in the autocollimator optics. This meant that the autocollimator readings varied with the shifted positions of a surface even if the angle position of that surface remained the same. As a result, the measurement must be compensated by shifting the surface in the opposite direction. This was accomplished by placing the artifact at 180° from its original position. Second, since the predicted curve repeated itself at every 180°, measuring the block at 180° from the original position yielded the same result as if the block were at the original position. This averaging method was useful since it resulted in good agreement between the measured and the predicted values.

Note also that the results of the first experiment as shown in Fig. 6 were overall better than those of the second as shown in Fig. 7. This was probably due to the better surface flatness of the artifact used in the experiment for Fig. 6 than that for Fig. 7.

7. Summary

A formula was developed which gives the quantitative error in optical angle measurements due to the presence of tilt. This formula, derived using vector analysis, shows that the error is a function of the tilt angle, the nominal angle, and the position angle of the artifact. For tilt angles that are less than 1°, the error can be simplified as the product of a coefficient and three terms. The three terms are: (1) the square of the tilt, (2) the sine of the artifact's nominal angle, and (3) the cosine of the artifact's nominal angle plus two times the artifact's position angle. It is shown that the error can be eliminated by placing the artifact at designated periodic positions.

Two experiments were performed to verify this formula. The first experiment measured the horizontal angle error of a 90° angle block at tilt angles of 3′, 9′, and 20′ as a function of block position. The second experiment measured the horizontal angle error of 30°, 60°, 90°, 120°, and 150° angle blocks with about 9′ of tilt as a function of block position. Remarkable agreement between the predicted and the experimental results was found; the largest difference observed was 0.17″. This good agreement was obtained even with large tilt angles. The formula may also be used for optical polygons to determine the tilt error for each of its adjacent surfaces.

8. Appendix A. Derivation of Horizontal Angle Error in Angle Block Measurements

8.1 Derivation of the Horizontal Angle Position for Surface 1

Initially, the mount has a tilt τ and is at position ω. Therefore,

$$M_{\text{norm}} = M_{\text{mid}} \times M_{\text{low}}$$

$$M_{\text{low}} = \cos(\tau)\sin(\omega)i + \cos(\tau)\cos(\omega)j - \sin(\tau)k$$

$$M_{\text{mid}} = \cos(\omega)i - \sin(\omega)j$$

which gives

$$M_{\text{norm}} = \sin(\tau)\sin(\omega)i + \cos(\omega)\sin(\tau)j + \cos(\tau)k.$$

Next, we have

$$P_1 \cdot M_{\text{low}} = \cos(\theta_1)$$

$$P_1 \cdot M_{\text{mid}} = \cos(\theta_2)$$

$$P_1 \cdot M_{\text{norm}} = \cos(\theta_3)$$

where

$$\theta_1 = \gamma - 90°$$

$$\theta_2 = \theta_1 - 90°$$

$$\theta_3 = 90°$$

which gives

$$\begin{bmatrix} \cos(\tau)\sin(\omega) & \cos(\tau)\cos(\omega) & -\sin(\tau) \\ \cos(\omega) & -\sin(\omega) & 0 \\ \sin(\tau)\sin(\omega) & \cos(\omega)\sin(\tau) & \cos(\tau) \end{bmatrix} \begin{bmatrix} P_{1x} \\ P_{1y} \\ P_{1z} \end{bmatrix}$$

$$= \begin{bmatrix} \cos(\gamma - 90°) \\ \cos((\gamma - 90°) - 90°) \\ \cos(90°) \end{bmatrix}.$$

Solving for P_1 in the above matrix yields its three components:

$$\begin{bmatrix} P_{1x} \\ P_{1y} \\ P_{1z} \end{bmatrix} = \begin{bmatrix} -\cos(\gamma)\cos(\omega) + \cos(\tau)\sin(\gamma)\sin(\omega) \\ \cos(\tau)\cos(\omega)\sin(\gamma) + \cos(\gamma)\sin(\omega) \\ -\sin(\gamma)\sin(\tau) \end{bmatrix}.$$

Next, we solve

$$N_1 = P_1 \times M_{\text{norm}}$$

which gives the three components of N_1:

$$\begin{bmatrix} N_{1x} \\ N_{1y} \\ N_{1z} \end{bmatrix} = \begin{bmatrix} \cos^2(\tau)\cos(\omega)\sin(\gamma) + \cos(\omega)\sin(\gamma)\sin^2(\tau) + \cos(\gamma)\cos(\tau)\sin(\omega) \\ \cos(\gamma)\cos(\tau)\cos(\omega) - \cos^2(\tau)\sin(\gamma)\sin(\omega) - \sin(\gamma)\sin^2(\tau)\sin(\omega) \\ -\cos(\gamma)\sin(\tau) \end{bmatrix}.$$

Further, we have

$$\theta_{\text{H:S}_1} = \arcsin\left(-\frac{N_{1y}}{\sqrt{N_{1x}^2 + N_{1y}^2}}\right)$$

which is equivalent to

$$\theta_{\text{H:S}_1} = -\arctan\left(\frac{N_{1y}}{N_{1x}}\right).$$

Therefore,

$$\theta_{\text{H:S}_1} = -\arctan\left(\frac{\cos(\tau)\cos(\gamma)\cos(\omega) - \sin(\gamma)\sin(\omega)}{\cos(\tau)\cos(\gamma)\sin(\omega) + \sin(\gamma)\cos(\omega)}\right).$$

8.2 Derivation of the Horizontal Angle Position for Surface 2

The mount is rotated to $\omega_{(\text{new})}$ such that surface S_2 is in alignment with the autocollimator as:

$$\omega_{(\text{new})} = \omega + (180° - \alpha).$$

Therefore,

$$M_{\text{low}} = \cos(\tau)\sin(\omega + 180° - \alpha)i + \cos(\tau)\cos(\omega + 180° - \alpha)j - \sin(\tau)k$$

$$M_{\text{mid}} = \cos(\omega + 180° - \alpha)i - \sin(\omega + 180° - \alpha)j$$

$$M_{\text{norm}} = \sin(\tau)\sin(\omega + 180° - \alpha)i + \cos(\omega + 180° - \alpha)\sin(\tau)j + \cos(\tau)k.$$

Also for surface 2,

$$\theta_{1(\text{new})} = \theta_{1(\text{old})} - (180° - \alpha).$$

As a result, the matrix for solving P_2 becomes

$$\begin{bmatrix} \cos(\tau)\sin(\omega + 180° - \alpha) & \cos(\tau)\cos(\omega + 180° - \alpha) & -\sin(\tau) \\ \cos(\omega + 180° - \alpha) & -\sin(\omega + 180° - \alpha) & 0 \\ \sin(\tau)\sin(\omega + 180° - \alpha) & \cos(\omega + 180° - \alpha)\sin(\tau) & \cos(\tau) \end{bmatrix} \begin{bmatrix} P_{2x} \\ P_{2y} \\ P_{2z} \end{bmatrix} = \begin{bmatrix} \cos(\gamma - 270° + \alpha) \\ \cos((\gamma - 270° + \alpha) - 90°) \\ \cos(90°) \end{bmatrix}.$$

Solving the above matrix yields

$$\begin{bmatrix} P_{2x} \\ P_{2y} \\ P_{2z} \end{bmatrix} = \begin{bmatrix} \cos(\alpha+\gamma)\cos(\omega+180°-\alpha)-\cos(\tau)\sin(\alpha+\gamma)\sin(\omega+180°-\alpha) \\ -\cos(\tau)\cos(\omega+180°-\alpha)\sin(\alpha+\gamma)-\cos(\alpha+\gamma)\sin(\omega+180°-\alpha) \\ \sin(\alpha+\gamma)\sin(\tau) \end{bmatrix}.$$

We now solve for N_2 from

$$N_2 = P_2 \times M_{\text{norm}}$$

to obtain

$$\begin{bmatrix} N_{2x} \\ N_{2y} \\ N_{2z} \end{bmatrix} = \begin{bmatrix} -\cos^2(\tau)\cos(\omega+180°-\alpha)\sin(\alpha+\gamma)-\cos(\omega+180°-\alpha)\sin(\alpha+\gamma)\sin^2(\tau)-\cos(\alpha+\gamma)\cos(\tau)\sin(\omega+180°-\alpha) \\ -\cos(\alpha+\gamma)\cos(\tau)\cos(\omega+180°-\alpha)+\cos^2(\tau)\sin(\alpha+\gamma)\sin(\omega+180°-\alpha)+\sin(\alpha+\gamma)\sin^2(\tau)\sin(\omega+180°-\alpha) \\ \cos(\alpha+\gamma)\sin(\tau) \end{bmatrix}.$$

Finally, we solve

$$\theta_{\text{H:}S_2} = -\arctan\left(\frac{N_{2y}}{N_{2x}}\right)$$

and obtain

$$\theta_{\text{H:}S_2} = -\arctan\left(\frac{\cos(\tau)\cos(\alpha+\gamma)\cos(\omega+180°-\alpha)-\sin(\alpha+\gamma)\sin(\omega+180°-\alpha)}{\cos(\tau)\cos(\alpha+\gamma)\sin(\omega+180°-\alpha)+\sin(\alpha+\gamma)\cos(\omega+180°-\alpha)}\right).$$

8.3 Derivation of the Horizontal Angle Error

The horizontal angle error, ϵ_{H}, is the difference in the horizontal angles derived above:

$$\epsilon_{\text{H}} = \theta_{\text{H:}S_2} - \theta_{\text{H:}S_1}$$

where

$$\theta_{\text{H:}S_1} = -\arctan\left(\frac{\cos(\tau)\cos(\gamma)\cos(\omega)-\sin(\gamma)\sin(\omega)}{\cos(\tau)\cos(\gamma)\sin(\omega)+\sin(\gamma)\cos(\omega)}\right)$$

$$\theta_{\text{H:}S_2} = -\arctan\left(\frac{\cos(\tau)\cos(\alpha+\gamma)\cos(\omega+180°-\alpha)-\sin(\alpha+\gamma)\sin(\omega+180°-\alpha)}{\cos(\tau)\cos(\alpha+\gamma)\sin(\omega+180°-\alpha)+\sin(\alpha+\gamma)\cos(\omega+180°-\alpha)}\right).$$

During calibration, it is customary to align the first surface of the artifact to the reference zero of the autocollimator as close as possible. Therefore, the position angle of the mount during setup is determined by the position of the artifact on the mount:

$$\omega = \arctan\left(\frac{\cos(\tau)\cos(\gamma)}{\sin(\gamma)}\right) \rightarrow \gamma \neq \pm(90N)°$$

$$\omega = 90° - \gamma \qquad \rightarrow \gamma = \pm(90N)°$$

where N is a whole number from 0 to ∞. This eliminates the independent variable, ω.

8.4 Simplification of the Error Equation

The error equation is expanded in a Taylor-series around τ to the sixth power:

$$\epsilon_{II} = \tau^2\left(\frac{\cos(\alpha+2\gamma)\sin(\alpha)}{2}\right)$$
$$+\tau^4\left(\frac{\cos(\alpha+2\gamma)\sin(\alpha)}{12}+\frac{\cos(\alpha+4\gamma)\sin(\alpha)}{16}+\frac{\cos(3\alpha+4\gamma)\sin(\alpha)}{16}\right)$$
$$+\tau^6\left(\frac{17\cos(\alpha+2\gamma)\sin(\alpha)}{1440}+\frac{\cos(\alpha+4\gamma)\sin(\alpha)}{48}+\frac{\cos(3\alpha+4\gamma)\sin(\alpha)}{48}\right.$$
$$\left.+\frac{\cos(\alpha+6\gamma)\sin(\alpha)}{96}+\frac{\cos(3\alpha+6\gamma)\sin(\alpha)}{96}+\frac{\cos(5\alpha+6\gamma)\sin(\alpha)}{96}\right)$$
$$+O_3(\tau)$$

where $O_3(\tau)$ represents the sum of the terms that are greater than the sixth power. The variables ϵ_{II} and τ are both expressed in radians. The above equation becomes:

$$\epsilon_{II} \approx \tau^2(2.424\times10^{-6})\cos(\alpha+2\gamma)\sin(\alpha)$$
$$+\tau^4((9.496\times10^{-18})\cos(\alpha+2\gamma)\sin(\alpha)+(7.122\times10^{-18})\cos(\alpha+4\gamma)\sin(\alpha)$$
$$+(7.122\times10^{-18})\cos(3\alpha+4\gamma)\sin(\alpha))$$
$$+\tau^6((3.162\times10^{-29})\cos(\alpha+2\gamma)\sin(\alpha)+(5.580\times10^{-29})\cos(\alpha+4\gamma)\sin(\alpha)$$
$$+(5.580\times10^{-29})\cos(3\alpha+4\gamma)\sin(\alpha)+(2.790\times10^{-29})\cos(\alpha+6\gamma)\sin(\alpha)$$
$$+(2.790\times10^{-29})\cos(3\alpha+6\gamma)\sin(\alpha)$$
$$+(2.790\times10^{-29})\cos(5\alpha+6\gamma)\sin(\alpha))+O_4(\tau)$$

for ϵ_{II} and τ expressed in arcseconds. This equation is an approximation because the coefficient in front of each term is only carried out to four significant digits. In most angle calibrations, the tilt angle is less than a degree. Therefore, using only the first term in the above equations is sufficient for determining the error to a hundredth of an arcsecond.

Acknowledgments

I would like to thank Dr. David Gilsinn for his help with the initial conceptualization of this work, John Horst for his help with the computer solution of the vector mathematics, and Dr. John Kramar for the simplification of the theoretical results.

9. References

[1] K. J. Hume, Metrology With Autocollimators, Hilger & Watts LTD., London (1965) p. 74.
[2] F. T. Fargo, Handbook of Dimensional Measurement, Industrial Press, Inc., Second Ed., New York (1982) pp. 276–280.
[3] P. J. Sim, Angle Standards and Their Calibration, in Modern Techniques In Metrology, P. L. Hewitt, ed., World Scientific Publishing Co. Pte Ltd., Singapore (1984) pp. 102–121.
[4] Y. H. Queen, Tilt Effects on Optical Angle Measurements, in International Progress In Precision Engineering, Proceedings of the 7th International Precision Engineering Seminar, N. Ikawa, S. Shimada, T. Moriwaki, P. A. McKeown, R. C. Spragg, eds., Butterworth-Heinemann, Kobe, Japan (1993) pp. 377–388.

About the author: Yun H. Queen is a physical scientist in the Precision Engineering Division of the NIST Manufacturing Engineering Laboratory. The National Institute of Standards and Technology is an agency of the Technology Administration, U.S. Department of Commerce.

Volume 99, Number 5, September–October 1994
Journal of Research of the National Institute of Standards and Technology

[J. Res. Natl. Inst. Stand. Technol. 99, 605 (1994)]

Optical Characterization in Microelectronics Manufacturing

Volume 99 Number 5 September–October 1994

S. Perkowitz[1] and D. G. Seiler

National Institute of Standards and Technology, Gaithersburg, MD 20899-0001

and

W. M. Duncan

Texas Instruments, Inc., Dallas, TX 75243

To successfully construct semiconductor devices, the semiconductor industry must measure fundamental material parameters, especially when developing new materials; measure the quality of the material as it is grown; accurately determine the details of thin films, quantum wells, and other microstructures that control or affect device performance; and measure properties of the devices themselves. Properties that need to be determined, therefore, include basic band structure and transport parameters, such as energy gap values and carrier scattering times; the presence and concentration of impurities and defects; alloy parameters; layer thicknesses; the distribution of materials in complex structures; and many others. This process of determining a wide range of material, structural, and device parameters is called characterization. The semiconductor industry uses many characterization methods which draw on electrical, chemical, and other approaches. Among these, optical characterization techniques, defined as those using electromagnetic radiation from the ultraviolet to the far infrared, stand out because they are nondestructive and require minimal sample preparation since no contacts are needed. These features are of great importance for production use or to examine finished devices. Another benefit is that, unlike electrical methods which require fixed contacts, optical techniques can give two- or three-dimensional maps of properties over the extent of a semiconductor wafer. The six techniques described in this paper (ellipsometry, infrared spectroscopy, microscopy, modulation spectroscopy, photoluminescence, and Raman scattering) were chosen because they are currently or potentially widely used in the industry; they measure a broad array of semiconductor parameters; and they operate in different regions of the electromagnetic spectrum. The discussion of each technique indicates the basic semiconductor quantities measured, gives the scientific basis of the technique, and indicates how the measurement is made. Illustrative examples from the literature are discussed in detail, showing applications to important semiconductor materials. More information can be obtained from the detailed list of references included.

Key words: ellipsometry; infrared spectroscopy; modulation spectroscopy; optical microscopy; photoluminescence; Raman scattering.

Accepted: July 21, 1994

Contents

[1] Consulting scientist. Present address: Department of Physics, Rollins Research Center, Emory University, Atlanta, GA 30322-2430.

1. Introduction

To successfully construct semiconductor devices, the microelectronics industry must measure fundamental material parameters, especially when developing new materials; measure the quality of the material as it is grown; accurately determine the structural details of thin films, quantum wells, and other microstructures at the heart of devices; and measure properties of the devices themselves. Properties that need to be determined, therefore, include basic band structure and transport parameters, such as gap values and carrier scattering times, the presence and concentration of impurities and defects, alloy parameters, layer thicknesses, the distribution of materials in complex structures, and many others.

The semiconductor industry uses many characterization methods which draw on electrical, chemical, and other approaches. Among these, optical characterization techniques, defined as those using electromagnetic radiation from the ultraviolet to the far infrared, stand out because they are nondestructive and require minimal sample preparation, since no contacts are needed. These features are of great importance for production use, for on-line applications, and for examination of finished devices. Another benefit is that optical techniques can give two- or three-dimensional maps of properties over the extent of a semiconductor wafer without requiring fixed contacts.

Six techniques are described in this paper (ellipsometry, infrared spectroscopy, optical microscopy, modulation spectroscopy, photoluminescence, and Raman scattering). They were chosen because they are currently widely used in the industry and because they measure a broad array of semiconductor parameters. The discussion of each technique indicates the basic semiconductor quantities measured (see Table 1), the physical basis of the technique, and how the measurement is made. Illustrative examples from the literature are discussed, showing applications to important semiconductor material systems. A more detailed review of infrared, Raman and photoluminescence spectroscopies is given in a book by Perkowitz [1]. A recent review of the optical properties of semiconductors is given by Amirtharaj and Seiler [2].

1.1 A Note on Units

Some regions of the electromagnetic spectrum, and some optical methods, refer to wavelength as a matter of usage; others use wavenumbers, or photon energy. Each section here uses the most common units for that technique, including wavelength in nanometers (nm) and micrometers (μm); wavenumber in cm^{-1}; and photon energy in electron volts (eV). Table 2 shows conversion factors for the main units of measure usually encountered.

Table 1. Semiconductor quantities (horizontal rows) and optical characterization methods (vertical columns, labeled as follows: ELL, ellipsometry; IR, infrared spectroscopy; MIC, microscopy; MOD, modulation spectroscopy; PL, photoluminescence; and RAM, Raman scattering). A bullet at the intersection of a given row and column means that the parameter can be determined by that technique using conventional methodology. Further details are given in the discussion

	ELL	IR	MIC	MOD	PL	RAM
Carrier density	•[a]				•[a]	
Carrier mobility		•[a]				•[a]
Carrier scattering time	•			•[b]		
Composition	•	•	•	•	•	•
Crystal orientation						•
Crystallinity	•	•			•	•
Defects		•	•		•	•
Energy gap		•		•	•	
Film thickness	•	•	•			
Impurities		•	•	•	•	•
Resistivity		•				•
Stress	•	•		•	•	•

[a] If the effective mass is known.
[b] Time resolved.

Table 2. Conversion factors for units of measure

λ/nm	$= 10^3\lambda/\mu m$
E_λ/eV	$= 1.2397/(\lambda/\mu m)$
	$= 1.2397\times10^{-4}\lambda^{-1}/cm^{-1}$
λ^{-1}/cm^{-1}	$= 10^4/(\lambda/\mu m)$

1.2 References

[1] S. Perkowitz, Optical Characterization of Semiconductors: Infrared, Raman, and Photoluminescence Spectroscopy, Academic Press, London (1993).
[2] P. Amirtharaj and D. G. Seiler, Optical Properties of Semiconductors, Chapter in Handbook of Optics, McGraw-Hill, to be published.

2. Ellipsometry

2.1 Introduction

Ellipsometry is a technique widely used to measure the thicknesses of films important to semiconductor technology, such as SiO_2 on Si. Thicknesses measured are typically in the range of several nm to several hundred nm. Surface cleanliness of semiconductor wafers during processing can also be determined. In spectroscopic ellipsometry, the ellipsometric data are obtained as a function of wavelength. Then appropriate modeling and fitting can yield the dielectric functions and thicknesses of the layers in complex semiconductor/oxide multilayer systems, such as SIMOX (Separation by IMplanted OXygen), a silicon-on-insulator material formed by high-energy oxygen ion implantation in silicon. The dielectric functions give a complete picture of composition for the entire layered structure.

2.2 Physical Basis

Ellipsometry is based on the polarization transformation that occurs when a beam of polarized light is reflected from (or transmitted through) an interface or film. For example, if plane- or linearly-polarized light impinges on the surface of an absorbing medium, the reflected light usually becomes elliptically polarized because the reflection process differently affects the in-plane component of the incident electric field E_p, relative to the perpendicular electric field component E_s. Each component is reflected with new values of amplitude and phase. The key parameters obtained from an ellipsometric measurement are the ellipsometric angles ψ and Δ. These appear in the complex reflection ratio ρ, defined as

$$\rho = \frac{r_p}{r_s} = \tan(\psi) e^{i\Delta}, \tag{1}$$

where the amplitude reflection coefficients r_p and r_s are

$$r_p = \frac{E_p \text{ (reflected)}}{E_p \text{ (incident)}} \tag{2}$$

$$r_s = \frac{E_s \text{ (reflected)}}{E_s \text{ (incident)}}. \tag{3}$$

The ellipsometric angles are defined as $\psi = \tan^{-1}|\rho|$, and Δ is the difference in phase between the p and s components.

2.3 Experimental and Technical Details

Ellipsometric measurements start with light of known polarization incident on the sample. The polarization of the reflected light is determined, from which further analysis gives the parameters such as refractive index and film thickness which determine the interaction between light and sample.

In its simplest form, single-wavelength ellipsometry requires a manual nulling to gather data. Light from the source (usually a laser for single-wavelength work) passes through a linear polarizer, then through a compensator which elliptically polarizes the light. The light continues to the sample, is reflected, passes through a polarization analyzer, and is finally detected. The null technique works by adjusting the angle of the polarizer with respect to compensator, sample, and analyzer until the reflection process just cancels the ellipticity the light gained from the compensator. Then the reflected light is linearly polarized and can be extinguished by choosing the appropriate angle for the analyzer, that is, until the photomultiplier shows a minimum signal. The two values of the angles yield ρ.

This null process is too slow for real-time measurements, or for spectroscopic ellipsometry. Three types of automatic ellipsometry (self-compensating, rotating element, and polarization-modulated), together with dedicated computers, allow rapid measurement and analysis. In the automatic self-compensating system [1], the angles of the linearly polarized light leaving the polarizer, and entering the analyzer, are rotated by Faraday or Pockels cells, until the null is achieved. This type of instrument can give fixed wavelength data within 1 ms, and spectroscopic data over a wide wavelength range in 3 s.

The optical layout of the rotating element system (Fig. 1) is like that of the self-compensating system with the compensator omitted [1]. The polarization analyzer rotates around the axis of the reflected light beam at a fixed angular velocity, typically corresponding to 50 Hz to 100 Hz. The rotating analyzer would produce a sine-squared signal with two maxima and two true zero minima every rotation, if the light were linearly polarized. For elliptically polarized light, the signal is also of sine-squared form, but with smaller maxima, and nonzero minima, which depend on the ellipticity of the reflected light. A Fourier analysis of the output of the rotating analyzer gives ρ and hence the angles ψ and Δ. For an analyzer rotating at 100 Hz, the measurement at a single wavelength can be completed in 5 ms.

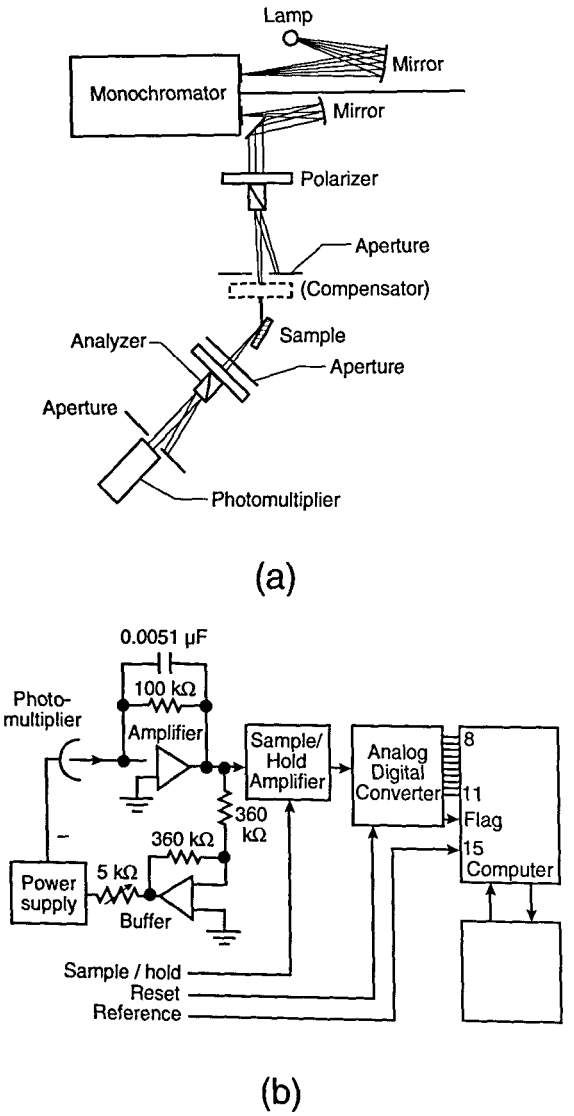

Fig. 1. Schematic diagrams of (a) optical elements and (b) signal processing system for a rotating analyzer spectroscopic ellipsometer designed for high-precision measurements of the optical properties of solids. (See Sec. 2.5, General Refs., Collins (1990), fig. 3, p. 2032.)

The fastest type of system is the polarization-modulated ellipsometer [1], where the compensator in the manual null system is replaced by a birefringent phase modulator (a piezobirefringent plate or a Pockels cell). In the phase modulator, the ellipticity imparted to the linearly polarized light varies sinusoidally with time, rather than remaining constant as in the self-compensating system. The signal which results at the detector can be Fourier analyzed or analyzed by a phase-sensitive detector to give ρ. A piezobirefringent modulator is a fast device, which can operate at 100 kHz or more; hence, this system can obtain data in an interval of 10 ms per wavelength measurement, which means that full scans over the range 400 nm to 700 nm can be obtained in a few seconds or less.

Of the three automatic systems, the polarization-modulated spectrometer is best for real-time rapid data acquisition. However, in the self-compensating and polarization-modulation cases, the compensator or modulator must be tuned for each wavelength; hence, these are more complex and can be less accurate than the rotating analyzer system.

For spectroscopic ellipsometry, a stable xenon lamp with output covering the near ultraviolet to near infrared is a commonly used source. The sample is mounted on a high-accuracy stage to allow careful angle alignment. Usually an autocollimator and apertures are used to control collimation and alignment. In general, available equipment gives good results over the near infrared to the near ultraviolet. The ellipsometric angles Δ and ψ can be measured to within millidegrees, resulting in uncertainties of less than one part in 10^3 for the index of refraction and tenths of a nanometer for the corresponding thicknesses.

Parameters for a complex semiconductor/oxide system examined by ellipsometry are determined by sophisticated computer software [1–2]. These fit the measured ellipsometric parameters versus wavelength, by assuming appropriate dielectric functions for each layer, and layer thicknesses. Commercial systems include appropriate software, and fitting routines are also available from other sources.

2.4 Illustrative Applications

An example of the kind of semiconductor analysis that can be achieved with spectroscopic ellipsometry is shown in Fig. 2 for a sample of SIMOX, an important silicon-on-insulator system. The ellipsometric angles Δ and ψ show complex spectra over the range 1.5 eV to 4.5 eV, with the large oscillations related to interference effects. Multiparameter regression analysis yields the fits displayed in the plots, which determine the sample's structural details as shown.

Table 3 presents typical sensitivities of quantities obtained by ellipsometry, such as thicknesses, composition, and temperature. For more specific details, the reader can refer to the citations given in the table.

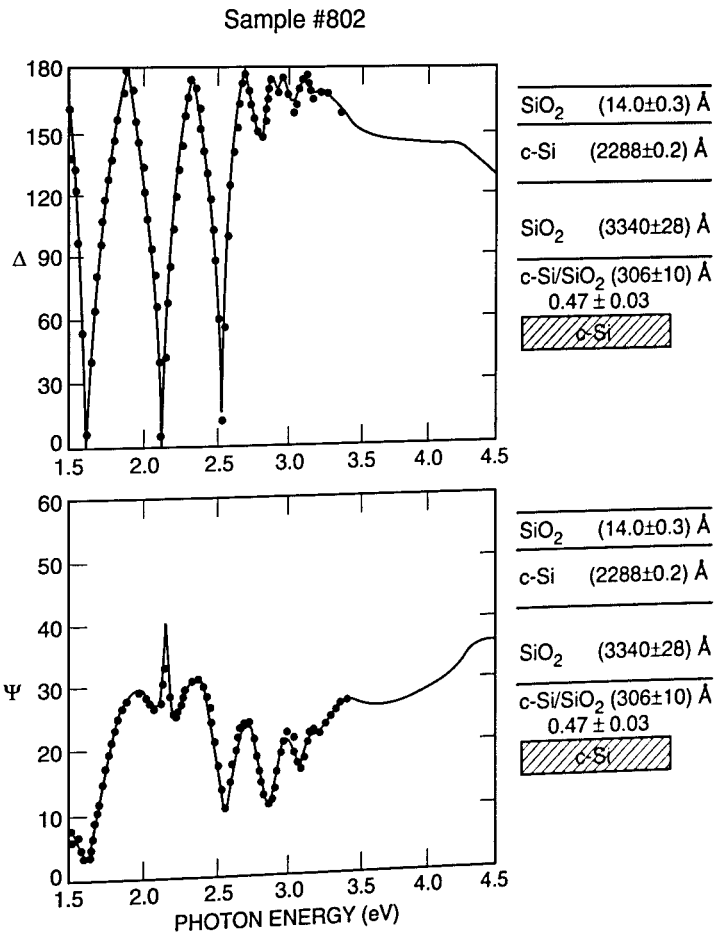

Fig. 2. Ellipsometric angles Δ and ψ versus photon energy for a SIMOX sample. Individual points, data obtained from rotating element spectroscopic ellipsometer. Solid line, fit obtained by regression analysis assuming structural layer thickness and composition shown on the right. The layer immediately below the 334 nm SiO_2 layer is modeled as a granular mixture of crystalline Si (c-Si) and SiO_2, with 47% volume fraction c-Si, using effective medium theory. Shown to the right of the figures are the thicknesses of the layers. The calculated uncertainties of the model parameters are set to one standard deviation as determined by the regression analysis. (After D. Chandler-Horowitz et al. (1991), unpublished data, National Institute of Standards and Technology.)

Table 3. Spectral ellipsometry sensitivity. Given are sensitivities for the measurement of thicknesses, composition, damage profile, and temperature in a number of systems. The notations used for the measured quantity column are the complex reflection ratio, ρ; the amplitude ratio, ψ; and the phase shift, Δ

Method	Matrix	Quantity	Measured quantity	Conversion	Sensitivity[a]	Ref. (see below)
SE	SiO_2/Si	SiO_2 thickness	ρ	Fresnel Equations[1] and Estimator[2] (FE&E)	±0.2 Å to ±0.6 Å @1000 Å to 2300 Å	3
SE	SiO_2/SiO_2+Si/Si	Interfacial SiO_2+Si thickness	ρ	FE&E and EMA[4]	±2 Å @ 7 Å	4
SE	SiO_2/SiO_2+Si/Si	SiO_2 thickness	ρ	FE&E and EMA	(1112.1±0.2) Å and (276.9±0.2) Å	5
SE	SiO_2/a-Si/c-Si+SiC/SiC/c-Si	Layer thicknesses	ρ	FE&E and EMA	±2 Å to ±25 Å	6
SE	Polysilicon	Polysilicon composition (e.g., void + c-Si+a-Si)	ρ	FE&E and EMA	c-Si: 0.14±0.02 void: 0.25±0.06	7
SE	Si	Damage profile	ρ	FE&E and EMA	Damage range (170±50) Å to (320±20) Å	8
SE	SiO_2/polysilicon/SiO_2/Si	Polysilicon and SiO_2 thicknesses	ρ	FE&E and EMA	Native oxide (15±0.3) Å; Poly±0.3 Å to ±3.9 Å @ (240 to 1030) Å; Oxide ±0.4 Å to ±1.7 Å @(50 to 130) Å	9
SE	SiO_2/Si/SiN/Si	Native oxide, Si, and nitride thickness	ρ	FE&E and EMA	–	10
SWE	SiO_2/Si	Temperature	ψ, Δ	polynomial	±10 °C	11
VASE	Oxide/GaAs/ $Al_xGa_{1-x}As$/ GaAs	Thicknesses and AlGaAs composition	ρ	FE&E and EMA	Oxide (34±3) Å GaAs (159±8) Å AlGaAs (865±14) Å AlGaAs, $x=0.35\pm0.02$	12
VASE	Oxide/GaAs/ $Al_xGa_{1-x}As$/ GaAs/Al_xGaAs_{1-x}/GaAs	Thicknesses and AlGaAs composition	ρ	FE&E and EMA	Oxide (26±1) Å GaAs (435±8) Å AlGaAs (413±14) Å AlGaAs, $x=0.37\pm0.005$ GaAs (142±10) Å AlGaAs/GaAs SLS 5@ (470±20) Å AlGaAs/GaAs SLS $x=0.32\pm0.001$	13
SE	$Al_xGa_{1-x}As$/GaAs	AlGaAs composition and thickness *in situ*	ρ	Trajectories in ϵ_1 and ϵ_2	$x=0.2\pm0.03$ ($x>0.2$)	14

[a] Typically calculated as the 90 % confidence interval from the mean square deviation and covariance matrix.

References

[1] R. M. A. Azzam and N. M. Bashara, Ellipsometry and Polarized Light, North Holland, Amsterdam (1989) Ch. 4.
[2] D. E. Aspnes, J. B. Theeten, and R. P. H. Chang, J. Vac. Sci. Technol. 16, 1374 (1979).

References to Table 3—Continued

[3] B. J. Mrstik, P. J. McMarr, J. R. Blanco, and J. M. Bennett, J. Electrochem. Soc. **138**, 1770 (1991).
[4] D. E. Aspnes and J. B. Theeten, J. Electrochem. Soc. **127**, 1359 (1980).
[5] G. E. Jellison, Jr., J. Appl. Phys. **69**, 7627 (1991).
[6] N. V. Nguyen and K. Vedam, J. Appl. Phys. **67**, 3555 (1990).
[7] D. E. Aspnes, J. Vac. Sci. Technol. **18**, 289 (1981).
[8] M. Fried, T. Lohner, W. A. M. Aarnink, L. J. Hanekamp, and A. van Silfhout, J. Appl. Phys. **71**, 2835 (1992).
[9] W. M. Duncan and S. A. Henck, Appl. Surf. Sci. **63**, 9 (1993).
[10] M. Fried, T. Lohner, J. M. M. de Nigs, A. van Silfhout, L. J. Hanekamp, Z. Laczik, M. Q. Khanh, and J. Gyulai, J. Appl. Phys. **66**, 5052 (1989).
[11] R. K. Sampson and H. Z. Massoud, J. Electrochem. Soc. **140**, 2673 (1993).
[12] P. G. Snyder, M. C. Rost, G. H. Bu-Abbud, J. A. Woollam, and S. A. Alterovitz, J. Appl. Phys. **60**, 3293 (1986).
[13] K. G. Merkel, P. G. Snyder, J. A. Woollam, S. A. Alterovitz, and A. K. Rai, Jpn. J. Appl. Phys. **28**, 1118 (1989); J. A. Woollam, P. G. Snyder, K. G. Merkel, and S. A. Alterovitz, Materials Sci. Engl. **B5**, 291 (1990).
[14] D. E. Aspnes, W. E. Quinn, and S. Gregory, Appl. Phys. Lett. **56**, 2569 (1969).

2.5 References

[1] O. Acher, E. Bigan, and B. Drevillon, Improvements of phase-modulated ellipsometry, Rev. Sci. Instrum. **60**, 65 (1989).
[2] R. M. A. Azzam and N. M. Bashara, Ellipsometry and Polarized Light, North-Holland, New York (1989).

General

D. E. Aspnes, The characterization of materials by spectroscopic ellipsometry, in Spectroscopic Characterization Techniques for Semiconductor Technology, Proceedings SPIE Vol. 452, F. H. Pollak and R. S. Bauer, eds., SPIE, Bellingham, Washington (1983) pp. 60–70.

D. E. Aspnes, The accurate determination of optical properties by ellipsometry, in Handbook of Optical Constants of Solids, E. D. Palik, ed., Academic Press, Orlando, Florida (1985) pp. 89–112.

D. E. Aspnes, Analysis of semiconductor materials and structures by spectroellipsometry, in Spectroscopic Characterization Techniques for Semiconductor Technology III, Proceedings SPIE Vol. 946, O. J. Glembocki, F. H. Pollak, and F. Ponce, eds., SPIE, Bellingham, Washington (1988) pp. 84–97.

R. W. Collins, Automatic rotating element ellipsometers: calibration, operation, and real-time applications, Rev. Sci. Instrum. **61**, 2029–2062 (1990).

J. F. Marchiando, Semiconductor Measurement Technology: A Software Program for Aiding the Analysis of Ellipsometric Measurements, Simple Spectroscopic Models, Natl. Inst. Stand. Technol. Special Publication 400–84, U.S. Government Printing Office, Washington, DC (1990).

B. A. Tirri, A. Turner, and P. C. Van Buskirk, Spectroellipsometric characterization of inhomogeneous films, in Modern Optical Characterization Techniques for Semiconductors and Semiconductor Devices, Proceedings SPIE Vol. 794, O. H. Glembocki, F. H. Pollak and J. J. Soong, eds., SPIE, Bellingham, Washington (1987) pp. 252–261.

Applications

D. E. Aspnes and A. A. Studna, Optical detection and minimization of surface overlayers on semiconductors using spectroscopic ellipsometry, in Optical Characterization Techniques for Semiconductor Technology, Proceedings SPIE Vol. 276, D. E. Aspnes, S. So, and R. F. Potter, eds., SPIE, Bellingham, Washington (1981) pp. 227–232.

D. E. Aspnes, J. P. Harbison, A. A. Studna, L. T. Florez, and M. K. Kelly, *In situ* optical measurements of the growth of GaAs and AlGaAs by molecular beam epitaxy, in Spectroscopic Characterization Techniques for Semiconductor Technology III, Proceedings SPIE Vol. 946, O. J. Glembocki, F. H. Pollak, and F. Ponce, eds., SPIE, Bellingham, Washington (1988) pp. 112–121.

R. W. Collins and J. M. Cavese, *In situ* ellipsometry characterization of the growth of thin film amorphous semiconductors, in Modern Optical Characterization Techniques for Semiconductors and Semiconductor Devices, Proceedings SPIE Vol. 794, O. H. Glembocki, F. H. Pollak, and J. J. Soong, eds., SPIE, Bellingham, Washington (1987) pp. 242–251.

Y. Demay, D. Arnoult, J. P. Gailliard, and P. Medina, *In situ* spectroscopic ellipsometry during molecular-beam epitaxy of cadmium mercury telluride, J. Vac. Sci. Technol. **A5**, 3139 (1987).

M. G. Doss, D. Chandler-Horowitz, J. F. Marchiando, S. Krause, and S. Seraphin, Analysis for the characterization of oxygen implanted silicon (SIMOX) by spectroscopic ellipsometry, Materials Research Society Symposia Proceedings Vol. 209, Materials Research Society, Pittsburgh, Pennsylvania (1991) pp. 493–498.

B. Drevillon, *In situ* analysis of the growth of semiconductor materials by phase modulated ellipsometry from UV to IR, in Surface and Interface Analysis of Microelectronic Materials Processing and Growth, Proceedings SPIE Vol. 1186, L. J. Brillson and F. H. Pollak, eds., SPIE, Bellingham, Washington (1989) pp. 110–121.

P. Dutta, G. A. Candela, D. Chandler-Horowitz, and J. F. Marchiando, Nondestructive characterization of oxygen-ion-implanted silicon-on-insulator using multiple-angle ellipsometry, J. Appl. Phys. **64**, 2754–2756 (1988).

K. G. Merkel, P. G. Snyder, J. A. Woollam, and S. A. Alterovitz, GaAs/AlGaAs superlattice characterization by variable angle spectroscopic ellipsometry, in Spectroscopic Characterization Techniques for Semiconductor Technology III, Proceedings SPIE Vol. 946, O. J. Glembocki, F. H. Pollak, and F. Ponce, eds., SPIE, Bellingham, Washington (1988) pp. 105–111.

P. G. Snyder, J. A. Woollam, and S. A. Alterovitz, Variable angle of incidence spectroscopic ellipsometric study of semiconductor multilayer structures, in Materials Characterization, Materials Research Society Symposia Proceedings Vol. 69, N. Cheung and M.-A. Nicolet, eds., Materials Research Society, Pittsburgh, Pennsylvania (1986) pp. 245–250.

P. G. Snyder, K. G. Merkel, and J. A. Woollam, Optical measurement of built-in and applied electric fields in AlGaAs/GaAs heterostructures, in Spectroscopic Characterization Techniques for Semiconductor Technology III, Proceedings SPIE Vol. 946, O. J. Glembocki, F. H. Pollak, and F. Ponce, eds., SPIE, Bellingham, Washington (1988) pp. 98–104.

E. Taft and L. Cordes, Optical evidence for a silicon-silicon oxide interlayer, J. Electrochem. Soc. 126, 131-134 (1979).

J. A. Woollam and P. G. Snyder, Fundamentals and applications of variable angle spectroscopic ellipsometry, Materials Sci. Eng. B5, 279–283 (1990).

3. Infrared Spectroscopy

3.1 Introduction

Infrared (IR) spectroscopy in the range from 10 cm^{-1} to 10,000 cm^{-1} can be used to determine impurity type and concentration in semiconductor materials, film thickness, semiconductor alloy composition, carrier density and scattering time. These determinations can be made for bulk, film, and microstructure systems. One application in Si measures the amount of interstitial oxygen, whose concentration is critical; correct values provide gettering action, reducing the level of other impurities, and hence, producing material with low leakage currents. Concentrations of oxygen in silicon and other impurities can be determined by infrared spectroscopic evaluation during processing.

3.2 Physical Basis

Infrared radiation interacts with semiconductor lattices, carriers, and impurities, and is affected by semiconductor layer thickness. Binary semiconductors like GaAs have vibrational lattice transverse optical (TO) modes which couple to infrared radiation, with resonant absorption when the incoming frequency matches the TO frequency. Ternary alloys like $Al_xGa_{1-x}As$ display two TO modes, whose strength and frequency vary with x.

Semiconductor impurities can absorb infrared energy by photoionization of their bound carriers, or may modify their immediate lattice environment to produce a so-called local vibrational mode (LVM). In the case of photoionization, the impurity must be in a populated or ground state; hence, this absorption process is normally observed at cryogenic temperatures. Local vibrational modes occur when an impurity atom is lighter than the host lattice. Impurities important to semiconductor processing such as oxygen and carbon in Si produce LVM absorptions in the infrared region. If a semiconductor film is not too highly absorbing (device grade material is often highly conductive, and, therefore, absorbing), interference between infrared radiation reflected from the front surface, and that reflected from the back, can produce fringes whose spacing is related to the film thickness. Finally, free charge carriers in a semiconductor also absorb electromagnetic radiation. The absorption increases with wavelength; hence, absorption can be significant at infrared wavelengths even for low carrier concentrations.

An important feature of optical processes such as those occurring in the IR region is that quantitative measurements can be made based on absorption, reflection, or transmission data, and then accurately described by simple theory. The infrared properties are specified by the complex dielectric function $\epsilon(\omega)=\epsilon_1(\omega)+i\epsilon_2(\omega)$, which is related to the complex refractive index $\tilde{n}(\omega)= n(\omega)+ik(\omega)$ by

$$n^2-k^2=\epsilon_1(\omega)$$

$$2nk=\epsilon_2(\omega)\,. \tag{4}$$

If $\tilde{n}(\omega)$ is known, then the reflection and transmission properties can be calculated. For instance, a semiconductor film has at normal incidence a front-surface reflection coefficient R,

$$R=\frac{[(n-1)^2+k^2]}{[(n+1)^2+k^2]} \tag{5}$$

and a transmission coefficient,

$$T=\frac{(1-R)^2e^{-\alpha d}}{(1-R^2e^{-2\alpha d})}\,, \tag{6}$$

where α is the absorption coefficient ($=4\pi k/\lambda$) and d is the film thickness. These expressions apply only when interference effects can be neglected, i.e., when noncoherent light is used.

For absorption due to lattice vibrations, or due to local impurity vibrational modes, the dielectric function ϵ is

$$\epsilon(\omega)=\epsilon_\infty+\frac{S\omega_R^2}{\omega_R^2-\omega^2-i\omega\Gamma}\,. \tag{7}$$

In this well-known Lorentzian form, ϵ_∞ is the high-frequency limit of $\epsilon(\omega)$; S is the oscillator strength; Γ is a damping term; and the resonant frequency ω_R is the TO frequency for a lattice oscillation, or characteristic fingerprint frequency for an impurity vibrational mode. For a ternary semiconductor like $Al_{1-x}Ga_xAs$, each TO mode is represented by a resonant term like that in Eq. (7), whose parameters depend on x.

If there are free carriers present, ϵ has an additional term $-\epsilon_\infty \omega_p^2/[\omega(\omega - i/\tau)]$, where τ is the carrier scattering time, and ω_p^2 is the plasma frequency $4\pi Ne^2/m^*\epsilon_\infty$, with N the carrier concentration and m^* the carrier effective mass. Hence, N and the drift mobility $\mu = e\tau/m^*$ can be found from these parameters if m^* is known. Also, the dc resistivity $\rho = m^*/ne^2\tau = \omega_p^2\tau$ can be found from these quantities, even if m^* is not known.

From the theory discussed above, measured reflection, transmission, and absorption data can be related to the microscopic semiconductor parameters. Thus, concentrations of impurity oxygen and carbon in silicon, for instance, in the parts-per-million range can be determined. Infrared analysis can also be used to determine carrier concentrations, mobilities, and resistivities for carrier concentrations as low as 10^{14} cm^{-3}, with results that agree well with conventional Hall effect and resistivity data.

Further, analysis of infrared reflectivity for thin films of semiconductors, which show interference effects, can be used to accurately determine the thicknesses of films in the micrometer range. For nonabsorbing films, the peaks of observed interference fringes occur at the wavelengths

$$\lambda_P = \frac{2n(\omega)d}{p} \tag{8}$$

where d is the layer thickness, $n(\omega)$ is the real part of the refractive index, and p is the interference order, an integer or half integer 1/2, 1, 3/2 . . . . $n(\omega)$ is known for semiconductors of interest, so that d can be derived from Eq. (8).

Infrared methods can also be used to determine the presence of shallow impurities. A shallow donor impurity behaves like a hydrogen atom immersed in a medium with dielectric constant ϵ and conduction band effective mass ratio m^*/m_0, where m_0 is the free electron mass. From the Bohr model, the ionization energy (in eV) is

$$E_{ion} = \frac{13.6}{\epsilon^2}\left(\frac{m^*}{m_0}\right) \tag{9}$$

which is approximately 6 meV for GaAs. This simple model cannot predict ionization energies for different impurities in different materials, but shows that shallow donor ionization energies lie in the infrared region. Their exact values, and hence identification of the particular impurity, can be found from infrared photoconductivity spectra.

The theory developed above can be used to analyze inhomogeneous microstructures composed of layers of different semiconductors. Each layer is described by the same infrared theory and parameters that define its bulk behavior, to give its complex refractive index. Then, using standard theory for the reflection and transmission at each interface, the total infrared response of the structure can be calculated by computer. This model works well in fitting such data to determine average carrier properties, layer thicknesses, and phonon behavior which is related to microstructure properties and quality.

3.3 Experimental and Technical Details

Infrared spectroscopy often requires only minimal sample preparation, and the low energy and power of infrared radiation sources guarantee that the samples are not altered by the measurement. Because infrared light typically penetrates several micrometers into a semiconductor, this radiation can also be used to examine the various layered regions of an entire microstructure such as a superlattice.

Low source intensity and low detector sensitivity in the infrared region make Fourier transform spectroscopy the method of choice for obtaining IR spectra. In the Fourier method, infrared light, having traversed or been reflected from a sample, is analyzed with an interferometer. The optical intensity reaching the detector through the interferometer is the optical Fourier transform of the desired transmission or reflection spectrum. The interference spectrum is computationally transformed back into an intensity spectrum by means of the Fast Fourier transform algorithm on a computer. The light throughput advantage of a large interferometer aperture rather than the narrow slit of a conventional dispersive monochromator is referred to as the Jacquinot advantage. In addition, the interferometer allows simultaneous observation of many wavelengths, the so-called Fellgett advantage.

Figure 3 is a schematic diagram of a Michelson interferometer. Radiation from a broad-band source, s, is divided by a beamsplitter, BS. Light reflected from the beamsplitter is also reflected

from fixed mirror M1, whereas light transmitted through the beamsplitter is reflected from a movable second mirror, M2. The two light beams recombine to produce a net intensity whose magnitude depends on the difference Δ between the paths that the two beams traverse. As mirror M2 moves, Δ varies continuously. The intensity function $I(\Delta)$, called the interferogram, is

$$I(\Delta)=\int_0^\infty S(f)\,[1+\cos(2\pi f\Delta)]\mathrm{d}f\,, \qquad (10)$$

where $S(f)$ is the intensity spectrum of the source as modified by the sample, and $f=\omega/\pi c$ is the optical frequency in cm^{-1}. Equation (10) is the cosine Fourier transform of $S(f)$, which can be calculated from the inverse transform

$$S(f)=\int_0^\infty \left[I(\Delta)-\frac{1}{2}I(0)\right]\cos(2\pi f\Delta)\mathrm{d}\Delta. \qquad (11)$$

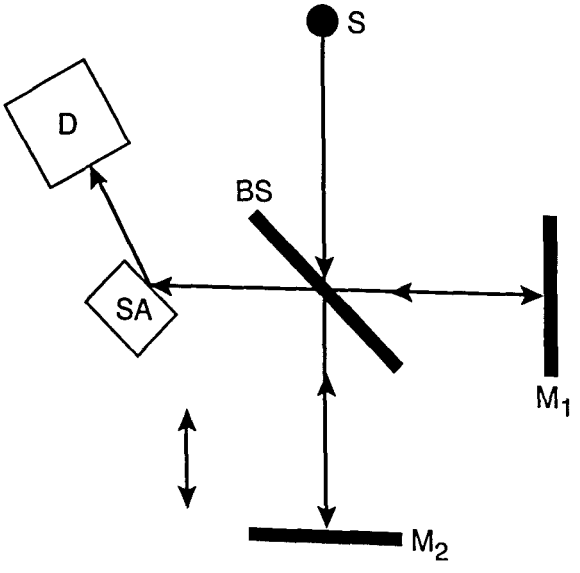

Fig. 3. Diagram of a Michelson interferometer configured for sample reflectance measurements. S, source; BS, beamsplitter; M1, fixed mirror; M2, movable mirror, which moves as indicated by the double-headed arrow; SA, sample; D, detector. The type of source and beamsplitter depends on the region of the infrared where data are to be obtained. The light beams reflected from M1 and M2 recombine to form the interferogram signal, which is measured by the detector.

This is implemented in the laboratory by processing the measured $I(\Delta)$ with a computer to carry out the inverse transform. The spectral resolution in wavenumbers of the Fourier system is $1/L$, where L is the total travel of the movable mirror. Most machines use a rapid scan method, where the mirror is swept through its entire travel in a short time. Many sweeps are averaged together to enhance the signal-to-noise ratio.

Because of the small intensities of infrared sources, especially at the very long wavelengths of the far infrared spectrum, high-quality detectors are important. Liquid helium bolometers give the highest sensitivity, but are expensive and complex to operate. Mercury-cadmium-telluride detectors operating at liquid nitrogen temperatures work well in the mid infrared spectrum. Pyroelectric detectors operate at room temperature and are simple and rugged. They are sufficiently sensitive, from ultraviolet to millimeter wavelengths, for much semiconductor work.

Commercial Fourier transform infrared systems are available that cover the near infrared to the far infrared spectrum, by suitable choice of light source, beam splitter, and detector. To avoid the effect of water vapor absorption on the desired spectrum, these spectrometers are evacuated. Often, semiconductor samples must be cooled in order to better study electronic properties by removing the effects of lattice vibrations or phonons in the absorption spectra. This can be accomplished to 77 K with liquid nitrogen, and to 4.2 K with a liquid helium cryogenic system or by a mechanical refrigerator.

3.4 Illustrative Applications

Figure 4 illustrates the absorption peaks for interstitial oxygen at 1107 cm^{-1} and substitutional carbon at 605 cm^{-1} in Czochralski-grown silicon. Such absorption data can be converted into oxygen concentration values, giving a rapid, nondestructive way to determine this important quantity. Figure 5 demonstrates how a semiconductor film, in this case an epitaxial layer of high-resistivity silicon deposited on low-resistivity silicon, gives clear interference fringes that can be used to measure the layer thickness. Figure 6 correlates resistivity obtained from infrared measurements with resistivity obtained from carrier transport measurements. The data, from epitaxial n- and p-type $Hg_xCd_{1-x}Te$ films, are compared to results from conventional electrical measurements, which require ohmic contacts that can be difficult to apply. Figure 7 shows infrared reflectance data for an AlAs-GaAs superlattice. As the caption discusses in detail, the TO phonon mode for each constituent material is clear, as are interference fringes and other features. The simple theory for infrared phonon response gives a

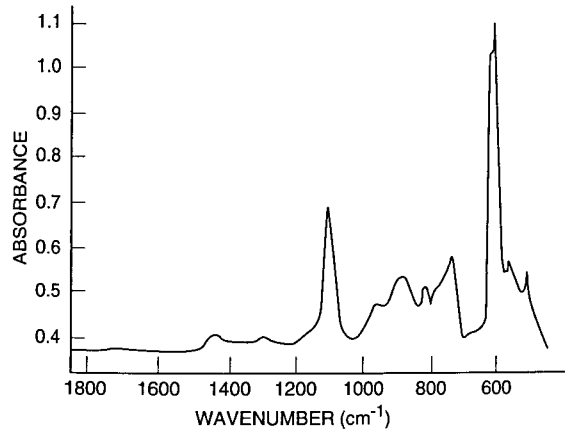

Fig. 4. Infrared absorbance for a Czochralski-grown silicon wafer 2 mm thick, derived from transmission spectra using a commercial Fourier spectrometer with a mercury-cadmium-telluride detector. The characteristic interstitial oxygen line at 1107 cm^{-1} and the substitutional carbon line at 605 cm^{-1} appear. Much of the remaining structure is due to silicon phonon modes. The absorbance at 1107 cm^{-1} is linearly related to the oxygen concentration. Calibration data exist to convert absorbance into oxygen concentration in parts per million atomic or atoms per cubic centimeter. (See Sec. 3.5, Applications Refs., Krishnan, Stout, and Watanabe, in Practical Fourier Transform Infrared Spectroscopy, J. R. Ferraro and K. Krishnan, Eds., Academic Press, San Diego (1990), fig. 5, p. 298.)

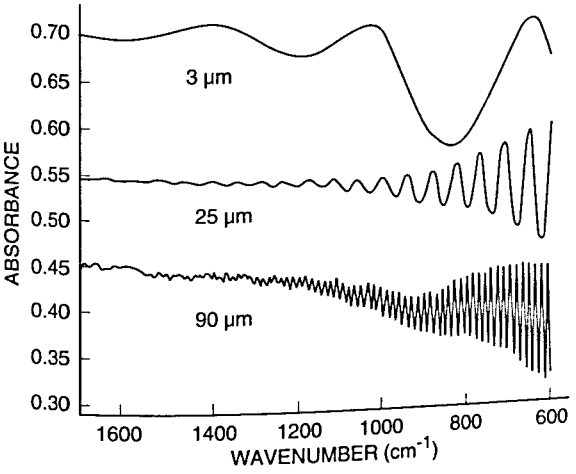

Fig. 5. Infrared reflectance spectra from structures consisting of low carrier concentration silicon epitaxial layers on high concentration silicon substrates, showing interference fringes that can be used to determine epitaxial layer thickness. Layers of different thickness produce different fringe spacings, according to Eq. (8). (See Sec. 3.5, Applications Refs., Krishnan, Stout, and Watanabe, in Practical Fourier Transform Infrared Spectroscopy, J. R. Ferraro and K. Krishnan, Eds., Academic Press, San Diego (1990), fig. 25, p. 333.)

fit which reproduces all the main features of the spectra, and allows an estimate of layer thickness.

Table 4 gives the sensitivities of typical quantities measured by infrared spectroscopy such as interstitial oxygen concentrations in Si and GaAs, substitutional carbon concentrations in Si and GaAs, and B, P, and As concentrations in Si. For more specific details, the reader should refer to the citations given in the table.

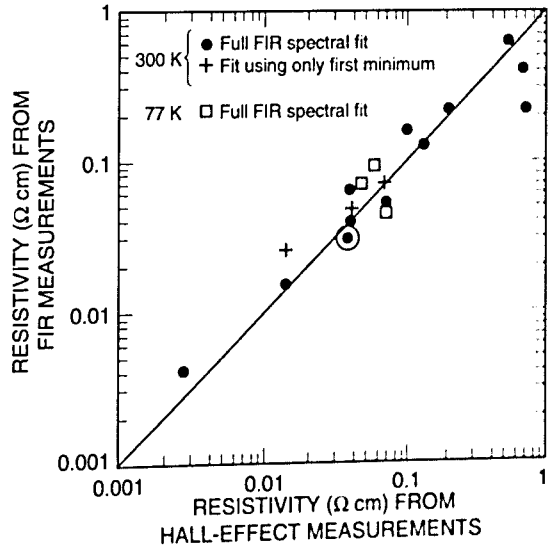

Fig. 6. Infrared values for dc resistivity compared to resistivity values from standard electrical (resistivity-Hall effect) measurements, for several n- and p-type $Hg_{1-x}Cd_xTe$ films on CdTe substrates. The films were typically several micrometers thick with x values of 0.2 to 0.4. Results at both 300 K and 77 K are shown. Resistivity values marked "Full FIR spectral fit" were derived from fits to the full far infrared (FIR) spectrum over the range 20 cm^{-1} to 230 cm^{-1}, using the theory developed in this section. Resistivity values marked "Fit using only first minimum" were derived from the measured position of one particular feature of the FIR spectra, the so-called plasmon-phonon minimum whose location depends on resistivity. The solid line represents perfect agreement between the infrared and the conventional electrical results. The contactless infrared method agrees well with the time-consuming and destructive electrical method requiring contacts. (See Sec. 3.5, Applications Refs., Jones, Boyd, Konkel, Perkowitz, and Braunstein (1986), fig. 2, p. 2057.)

3.5 References

General

R. J. Bell, Introductory Fourier Transform Spectroscopy, Academic Press, New York (1972).

G. L. Carr, S. Perkowitz, and D. B. Tanner, Far infrared properties of inhomogeneous materials, in Infrared and Millimeter Waves, Vol. 13, K. J. Button, ed., Academic Press, New York (1985) pp. 171–263.

E. D. Palik and R. T. Holm, Optical characterization of semiconductors, in Nondestructive Evaluation of Semiconductor Materials and Devices, J. N. Zemel, ed., Plenum, New York (1979) pp. 315–345.

S. Perkowitz, Submillimeter solid state physics, in Infrared and Millimeter Waves, Vol. 8, K. J. Button, ed., Academic Press, New York (1983) pp. 71–125.

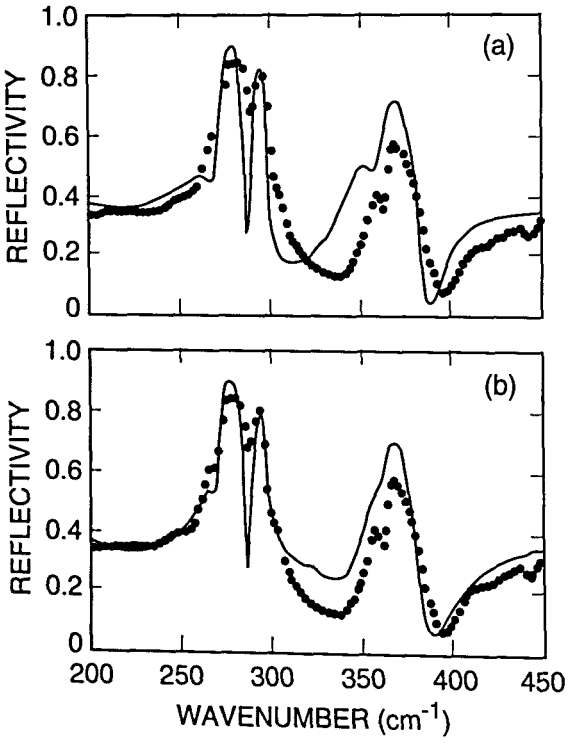

Fig. 7. Infrared reflectivity spectra for an AlAs-GaAs superlattice with 50 layer pairs. Panels (a) and (b) show the same data points. The peaks at 275 cm^{-1} and 365 cm^{-1} are the GaAs TO mode and AlAs TO mode, respectively. The peak at 290 cm^{-1} and shoulder at 355 cm^{-1} are interference fringes. The minima in the spectra lie at the positions of the structure's longitudinal optical phonon modes, which are sensitive to layer thickness. In Panel (a), the fitted solid line uses known phonon parameters for GaAs and AlAs, and the grower's nominal layer thickness $d_{AlAs} = d_{GaAs} = 10$ nm. The improved fit in Panel (b) uses the same phonon parameters, but allowed each layer thickness to vary for the best result. The numbers reported by Sudharsanan et al. gave $d_{AlAs} = (7.5 \pm 0.2)$ nm and $d_{GaAs} = (8.2 \pm 0.2)$ nm, in agreement with the x-ray results $d_{AlAs} = (8.3 \pm 0.8)$ nm and $d_{GaAs} = (8.3 \pm 0.8)$ nm. (See Sec. 3.5, Applications Refs., Sudharsanan, Perkowitz, Lou, Drummond, and Doyle (1988), fig. 1, p. 658.)

Applications

P. M. Amirtharaj, G. Holah, and S. Perkowitz, Far infrared spectroscopic study of $In_{1-x}Ga_xAs_yP_{1-y}$, Phys. Rev. B **21**, 5656–5661 (1980).

G. J. Brown and W. C. Mitchel, Mid-infrared spectral response of semi-insulating GaAs, in Impurities, Defects and Diffusion in Semiconductors: Bulk and Layered Structures, Materials Research Society Symposia Proceedings Vol. 163, D. J. Wolford, J. Bernholc, and E. E. Haller, eds., Materials Research Society, Pittsburgh, Pennsylvania (1989) pp. 157–162.

J. P. Fillard, M. Castagne, J. Bonnafe, and J. Gall, Scattering and absorption of infrared light on EL2 clusters in GaAs semi-insulating materials, in Materials Characterization, Materials Research Society Symposia Proceedings Vol. 69, N. Cheung and M.-A. Nicolet, eds., Materials Research Society, Pittsburgh, Pennsylvania (1986) pp. 231–236.

D. K. Gaskill, J. Davis, R. S. Sillmon, and M. N. Sydor, Nondestructive characterization of carrier concentration and thickness uniformity for semiconductors using infrared reflectance spectroscopy, in Modern Optical Characterization Techniques for Semiconductors and Semiconductor Devices, Proceedings SPIE Vol. 794, O. H. Glembocki, F. H. Pollak, and J. J. Soong, eds., SPIE, Bellingham, Washington (1987) pp. 231–241.

J. Geist, Infrared absorption cross section of arsenic in silicon in the impurity band region of concentration, Appl. Optics **28**, 1193–1199 (1988).

C. E. Jones, T. N. Casselman, J. P. Faurie, S. Perkowitz, and J. Schulman, Infrared properties and bandgaps of HgTe/CdTe superlattices, Appl. Phys. Lett. **47**, 140–142 (1985).

C. E. Jones, M. E. Boyd, W. H. Konkel, S. Perkowitz, and R. Braunstein, Noncontact electrical characterization of epitaxial HgCdTe, J. Vac. Sci. Technol. **A4**, 2056–2060 (1986).

K. Krishnan, Precise and Rapid Measurement of Interstitial Oxygen Concentration in Silicon, Bio-Rad Semiconductor Notes No. 102, Bio-Rad Semiconductor Measurement Systems, 237 Putnam Ave., Cambridge, MA 02139, April 1983.

K. Krishnan, A study of the spatial distribution of the oxygen content in silicon wafers using an infrared transmission microscope, Bio-Rad Semiconductor Notes No. 105, Bio-Rad Semiconductor Measurement Systems, 237 Putnam Ave., Cambridge, MA 02139, January 1985.

K. Krishnan and R. B. Mundhe, Characterization of semiconducting silicon using FT-IR spectroscopy, in Spectroscopic Characterization Techniques for Semiconductor Technology, Proceedings SPIE Vol. 452, F. H. Pollak and R. S. Bauer, eds., SPIE, Bellingham, Washington (1983) pp. 71–78.

K. Krishnan, P. J. Stout, and M. Watanabe, Characterization of semiconductor silicon using Fourier transform infrared spectrometry, in Practical Fourier Transform Infrared Spectroscopy, J. R. Ferraro and K. Krishnan, eds., Academic Press, San Diego (1990) pp. 285-349.

B. Lou, S. Perkowitz, and R. Sudharsanan, Anisotropy and infrared response of the AlAs-GaAs superlattice, Phys. Rev. B **38**, 2212–2214 (1988). [Erratum: Phys. Rev. B **39**, 1387 (1989)]

E. Merk, J. Heyman, and E. E. Haller, Infrared absorption study of zinc-doped silicon, in Impurities, Defects and Diffusion in Semiconductors: Bulk and Layered Structures, Volume 163, Materials Research Society Symposia Proceedings, D. J. Wolford, J. Bernholc, and E. E. Haller, eds., Materials Research Society, Pittsburgh, Pennsylvania (1989) pp. 15–20.

W. J. Moore, Infrared transmission characterization of p-type gallium arsenide, in Optical Characterization Techniques for Semiconductor Technology, Proceedings SPIE Vol. 276, D. E. Aspnes, S. So, and R. F. Potter, eds., SPIE, Bellingham, Washington (1981) pp. 101–103.

R. C. Newman, Localized vibrational mode spectroscopy of impurities in semiconductor crystals, in Growth and Characterization of Semiconductors, R.A. Stradling and P.C. Klipstein, eds., Adam Hilger, Bristol (1990) pp. 105-118.

S. Perkowitz and J. Breecher, Characterization of GaAs by far infrared reflectivity, Infrared Phys. **13**, 321–326 (1973).

S. Perkowitz, Far infrared characterization of $Hg_xCd_{1-x}Te$ and related electronic materials, J. Electronic Materials **14**, 551–562 (1985).

S. Perkowitz, D. Rajavel, I. K. Sou, J. Reno, J. P. Faurie, C. E. Jones, T. Casselman, K. A. Harris, J. W. Cook, and J. F. Schetzina, Far infrared study of alloying in HgTe-CdTe superlattices, Appl. Phys. Lett. **49**, 806–809 (1986).

S. Perkowitz, Far infrared spectroscopy of $Hg_xCd_{1-x}Te$ and related materials, in Far-Infrared Science and Technology, Proceedings SPIE Vol. 666, J. R. Izatt, ed., SPIE, Bellingham, Washington (1986) pp. 120–125.

S. Perkowitz, R. Sudharsanan, and S. S. Yom, Far infrared analysis of alloy structure in HgTe-CdTe superlattices, J. Vac. Sci. Technol. **A5**, 3157–3160 (1987).

S. Perkowitz, R. Sudharsanan, S. S. Yom, and T. J. Drummond, AlAs phonon parameters and heterostructure characterization, Solid State Commun. **62**, 645–647 (1987).

B. Senitzky and S. P. Weeks, Infrared reflectance spectra of thin-epitaxial silicon layers, in Optical Characterization Techniques for Semiconductor Technology, Proceedings SPIE Vol. 276, D. E. Aspnes, S. So, and R. F. Potter, eds., SPIE, Bellingham, Washington (1981) pp. 222–226.

R. Sudharsanan, S. Perkowitz, S. S. Yom, and T. J. Drummond, Far infrared reflectance spectroscopy of AlAs-GaAs microstructures, in Modern Optical Characterization Techniques for Semiconductors and Semiconductor Devices, Proceedings SPIE Vol. 794, O. H. Glembocki, F. H. Pollak, and J. J. Soong, eds., SPIE, Bellingham, Washington (1987) pp. 197–201.

R. Sudharsanan, S. Perkowitz, B. Lou, T. J. Drummond, and B. L. Doyle, Far-infrared characterization of AlAs-GaAs superlattice structure, Superlattices and Microstructures **4**, 657–660 (1988).

L. E. Taroff, C. J. Miner, and A. J. Springthorpe, Epitaxial layer thickness measurements by reflection spectroscopy, J. Electronic Materials **18**, 361–367 (1989).

W. M. Theis, C. W. Litton, and K. K. Bajaj, Infrared localized mode spectroscopy of carbon-implanted GaAs, in Optical Characterization Techniques for Semiconductor Technology, Proceedings SPIE Vol. 276, D. E. Aspnes, S. So, and R. F. Potter, ed., SPIE, Bellingham, Washington (1981) pp. 109–112.

J. Vindevoghel, M. Vindevoghel, and Y. Leroy, Millimetric and far infrared conductivity for p-Si. Evidence for interband transitions, Infrared Phys. **18**, 99–105 (1978).

J. M. Zavada, H. A. Jenkinson, and T. J. Gavanis, Optical properties of proton implanted n-type GaAs, in Optical Characterization Techniques for Semiconductor Technology, Proceedings SPIE Vol. 276, D. E. Aspnes, S. So, and R. F. Potter, eds., SPIE, Bellingham, Washington (1981) pp. 104–108.

4. Optical Microscopy

4.1 Introduction

In applications where the dimensions of interest are below the optical diffraction limit (~0.8 μm), electron microscopy is used by necessity. However, traditional optical methods remain useful for a large number of applications such as examining topological features larger than ~1.0 μm, examining defects, or counting etchpits. Several specialized forms of optical microscopy are highly valuable: Nomarski, scanning laser, and microspectrophotometry. In Nomarski microscopy, interference methods are used to increase the contrast between small differences in the surface level of a semiconductor wafer. Scanning microscopy in both the visible and infrared spectral ranges allows two-dimensional imaging of features in a layer or structure. Finally, microspectrophotometry allows film thickness determination from spectral analysis of reflected light.

Scanning microscopy is also used in both the visible and the infrared spectral ranges to form two-dimensional images of inhomogeneities in a semiconductor. The form called confocal microscopy produces three-dimensional images [1]. One visible light-scanning technique of special interest is the optical-beam-induced current method (abbreviated OBIC, or sometimes LBIC, for laser-beam-induced current), which detects grain boundaries, dislocations, and other defects in semiconductors and semiconductor devices. OBIC images represent spatial distributions of electrically active defects that include inclusions, strain, damage, precipitates, stacking faults, twin boundaries, dislocation clusters, and bandgap and doping variations. In this technique, a focused laser beam is scanned across the surface of the sample, and the induced current between two remote contacts on the sample is measured as a function of the laser beam position. The induced current is a result of the charge-separation effect of the regions in the vicinity of the light. Light incident on the area of the sample which is homogeneous and defect-free does not generate any induced current. Infrared scanning has been used to study individual precipitate particles in Si ingots, and to examine GaAs and other materials.

Table 4. Infrared sensitivity. Given are sensitivities for the measurement of interstitial oxygen [O_i], substitutional carbon [C_s], and nitrogen [Si-N-Si], in crystalline Si and substitutional carbon [C_{Ga}] and interstitial oxygen [O_i] in crystalline GaAs. Also given are sensitivities for measurement of compositions, x, of $Al_xGa_{1-x}As$ and $Hg_xCd_{1-x}Te$ and for carrier concentrations, N_d, in Si and GaAs. The sensitivity of far infrared low-temperature absorption measurements for substitutional boron [B_s]; phosphorus [P_s]; and arsenic [As_s] are also given. The notations used for the measured quantity column are absorption coefficients, α, at subscripted wavelength in cm^{-1}, e.g., α_{1107}; absorption coefficient full width product, $\alpha\Delta$, at subscripted wavelength, e.g., $\alpha\Delta_{845}$; LO phonon frequency, ω_{LO}; plasma resonance frequency, ω_P; transmission, T; and frequency, ω

Method	Matrix	Quantity	Measured quantity	Conversion	Sensitivity[a]	Ref. (see below)
LVM	Si	$[O_i]$	α_{1107} @300 K	$[O_i]=\alpha\times3.03\pm0.02\times10^{17}\ cm^{-2}$	$\pm2\times10^{15}\ cm^{-3}$	1
LVM	Si	$[O_i]$	α_{1107} @300 K	$[O_i]=\alpha\times3.14\times10^{17}\ cm^{-2}$	$\pm2\times10^{15}\ cm^{-3}$	2
LVM	Si	$[C_s]$	α_{605} @300 K	$[C_s]=\alpha\times1.1\times10^{17}\ cm^{-2}$	$\pm2\times10^{16}\ cm^{-3}$	3
Absorption	Si	[Si-N-Si]	α_{963} @300 K	$[N_s]=\alpha\times1.3\times10^{17}\ cm^{-2}$	$\pm2\times10^{15}\ cm^{-3}$	4
LVM	GaAs	$[C_{Ga}]$	$\alpha\Delta_{583}$ @77 K	$[C_s]=\alpha\Delta\times1.1\times10^{16}\ cm^{-1}$ $[C_s]=\alpha\Delta\times8\pm2\times10^{15}\ cm^{-1}$	$\pm2\times10^{14}\ cm^{-3}$	5 6
LVM	GaAs	$[O_i]$	$\alpha\Delta_{845}$ @10 K	$[C_s]=\alpha\Delta\times8\times10^{16}\ cm^{-1}$	$\pm2\times10^{15}\ cm^{-3}$	7
Phonon frequency	$Al_xGa_{1-x}As$	x	ω_{LO} or ω_{TO} @300 K	$(\omega_{LO}/2\pi c)/cm^{-1}=$ $292.4+70.8x-26.8x^2-41.13x^3$		8
IR cut off	$Hg_xCd_{1-x}Te$	x	T vs ω	Ref. 9		9
IR plasma frequency	Si	N_d	ω_p @300 K	$\omega_p^2=4\pi N_e e^2/\epsilon m^*$		10
IR plasma frequency	GaAs	N_d	ω_p @300 K	$\omega_p^2=4\pi N_e e^2/\epsilon m^*$		11
Absorption	Si	$[B_s]$	$\alpha\Delta_{320}$ @12 K	$[B_s]=\alpha\times1.1\times10^{17}\ cm^{-2}$	$\pm1.5\times10^{12}\ cm^{-3}$	12
Absorption	Si	$[P_s]$	$\alpha\Delta_{316}$ @12 K	$[P_s]=\alpha\times1.1\times10^{17}\ cm^{-2}$	$\pm1.5\times10^{12}\ cm^{-3}$	12
Absorption	Si	$[As_s]$	$\alpha\Delta_{382}$ @12 K	$[As_s]=\alpha\times1.1\times10^{17}\ cm^{-2}$	$\pm1.5\times10^{12}\ cm^{-3}$	12

[a] Calculated as the concentration-equivalent-of-noise assuming ±0.1 % noise in transmission.

References

[1] T. Iizuka, S. Takasu, M. Tajima, T. Arai, T. Nozaki, N. Inoue, and M. Watanabe, J. Electrochem. Soc. **132**, 1707 (1985).
[2] A. Baghdadi, W. M. Bullis, M. C. Croarkin, Yue-Zhen Li, R. I. Scace, R. W. Series, P. Stallhofer, and M. Watanabe, J. Electrochem. Soc. **136**, 2015 (1989); ASTM Standard F1188, Annual Book of ASTM Standards, **10.05** (ASTM, Philadelphia, PA (1991).
[3] R. C. Newman and J. B. Willis, J. Phys. Chem. Solids **26**, 373 (1965).
[4] H. J. Stein, Appl. Phys. Lett. **47**, 1339 (1985); Y. Itoh, T. Nozaki, T. Masui and T. Abe, Appl. Phys. Lett. **47**, 488 (1985).
[5] A. T. Hunter, H. Kimura, J. P. Baukus, H. V. Winston, and O. J. Marsh, Appl. Phys. Lett. **44**, 74 (1984)
[6] M. R. Brozel, E. J. Foulkes, R. W. Series, and D. T. J. Hurle, Appl. Phys. Lett. **49**, 337 (1986).
[7] M. Skowronski, S. T. Neild, and R. E. Kremer, Appl. Phys. Lett. **58**, 1545 (1991).
[8] O. K. Kim and W. G. Spitzer, J. Appl. Phys. **50**, 4362 (1979); S. Adachi, J. Appl. Phys. **58**, R1 (1985).
[9] E. Finkman and Y. Nemirovsky, J. Appl. Phys. **50**, 4356 (1979).
[10] W. G. Spitzer and H. Y. Fan, Phys. Rev. **106**, 882 (1957).
[11] J. K. Kung and W. G. Spitzer, J. Electrochem. Soc. **121**, 1482 (1971).
[12] S. C. Baber, Thin Solid Films **72**, 201 (1980).

4.2 Physical Basis

4.2.1 Nomarski Microscopy In Nomarski microscopy, two microscopic images of a surface are formed so that they are slightly displaced in space and of opposite phase. Interference bands appear where the images overlap. The physical displacement and the interference bands heighten the visibility of small variations in surface levels.

4.2.2 Scanning Microscopy In scanning microscopy, a spot of light, whose size is limited by diffraction, is scanned over a specimen. The image of the specimen is developed point by point in sequential fashion, to be displayed or stored for analysis. If the specimen is broadly illuminated and scanned in a raster pattern by a point detector (or raster scanned by a point source, with the light sensed by a broad area detector), a two-dimensional image results. In the variation known as confocal scanning, the specimen is illuminated in only a small region at any one time, and a point detector senses light only from that same region. This makes it possible to develop a three-dimensional image. Confocal scanning also enhances resolution.

The light can be sensed by any of several conventional detectors. In the OBIC method, however, the detector is an external circuit that measures the current produced locally by the incident light. Light intensity from a laser of even modest power creates a high density of carriers in the sample, due to electron-hole excitation. The electrons and holes are affected by the electric fields associated with macroscopic defects, such as grain boundaries in polycrystalline silicon, so that the motion of the electrons and holes induces a current which is sensed by an external circuit. Hence, OBIC images clearly show the presence of defects, and map out their locations.

4.2.3 Microspectrophotometry Reflection spectrophotometry depends on the interference pattern caused by reflections from top and bottom surfaces of a transparent film. The equations governing reflection from stratified dielectric media are derived in most optics texts [2]. Microspectrophotometry is normally used for determining the film thickness of a single layer on a substrate or the film thicknesses in a relatively simple multilayer stack. As in ellipsometry, values of the functions $n(\omega)$ and $k(\omega)$ for each of the layers of interest are needed to determine the thicknesses. The advantages of reflectometry relative to ellipsometry are that most of the information is carried in the wavelength dependences, and it is relatively simple to focus the beam down to spot sizes on the order of micrometers [3].

4.3 Experimental and Technical Details

4.3.1 Nomarski microscopy In Nomarski microscopy, two microscopic images of a surface are formed by a Wollaston prism. The prism is placed between the eyepiece and the objective of the microscope, as shown in Fig. 8.

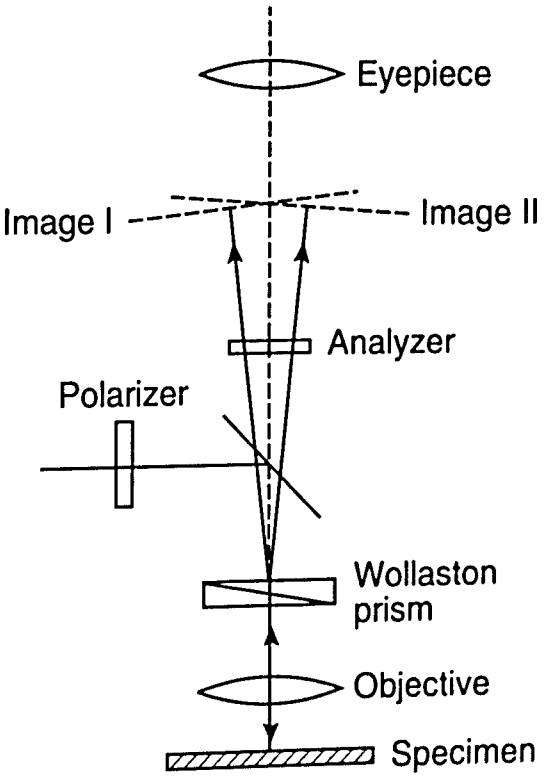

Fig. 8. Schematic diagram of a Nomarski interference microscope. The Wollaston prism consists of identical prisms of crystalline quartz, one with its optical axis parallel to the plane of the paper and the specimen surface, the other perpendicular to the plane of the paper. (See Sec. 4.5, General Refs., Modin and Modin (1973), fig. 3.17, p. 130.)

Light traversing the prism is divided into two beams polarized at right angles to each other and diverging by some angle, giving two microscopic images. The microscope includes a polarizer set so that the incident light lies at 45° to the plane of vibration of the prism. With an analyzer set at right angles to the polarizer, this gives two images of the same intensity but 180° apart in phase. Hence, interference bands form where the images overlap. These fringes, combined with the displacement of the images, magnify surface variations. The edges of surface features become clearly visible, and the thickness of films deposited on the surface can be found.

4.3.2 Scanning Microscopy Figure 9 shows the main components of a scanning microscope. It includes a light source, usually a laser; a scanning system, which either moves the laser beam across a fixed sample or moves the sample relative to a fixed optical system; optical elements to focus and manipulate the beam; and a detector. The type of detector used depends on the scanning and imaging methods and on the wavelengths; it may be a single photomultiplier tube or a detector array. In the OBIC method, it is an external circuit that measures the photocurrent.

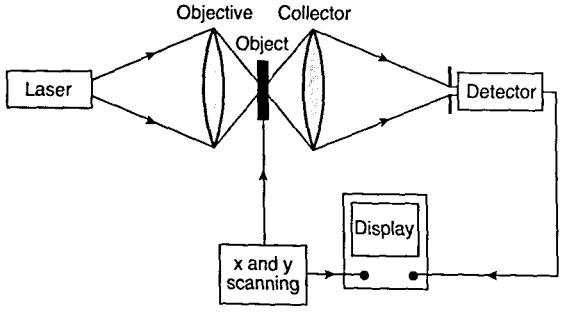

Fig. 9. Schematic diagram showing the main elements of a scanning microscope. (See Sec. 4.5, General Refs., Wilson and Sheppard (1984), fig. 1.1, p. 2.)

As stated above, in some systems, the light beam is scanned across a fixed sample. This allows rapid acquisition and display of images; however, there are complications in designing the movable optical system, and in maintaining good image quality. In other designs, the light beam is fixed and the sample is moved to produce the raster pattern. Although these systems are relatively slow, the optical design is simple and produces images of high quality.

The OBIC technique (a typical experimental arrangement is illustrated in Fig. 10) is one of the most important for semiconductor materials and devices, and can readily be implemented with small lasers as sources. A 1 mW HeNe laser produces 3×10^{15} photons per second. Based on a calculation using typical parameters for electron-hole generation in a semiconductor, this intensity is enough to generate a large density of electron-hole pairs, about 10^{20} cm^{-3}. The electric fields associated with defects or doped regions separate the electron and hole in each pair. These separated carriers can induce a current by flowing through an appropriate external circuit. (Depending on whether the sample includes a p-n junction or not and on the nature of the circuit, either photovoltages or photocurrents can be measured.)

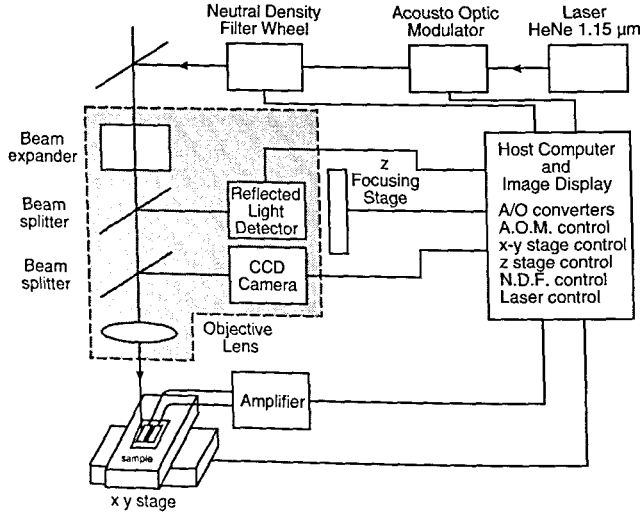

Fig. 10. Schematic diagram of an optical-beam-induced current (OBIC) system, also called LBIC (laser-beam-induced current). (See Sec. 4.5, General Refs., Moore, Hennessy, Bajaj, and Tennant (1988), fig. 1.)

Scanning methods can be used equally well in the visible and in the infrared regions. In one typical infrared system, the source is a semiconductor laser operating at 1.3 μm wavelength (giving a spot diameter of about 2 μm), with detection accomplished by germanium photodiodes. The sample is mechanically moved to produce raster scanning, and the resulting images are taken at resolutions of 512 pixels by 512 pixels.

4.3.3 Microspectrophotometry Interference of light waves reflected from each interface of a multilayer film structure determines the reflectance of the structure. The reflectance spectrum depends on angle of incidence of the radiation, the refractive indices of the media, polarization of the radiation, and film thicknesses [4]. Whereas the same equations describing reflection and transmission apply in both ellipsometry and reflectance spectrophotometry, the problem is somewhat simplified in the case of reflectometry, where polarization is usually ignored. Normally, the reflected light intensity is recorded versus wavelength. Then, the thicknesses are calculated by fitting measured spectra to calculated spectra based on a model of the layer structure and known dielectric constants. Measurements can also be made of the reflectance versus polarization angle or versus angle of incidence, but this is not normally done in microscopic measurements because these parameters are difficult to change systematically within the microscope environment. The most frequent application of microspectrophotometry is the determination of thicknesses of simple dielectric stacks on a substrate; but microspectrophotometry can also be used like ellipsometry to find the dielectric function of film layers and, hence, film layer composition [4]. Because of the relaxed constraint on the angle of incidence and the relative speed of processing data, microspectrophotometry is an ideal way to map the uniformity of wafer film thickness.

4.4 Illustrative Applications

Figure 11 shows the power of OBIC imaging to detect flaws in semiconductor materials such as silicon, even when the material is incorporated in an operating device such as a transistor. Figure 12 shows an infrared scanning system micrograph of oxide particles embedded in Czochralski-grown silicon, even displaying those particles smaller than the infrared beam diameter of 2 μm. By focusing to different depths in the sample, it is possible to obtain some depth-dependent information as well.

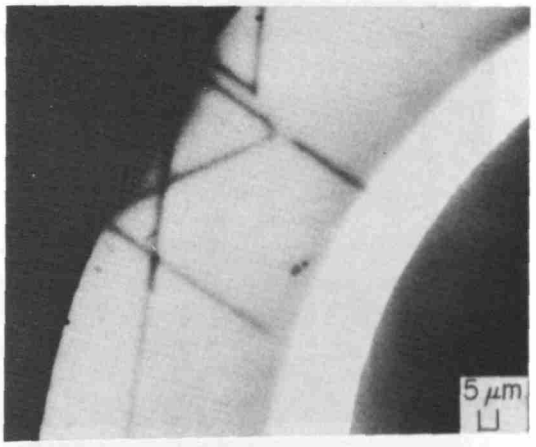

Fig. 11. An OBIC image formed by monitoring the emitter-base current in a silicon transistor while a laser beam is scanned across the transistor. The dark straight lines are lines of dislocations in the silicon. (See Sec. 4.5, General Refs., Wilson and Sheppard (1984), fig. 1.6, p. 8.)

4.5 References

[1] G. Q. Ziao, T. R. Corle, and G. S. Kino, Real-time confocal scanning optical microscope, Appl. Phys. Lett. **53**, 716 (1988).

[2] M. Born and E. Wolf, Principles of Optics, Pergamon Press, New York (1975) p. 61.

[3] P. Burggraf, How thick are your thin films?, Semiconductor International (1988) p. 96.

[4] S. E. Stokowski, Measuring refractive indices of films on semiconductors by microreflectometry, in Integrated Circuit Metrology, Inspection, and Process Control IV, Proceedings SPIE, W. H. Arnold, ed., SPIE, Bellingham, Washington (1990) p. 253.

General

Microscopy of Semiconducting Materials, Institute of Physics Conference Proc. 60, A. G. Cullis and D. C. Joy, eds., Institute of Physics, Adam Hilger, Bristol (1981).

Microscopy of Semiconducting Materials, Institute of Physics Conference Proc. 67, A. G. Cullis, S. M. Davison, and G. R. Booker, eds., Institute of Physics, Adam Hilger, Bristol (1983).

Microscopy of Semiconducting Materials, Institute of Physics Conference Proc. 76, A. G. Cullis and D. B. Holt, eds., Adam Hilger, Bristol (1985).

Microscopy of Semiconducting Materials, Institute of Physics Conference Proc. 87, A. G. Cullis and P. D. Augustus, eds., Institute of Physics, Adam Hilger, Bristol (1987).

Microscopy of Semiconducting Materials, Institute of Physics Conference Proc. 100, A. G. Cullis and J. L. Hutchinson, eds., Institute of Physics, Adam Hilger, Bristol (1989).

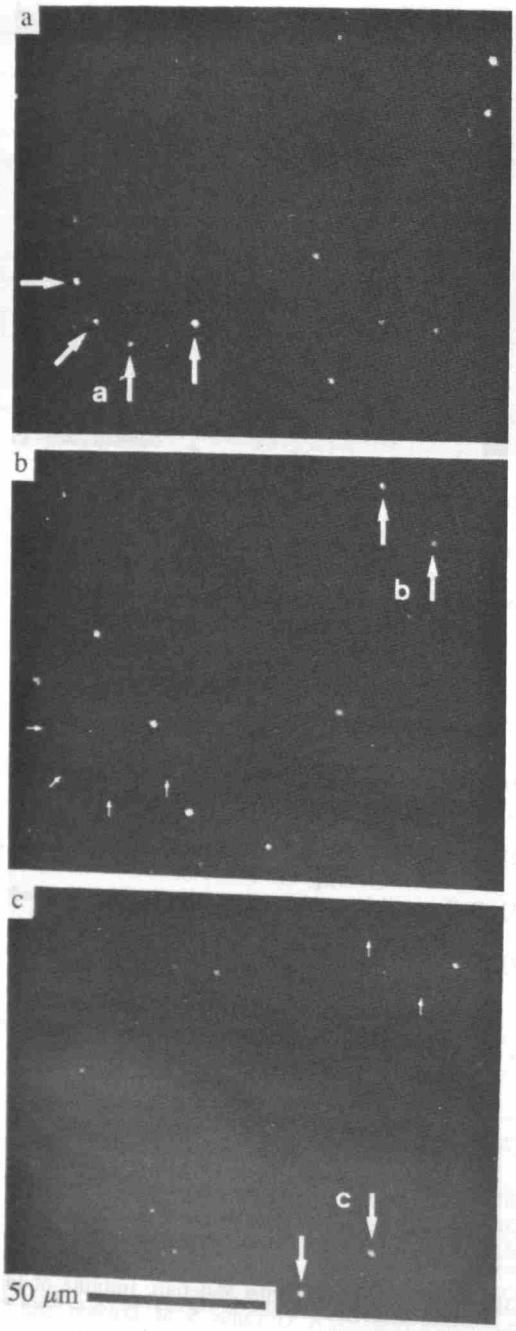

Fig. 12. Infrared scanning microscope images of oxide particles in heat-treated (100) Czochralski silicon. The microscope used a semiconductor laser emitting at 1.3 μm, to give a spot size of ~2 μm. Particles of this size or greater are directly imaged. Smaller particles can still be seen, although as spots 2 μm across, because the system can detect intensity variations of about 0.5 %. The depth of focus is 30 μm. Panels (b) and (c) show successively deeper probes into the sample, relative to Panel (a). The focal plane is 60 μm deeper in Panel (b) and 120 μm deeper in Panel (c). The sets of oxide images marked "a," "b," and "c" can be followed in and out of focus through the panels. (See Sec. 4.5, Applications Refs., Laczik, Booker, Falster, and Shaw (1989), fig. 1, p. 808.)

Microscopy of Semiconducting Materials, Institute of Physics Conference Proc. 117, A. G. Cullis and N. J. Long, eds., Institute of Physics, Bristol (1991).

S. Hildebrandt and W. Hergert, Unified theoretical description of the CL, EBIC, PL, and EBIC contrast profile area of an individual surface-parallel dislocation. Phys. Stat. Sol (a) **119**, 689–699 (1990).

R. Keeler, Confocal microscopes, R&D Magazine (April 1991) pp. 40–42.

H. Modin and S. Modin, Metallurgical Microscopy, John Wiley, New York (1973).

T. Wilson and C. Sheppard, Theory and Practice of Scanning Optical Microscopy, Academic Press, London (1984).

Applications

J. Bajaj, L. O. Bubulac, P. R. Newman, and W. Tennant, Spatial characterization of semiconductors using laser beam induced current (LBIC), in Modern Optical Characterization Techniques for Semiconductors and Semiconductor Devices, Proceedings SPIE Vol. 794, O. J. Glembocki, F. H. Pollak, and J. J. Song, eds., SPIE, Bellingham, Washington (1987) pp. 136–141.

J. Bajaj, W. E. Tennant, and P. R. Newman, Laser beam induced current imaging of surface nonuniformity at the HgCdTe/ZnS interface. J. Vac. Sci. Technol. A **6**, 2757 (1988).

S. Haq, G. Hobson, K. E. Singer, W. S. Truscott, and J. O. Williams, A transmission electron microscopy investigation of $GaAs_{1-y}Sb_y$-GaAs superlattices grown by molecular beam epitaxy, in Microscopy of Semiconducting Materials, Institute of Physics Conference Proc. 100, A. G. Cullis and J. L. Hutchinson, eds., Adam Hilger, Bristol (1989) pp. 337–341.

P. Kidd, G. R. Booker, and D. J. Stirland, 3-D distribution of inhomogeneities in LEC GaAs using infra-red laser scanning microscopy, in Microscopy of Semiconducting Materials, Institute of Physics Conference Proc. 87, A. G. Cullis and P. D. Augustus, eds., Adam Hilger, Bristol (1987) pp. 275–280.

Z. Laczik, G. R. Booker, R. Falster, and N. Shaw, Investigation of precipitate particles in Si and CdTe ingot material using the scanning infrared-red microscope (SIRM), in Microscopy of Semiconducting Materials, Institute of Physics Conference Proc. 100, A. G. Cullis and J. L. Hutchinson, eds., Adam Hilger, Bristol (1989) pp. 807–812.

Y-C., Lu, R. K. Route, D. Elwell, and R. S. Feigelson, Etch pit studies in CdTe crystals. J. Vac. Sci. Technol. A **3**, 264 (1985).

J. L. Mariani, B. Pichaud, F. Minari, and S. Martinuzzi, Direct determination of the recombination activity of dislocations in FZ silicon by LBIC measurements, in Microscopy of Semiconducting Materials, Institute of Physics Conference Proc. 100, A. G. Cullis and J. L. Hutchinson, eds., Adam Hilger, Bristol (1989) pp. 801–806.

C. J. L. Moore, J. Hennessy, J. Bajaj, and W. E. Tennant, Finding faults in focal plane arrays, Photonics Spectra (September 1988) pp. 161–166.

M. Ogura, M. Tajima, and Y. Tokumaru, Scanning optical fiber microscope for high resolution laser beam induced current images of semiconductor materials, in Materials Characterization, Materials Research Society Symposia Proceedings Vol. 69, N. Cheung and M.-A. Nicolet, eds., Materials Research Society, Pittsburgh, Pennsylvania (1986) pp. 251-256.

D. J. Stirland, P. Kidd, G. R. Booker, S. Clark, D. T. J. Hurle, M. R. Brozel, and I. Grant, The behaviour of arsenic-rich defects in quenched semi-insulating GaAs, in Microscopy of Semiconducting Materials, Institute of Physics Conference Proc. 100, A. G. Cullis and J. L. Hutchinson, eds., Adam Hilger, Bristol (1989) pp. 373-378.

5. Modulation Spectroscopy

5.1 Introduction

Modulation spectroscopy is a sensitive technique which can determine fine details of interband transitions in semiconductors. In semiconductor superlattices and other microstructures, detailed knowledge of the complex interband transitions can be used to characterize quantum well widths, potential barrier heights and widths, electric fields, and the amount of strain in strain layer systems.

5.2 Physical Basis

The principle behind modulation spectroscopy is that a periodic physical perturbation applied to a sample elicits the derivative of the sample's optical response to that perturbation. The derivative feature amplifies weak features in the response function and suppresses large constant background levels. This gives modulation methods very high sensitivity to small spectral features that are invisible in conventional spectroscopy.

To illustrate the origin of the derivative response, consider the reflectivity R of a sample. This depends on the sample's dielectric function, which depends on many physical properties. For example, the dielectric function depends on an applied electric field E; hence, R also depends on E. If the applied electric field has a dc component E_0 and a small ac component $E_1 \cos\Omega t$ (Ω is the modulation angular frequency), the reflectivity can be written as $R(E)=R(E_0+E_1\cos\Omega t)$. If $E_1 << E_0$, this expression can be expanded in a Taylor series, where only the first two terms are kept; that is

$$R(E)\cong R(E_0)+\frac{dR}{dE}(E_1\cos\Omega t)\,. \qquad (12)$$

The first term depends on E_0 but not on time, whereas the second term is a periodic function of time at the modulation frequency Ω. Hence, the ac portion of the reflectance at frequency Ω can be detected with a lock-in amplifier; this signal is proportional to the derivative dR/dE. Thus, small structures in the optical spectrum of $R(E)$ are enhanced, even with the sample at room temperature. A periodic perturbation can be applied to any physical property affecting the sample's optical response. Examples are electroreflectance, where a periodic electric field is applied to a sample while its reflectance spectrum is measured; and photoreflectance, where optically injected carriers from a chopped laser beam modulate the "built-in" surface or internal electric fields, thereby modulating the reflectance of the sample. Other forms of modulation spectroscopy have been reviewed by Aspnes [1]. The following discussion concentrates on electroreflectance and photoreflectance, two forms of modulation spectroscopy currently in common usage. Because photoreflectance results from the modulation of "built-in" electric fields, this discussion applies generally to either electroreflectance or photoreflectance.

The enhancement of spectroscopic structures that appear at energies corresponding to energy gaps and other critical points in the joint density of states of the material under study is one useful result of modulation methods. The method becomes more useful still when the measured spectral line shapes can be connected to microscopic parameters through theory. The relationship that makes this connection is [2]

$$\frac{\Delta R}{R}=\alpha\Delta\epsilon_1+\beta\Delta\epsilon_2, \qquad (13)$$

where ΔR is the change in reflectivity due to the applied modulation, $\Delta\epsilon_1$ and $\Delta\epsilon_2$ are the changes in the real and imaginary parts, respectively, of the complex dielectric function $\epsilon=\epsilon_1+i\epsilon_2$, and α and β are called the Seraphin coefficients. Near the energy gap of a bulk sample, $\beta=0$; however, for complex microstructures where interference effects occur, both α and β need to be considered, and hence $\Delta\epsilon_1$ and $\Delta\epsilon_2$ must both be known. These can be calculated from general band theory and from dielectric function theory. In the case of electroreflectance and photoreflectance, different spectral line shapes are obtained, and concomittantly different analyses are required, depending on the magnitude of the electric field. The modulation field is usually described in terms of three regimes [2]: high field (Stark effect), intermediate field (Franz-Keldysh effect), or low field. The high field case is

not usually studied under modulation conditions, as a high electric field breaks down the normal selection rules and results in a Stark shift of the band structure. The analysis of spectra based on intermediate and low field theories is discussed in reference to representative spectra, in the illustrative applications section below.

5.3 Experimental and Technical Details

A modulation measurement requires a light source, a monochromator, and a detector as in conventional spectroscopy, and a means to apply the modulation to the sample. These elements are shown in Fig. 13. The source can be an incandescent or discharge lamp. Generally, a monochromator of 0.25 m focal length provides adequate energy resolution, but higher resolution may be needed in some cases.

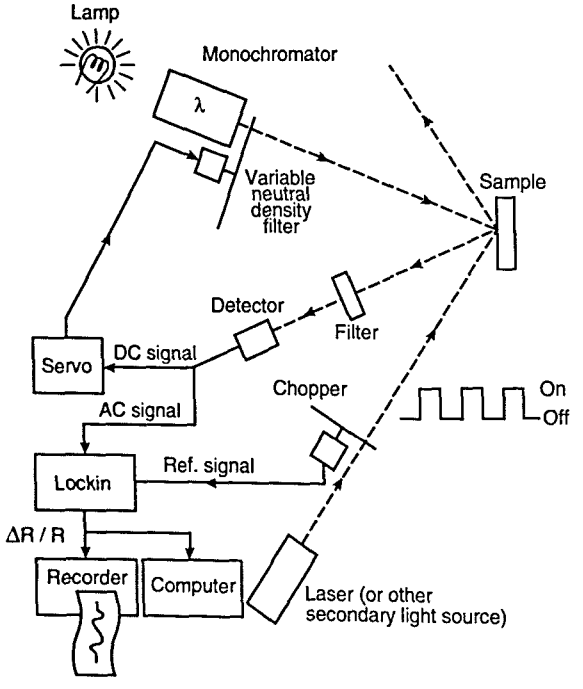

Fig. 13. Diagram of a photoreflectance spectrometer, illustrating lamp with following optics and electronics to obtain the spectrum, and a laser to supply modulated light. The variable neutral density filter holds the constant part of the detected signal independent of wavelength, facilitating evaluation of the ratio of $\Delta R/R$. (See Sec. 5.5, General Refs., Pollak and Glembocki (1988), fig. 4, p. 25.)

The light reflected from the sample is detected by a photomultiplier tube or a photodiode. It contains a steady (dc) component RI_0 (I_0 is the incident light intensity) and a periodically modulated (ac) component ΔRI_0. To obtain $\Delta R/R$, the dc signal and the ac signal must be separately measured and then a ratio of these signals is taken. It is also possible to electronically hold the dc signal (corresponding to RI_0) constant during the measurement. This can be done by a feedback loop that changes the gain of the detector to keep its dc output constant, or, as shown in Fig. 13, by mounting a circular continuously variable neutral density filter on a servo motor and inserting it before the sample.

For photoreflectance, light from a modulated optical source such as a laser, whose photon energy exceeds the sample's energy gap, impinges on the sample. For electroreflectance of a doped semiconductor, the varying electric field can be applied between an ohmic contact on the sample's back surface, and a transparent gate electrode on the front of the sample; 5 nm to 10 nm of deposited gold or aluminum is an adequate electrode. A second method is to put the sample in an electrolyte such as a KCl solution, or an acidic solution. The resulting electric field at the sample surface can be changed by varying a voltage applied between the sample and a platinum counter electrode. Photoreflectance and electroreflectance spectroscopy both provide highly detailed spectra even at room temperature, so that sample cooling is usually not needed.

5.4 Illustrative Applications

Figure 14a shows the sensitivity of modulation spectroscopy, by comparing the reflectivity spectrum of GaAs in the interband region to the much more detailed $\Delta R/R$ spectrum obtained by electroreflectance. Figure 14a is illustrative of the low field case. Here the spectra near the energy gap can be fitted using [3]

$$\frac{\Delta R}{R} = R[e^{i\theta}(\hbar\omega - E_g + i\Gamma)^{-m}], \qquad (14)$$

where $\hbar\omega$ is the photon energy, E_g is the gap energy, θ is the phase factor, Γ is the lifetime broadening parameter, and the quantity m takes on the values 2, 2.5, and, 3 for excitonic, three-dimensional, and two-dimensional critical points, respectively. Hence, the critical point type and energy can be determined from fitting this line shape. Aspnes [3] has also developed a "three-point" method for extracting critical point energies which for simple spectra eliminates the need for a full spectrum fit.

Shown in Fig. 14b [4] is the photoreflectance spectra of a moderately n-type doped

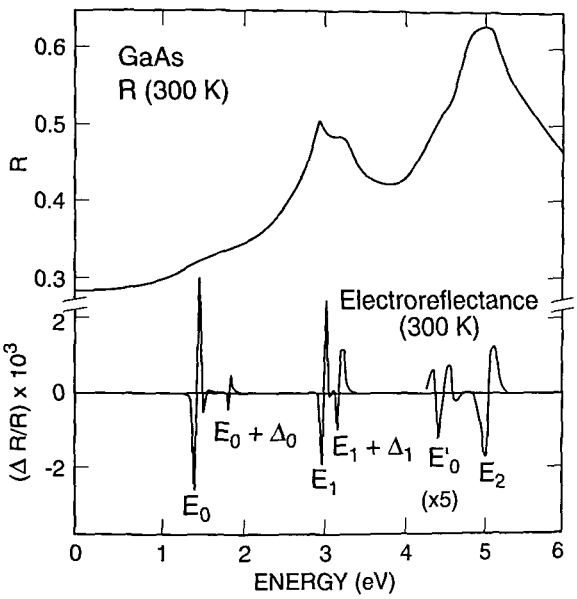

Fig. 14a. Conventional interband reflectivity spectrum for GaAs at 300 K, compared to the interband $\Delta R/R$ spectrum at 300 K obtained by electroreflectance. The broad features in the plot for reflectivity R, such as the shoulder at the gap energy E_0, become obvious sharp lines in the $\Delta R/R$ data which lie on a baseline of zero signal. Structure at $E_0 + \Delta_0$ which was invisible in the reflectivity spectrum is apparent in the $\Delta R/R$ curve. (See Sec. 5.5, General Refs., Pollack and Glembocki (1988), fig. 1, p. 25.)

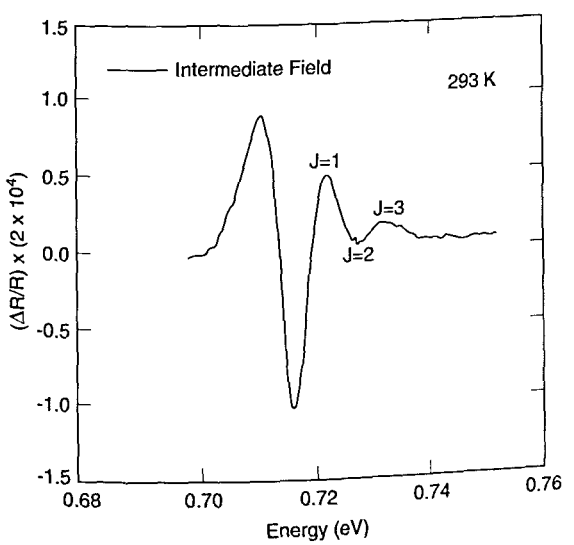

Fig. 14b. Photoreflectance spectra for the intermediate field case for a moderately doped sample of InGaAs/InP with labeled extrema ($J = 1, 2, 3$).

($\sim 1 \times 10^{16}$ cm^3) sample of $In_{0.53}Ga_{0.47}As$ illustrating the intermediate field line shape. This case can be identified by the presence of oscillatory behavior, the so-called Franz-Keldysh oscillations at energies greater than the energy gap of the material. Modulation intensities are usually greater for the high field case than for the low field case. Materials information (electric fields and energy gap values) is typically extracted from Franz-Keldysh oscillations using the Aspnes asymptotic approximation [5]

$$\frac{\Delta R}{R} = (\hbar\omega - E_g)^{-1} \exp \frac{\Gamma(\hbar\omega - E_g)^{1/2}}{(\hbar\Omega)^{3/2}}$$

$$\times \cos\left[\theta + \frac{2}{3}\left(\frac{\hbar\omega - E_g}{\hbar\Omega}\right)^{3/2}\right], \qquad (15)$$

where θ, Γ, and E_g are defined above, and $\hbar\Omega$ is the electro-optic parameter $[e^2E^2\hbar^2/32\pi^2\mu]^{1/3}$. Here, e is the electron charge, E is the dc electric field, $\hbar$ is Planck's constant, and μ is the reduced interband effective mass. Since successive extrema represent a change of π in the argument of the cosine term in Eq. 15, the energy of the jth extrema [5] can be written as

$$j\pi = \theta + \frac{2}{3}\left[\frac{(\hbar\omega - E_g)_j}{\hbar\Omega}\right]^{3/2}. \qquad (16)$$

Hence, the phase factor and electro-optic energy can be obtained from the intercept and slope of a plot of $(\hbar\omega - E_g)_j^{3/2}$ vs j. It is noteworthy that the electric field in a structure under study can be extracted from the electro-optic energy, requiring only independent knowledge of the effective mass of the material. Hence, electroreflectance and photoreflectance provide very important methods for nondestructive determination of surface and junction electric fields. These fields can, in turn, be related to doping densities in a space charge region [6] through the Schottky equation.

Figure 15 presents photoreflectance data used to characterize a GaAs/$Al_{0.24}Ga_{0.76}As$ multiple quantum well. The chopped laser beam, 100 μm in diameter, had been moved along the structure to give spectra from different spatial regions. Each of the resulting spectra was theoretically fitted, to determine how the well width and Al mole fraction value changed with position over a distance of 1.4 cm.

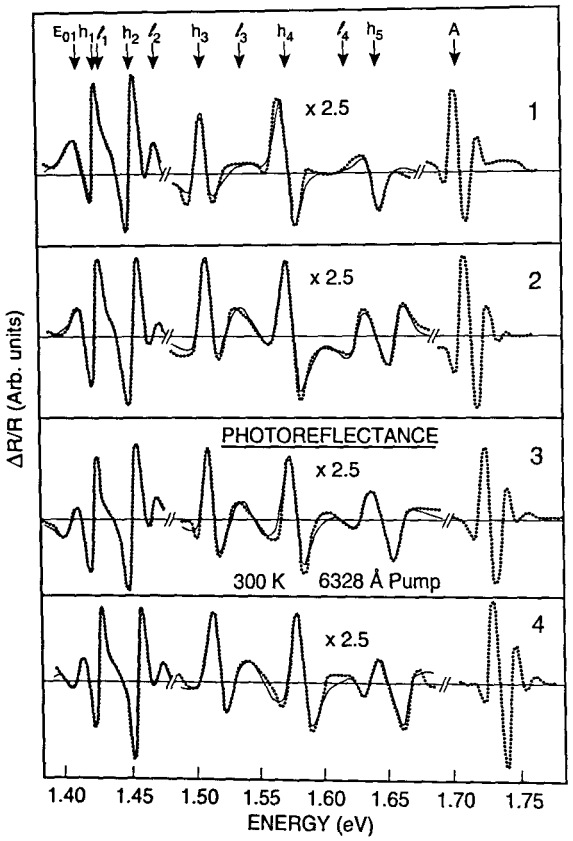

Fig. 15. Photoreflectance spectra of GaAs/$Al_xGa_{1-x}As$ multiple quantum well (MQW) with nominal x value 0.24, and nominal barrier and well thickness of 15 nm and 22 nm, respectively. Spectra (1) to (4) were measured at locations spaced 0.47 cm apart along a straight line. In each, the peak at 1.42 eV marked E_{01} comes from the direct gap of the GaAs substrate, the peak marked "A" near 1.72 eV comes from the direct gap of the $Al_xGa_{1-x}As$ barriers, and the remaining features marked l_n and h_n ($n = 1, 2, 3 \ldots$) between 1.43 and 1.68 eV come from light and heavy hole interband transitions characteristic of the MQW energy bands. The $Al_xGa_{1-x}As$, h_1, and l_1 features shift with spatial position. Fits to the data show that the well width ranges from 21.4 nm to 21.0 nm, and x ranges from 0.225 to 0.247, between positions (1) and (4), 1.4 cm apart. (See Sec. 5.5, Applications Refs., Parayanthal, Shen, Pollak, Glembocki, Shanabrook, and Beard (1986), fig. 1, p. 1261.)

Table 5 presents the sensitivities to typical quantities measured by photoreflectance spectroscopy such as composition, stress, electric field strength, surface photovoltage, and doping density. For more specific details, the reader should refer to the citations given in the table.

5.5 References

[1] D. E. Aspnes, Modulation spectroscopy/electric field effects on the dielectric function of semiconductors, in Handbook on Semiconductors, Vol. 2, T. S. Moss and M. Balkanski, eds., North-Holland, New York (1980) p. 109.

[2] B. O. Seraphin and N. Bottka, Franz-Keldysh effect of the refractive index in semiconductors, Phys. Rev. **139** A560 (1965).

[3] D. E. Aspnes, Third-derivative modulation spectroscopy with low-field electroreflectance, Surface Science **37**, 418 (1973).

[4] J. P. Estrera, W. M. Duncan, Y. C. Kao, H. Y. Liu, and E. A. Beam, Systematic optical and x-ray study of $In_xGa_{1-x}As$ on InP, J. Electronic Materials **20**, 983 (1991).

[5] D. E. Aspnes and A. A. Studna, Schottky-barrier electroreflectance: application to GaAs, Phys. Rev. B **7**, 4605 (1973).

[6] W. M. Duncan and A. F. Schreiner, Surface state study of ion implanted GaAs (Se) from photoreflectance, Solid State Communications **31**, 457 (1979).

General

J. I. Pankove, Optical Processes in Semiconductors, Prentice Hall, Englewood Cliffs (1971) pp. 391–407.

F. H. Pollak and O. J. Glembocki, Modulation spectroscopy of semiconductor microstructures: an overview, in Spectroscopic Characterization Techniques for Semiconductor Technology III, Proceedings SPIE Vol. 946, O. J. Glembocki, F. H. Pollak, and F. Ponce, eds., SPIE, Bellingham, Washington (1988) pp. 2–35.

Applications

P. M. Amirtharaj, J. H. Dinan, J. J. Kennedy, P. R. Boyd, and O. J. Glembocki, Photoreflectance study of $Hg_{0.7}Cd_{0.3}Te$ and $Cd_xZn_{1-x}Te$ E_1 transition, J. Vac. Sci. Technol. A **4**, 2028 (1986).

R. N. Bhattacharya, H. Shen, P. Parayanthal, and F. H. Pollak, Electroreflectance and photoreflectance characterization of the space charge region in semiconductors: ITO/InP as a model system, in Modern Optical Characterization Techniques for Semiconductors and Semiconductor Devices, Proceedings SPIE Vol. 794, O. H. Glembocki, F. H. Pollak, and J. J. Soong, eds., SPIE, Bellingham, Washington (1987) pp. 81–87.

R. C. Bowman, R. L. Alt, and K. W. Brown, Photoreflectance spectroscopy studies of alloy composition and ion implant damage in zincblende-type semiconductors, in Modern Optical Characterization Techniques for Semiconductors and Semiconductor Devices, Proceedings SPIE Vol. 794, O. H. Glembocki, F. H. Pollak, and J. J. Soong, eds., SPIE, Bellingham, Washington (1987) pp. 96–104.

R. C. Bowman, D. N. Jamieson, and P. M. Adamson, Optical and structural characterization of boron implanted GaAs, in Spectroscopic Characterization Techniques for Semiconductor Technology III, Proceedings SPIE Vol. 946, O. J. Glembocki, F. H. Pollak, and F. Ponce, eds., SPIE, Bellingham, Washington (1988) pp. 65–75.

J. P. Estrera, W. M. Duncan, Y. C. Kao, H. Y. Liu, and E. A. Beam, Systematic optical and x-ray study of $In_xGa_{1-x}As$ on InP, J. Electronic Materials **20**, 983–987 (1991).

O. J. Glembocki, Ellipsometric-electrolyte electro-reflectance study of the Si/SiO_2 interface, in Spectroscopic Characterization Techniques for Semiconductor Technology, Proceedings SPIE Vol. 452, F. H. Pollak and R. S. Bauer, eds., SPIE, Bellingham, Washington (1983) pp. 130–141.

O. J. Glembocki and B. V. Shanabrook, Photoreflectance characterization of microstructures using a dye laser system, in Modern Optical Characterization Techniques for Semiconductors and Semiconductor Devices, Proceedings SPIE Vol. 794, O. H. Glembocki, F. H. Pollak, and J. J. Soong, eds., SPIE Bellingham, Washington (1987) pp. 74–80.

R. Glosser and N. Bottka, Comparative response of electroreflectance and photoreflectance in GaAs, in Modern Optical Characterization Techniques for Semiconductors and Semiconductor Devices, Proceedings SPIE Vol. 794, O. H. Glembocki, F. H. Pollak, and J. J. Soong, eds., SPIE, Bellingham, Washington (1987) pp. 88–95.

T. K. Gupta, Effective bandgap shrinkage measurement in silicon solar cell by electroreflectance method, in Spectroscopic Characterization Techniques for Semiconductor Technology III, Proceedings SPIE Vol. 946, O. J. Glembocki, F. H. Pollak, and F. Ponce, eds., SPIE, Bellingham, Washington (1988) pp. 76–81.

B. K. Janousek and R. C. Carscallen, Approaches to enhancing the sensitivity of direct coupled photoacoustic spectroscopy as applied to GaAs, in Spectroscopic Characterization Techniques for Semiconductor Technology, Proceedings SPIE Vol. 452, F. H. Pollak and R. S. Bauer, eds., SPIE, Bellingham, Washington (1987) pp. 121–127.

C. E. Jones, M. E. Boyd, W. H. Konkel, S. Perkowitz, and R. Braunstein, Noncontact electrical characterization of epitaxial HgCdTe, J. Vac. Sci. Technol. A 4, 2056–2060 (1986).

Y. R. Lee, A. K. Ramdas, F. A. Chambers, J. M. Meese, and L. R. Ram Mohan, Piezomodulated electronic spectra of semiconductor heterostructures: GaAs/AlGaAs quantum well structures, in Spectroscopic Characterization Techniques for Semiconductor Technology, Proceedings SPIE Vol. 452, F. H. Pollak and R. S. Bauer, eds., SPIE, Bellingham, Washington (1987) pp. 105–110.

T. W. Nee, T. L. Cole, A. K. Green, M. E. Hills, C. K. Lowe-Ma, and V. Rehn, Infrared-wavelength modulation spectra of InGaAs grown by MBE and LPE, in Spectroscopic Characterization Techniques for Semiconductor Technology, Proceedings SPIE Vol. 452, F. H. Pollak and R. S. Bauer, eds., SPIE, Bellingham, Washington (1987) pp. 142–151.

G. Niquet, J. F. Dufour, G. Chabrier, M. Q'Jani, and P. Vernier, Characterization by electroreflectance of thin films and thin film interfaces in layered structures, in Modern Optical Characterization Techniques for Semiconductors and Semiconductor Devices, Proceedings SPIE Vol. 794, O. H. Glembocki, F. H. Pollak, and J. J. Soong, eds., SPIE, Bellingham, Washington (1987) pp. 111–115.

P. Parayanthal, H. Shen, F. H. Pollak, O. J. Glembocki, B. V. Shanabrook, and W. T. Beard, Photoreflectance of GaAs/GaAlAs multiple quantum wells: topographical variations in barrier height and well width, Appl. Phys. Lett. 48, 1261–1263 (1986).

U. K. Reddy, G. Ji, R. Houdre, H. Unlu, D. Huang, and H. Morkoc, Study of GaAs/AlGaAs and InGaAs/GaAs multiple quantum wells grown on non-polar substrates by photoreflectance, in Modern Optical Characterization Techniques for Semiconductors and Semiconductor Devices, Proceedings SPIE Vol. 794, O. H. Glembocki, F. H. Pollak, and J. J. Soong, eds., SPIE, Bellingham, Washington (1987) pp. 116–120.

H. Shen, S. H. Pan, F. H. Pollak, and R. N. Sacks, Photoreflectance and thermoreflectance of a $GaAs/Ga_{0.82}Al_{0.18}As$ multiple quantum well, in Spectroscopic Characterization Techniques for Semiconductor Technology III, Proceedings SPIE Vol. 946, O. J. Glembocki, F. H. Pollak, and F. Ponce, eds., SPIE, Bellingham, Washington (1988) pp. 36–42.

H. Shen, Z. Hang, F. H. Pollak, K. Capuder, and P. E. Norris, *In situ* monitoring of OMVPE of GaAs and $Ga_{1-x}Al_xAs$ ($x = 0.17$) by contactless photoreflectance, in Surface and Interface Analysis of Microelectronic Materials Processing and Growth, Proceedings SPIE Vol. 1186, L. J. Brillson and F. H. Pollak, eds., SPIE, Bellingham, Washington (1989) pp. 27–35.

X. Yin, F. H. Pollak, J. T. Fitch, C. H. Bjorkman, and G. Lucovsky, Photoreflectance study of strain at Si/SiO_2 interfaces prepared by thermal oxidation of silicon, in Surface and Interface Analysis of Microelectronic Materials Processing and Growth, Proceedings SPIE Vol. 1186, L. J. Brillson and F. H. Pollak, eds., SPIE, Bellingham, Washington (1989) pp. 122–130.

6. Photoluminescence

6.1 Introduction

Photoluminescence (PL) depends on the fact that electrons residing in the valence band of a semiconductor can be excited via optical absorption to the conduction band, to an impurity, or to a defect level in the energy gap. PL can be used to determine the energy gap of a semiconductor sample. This technique is especially useful for III-V and II-VI ternary alloys like $Al_xGa_{1-x}As$ and $Zn_xCd_{1-x}Te$, because the energy gap, which varies with the compositional parameter x, must be accurately known for most applications. When this process is inverted, x can be found from the gap value and the known relation between gap energy and composition. Photoluminescence also detects the presence of impurities and crystalline defects in semiconductors, which affect materials quality and device performance. Each impurity produces a characteristic feature or set of features in the spectrum. Hence, the impurity type can be identified, and multiple impurities can be detected in a single PL spectrum. In some cases, PL can measure the concentration of impurities. Comparison of PL peak halfwidths from sample to sample gives an indication of impurity concentration, carrier concentration, and crystal perfection.

6.2 Physical Basis

Photoluminescence results from radiative relaxation of an optically excited population. In order to cause this excitation, the incoming photon energy

Table 5. Photoreflectance spectroscopy sensitivity. Given are sensitivities for the measurement of crystallinity, x; stress, χ; field strength, F_{dc}; surface photovoltage, V_f; and doping density, N_d. The notations used for the measured quantity column are intensity, I; energy, $h\nu$; damping, Γ; bandgap, E_g; splitting energy, ΔE_{split}; deformation potential, b; compliances, S_{11} and S_{12}; energy of Franz Keldysh oscillation lobe, E_m; oscillation number, m; energy difference, E_2-E_1; shift of critical point, δE_{cp}; and spacing of Franz Keldysh oscillations, ΔE_{FKO}. ΔV is the built-in potential minus the photovoltage of the laser minus the thermal energy

Method	Matrix	Quantity	Measured quantity	Conversion	Sensitivity[a]	Ref. (see below)
PR	Si	crystallinity	$I, h\nu, \Gamma$	qualitative		1
PR	$In_xGa_{1-x}As$	x	E_g	$E_g/eV = 1.425 - 1.337x + 0.270x^2$	$x = 0$ to 0.15	2
PR	GaAs/Si	stress	ΔE_{split}	$\Delta E_{split} = 2b(S_{11} - S_{12})\chi$	$\chi = (150 \pm 50)$ MPa	3
PR	GaAs/GaAlAs	field strength	E_m vs m	$m\pi = \theta + (4/3)[(E_m - E_0)/\hbar O]^{3/2}$	$F_{dc} \sim (2$ to $4) \times 10^5$ V/cm	4
PR	metal/GaAs	surface photovoltage	E_m vs m	$m\pi = \theta + (4/3)[(E_m - E_0)/\hbar O]^{3/2}$	$V_F = (0.73 \pm 0.02)$ V	5
PR	GaAs	doping density	$E_2 - E_1$	$N_d = (\Delta V)N_d = (E_2 - E_1)^3(3.46 \times 10^{20})$ cm^{-3}	$N_d = (1 \times 10^{14}$ to $1 \times 10^{16})$ cm^{-3}	6
PR	GaAs	doping density	δE_{cp}	$\delta E_{cp}/\delta N_d = (5.8 \pm 0.5) \times 10^{-20}$ eV cm^3	$N_d > 1 \times 10^{16}$ cm^{-3}	7
PR	GaAs	doping density	ΔE_{FKO}	$\Delta E_{FKO} = \text{const.} \times N_d^{1/3}$	$N_d = (6 \times 10^{17}$ to $3 \times 10^{18})$ cm^{-3}	8

[a] Values quoted in references below.

References

[1] A. Giordana, R. Glosser, K. Joyner, and G. Pollack, J. Electronic Mat. **20**, 949 (1991).
[2] R. E. Nahory, M. A. Pollack, and J. C. DeWinter, J. Appl. Phys. **46**, 775 (1975).
[3] A. Dimoulas, P. Tzanetakis, A. Georgakilas, O. J. Glembocki, and A. Christou, J. Appl. Phys. **67**, 4389 (1990); T. Kanata, H. Suzawa, M. Matsunaga, H. Takakura, Y. Hamakawa, H. Kato, and T. Nishino, Phys. Rev. **B41**, 2936 (1990).
[4] X. Yin, F. H. Pollak, L. Pawlowicz, T. O'Neill, and M. Hafizi, Appl. Phys. Lett. **56**, 1278 (1990); N. Bottka, D. K. Gaskill, P. D. Wright, R. W. Kaliski, and D. A. Williams, J. Crystal Growth **107**, 893 (1991).
[5] X. Yin, H-M. Chen, F. H. Pollak, Y. Chan, P. A. Montano, P. D. Kirchner, G. D. Pettit, and J. M. Woodall, Appl. Phys. Lett. **58**, 260 (1991).
[6] M. Sydor, J. Angelo, W. Mitchel, T. W. Haas, and M-Y. Yen, J. Appl. Phys. **66**, 156 (1989).
[7] L. Peters, L. Phaneuf, L. W. Kapitan, and W. M. Theis, J. Appl. Phys. **62**, 4558 (1987).
[8] W. M. Duncan and A. F. Schreiner, Solid State Commun. **31**, 457 (1979).

must equal or exceed the energy difference between the initial and final states of the electron. Such an excited electron usually returns to its initial state after a short time. If the excited electron returns to its initial state by radiative means, the process emits a photon whose energy is the difference between the excited and the initial state energies. The spectral distribution of the emitted photons shows an emission peak at the energy (or wavelength) corresponding to each excited level.

Photoluminescence is complicated by the behavior of the electron during its excited period. The excited electron leaves behind it a deficiency in the valence band, a mobile hole. The Coulomb attraction between the excited electron and the hole can bind the two particles into a system called a free exciton, much as a proton and an electron form a bound hydrogen atom. The exciton can move as a unit through the crystal, but carries no current because its net charge is zero. From this perspective, the return of the electron to its initial state can be viewed as the collapse of the temporary excitonic state, when the electron recombines with the hole.

The exciton influences the PL spectrum in several ways. Because it is a bound state, the excited state energy is slightly less than the bandgap energy, generally by a few meV. Hence, for PL near the energy gap, the equation for the energy of the emitted photon is

$$\hbar\omega = E_g - E_{ex} , \tag{17}$$

where E_{ex} is the binding energy of the excitonic state. This equation applies for a direct energy gap semiconductor. For an indirect gap semiconductor, a phonon must also be involved to properly conserve momentum. Then the equation for the emitted photon energy is (E_{ph} is the photon energy)

$$\hbar\omega = E_g - E_{ex} - E_{ph} . \tag{18}$$

However, this free exciton recombination dominates only when the sample is very pure. When donor, acceptor, or neutral impurities are present, free excitons respond to the Coloumb fields of these defects to form bound excitons. Each type of exciton produces a PL peak when recombination occurs, and each can be identified in the spectrum.

6.3 Experimental and Technical Details

Figure 16 shows the main elements of a standard PL arrangement. Any of several commercially available types of laser may be used, provided that the energy of the laser's photons exceeds the energy gap of the material, and the laser power is adequate to excite a usable PL signal. An argon ion laser is suitable for many semiconductors of technological interest such as Si (1.12 eV), $Al_xGa_{1-x}As$ (1.42 eV to 2.16 eV) and $Zn_xCd_{1-x}Te$. Laser powers $\leq$50 mW are usually adequate, but power densities must be minimized to avoid sample heating effects. It is generally possible to avoid heating and still obtain adequate signal to noise by defocusing the laser or reducing the incident laser power.

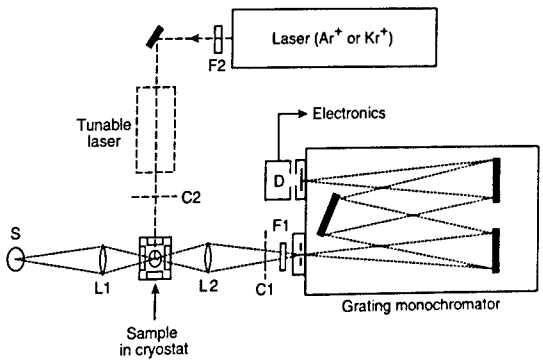

Fig. 16. Schematic diagram of a photoluminescence arrangement, showing the exciting Ar^+ or Kr^+ laser, filter F2 to block unwanted laser lines, the sample mounted in a cryostat, lens L2 to bring the PL radiation to the monochromator entrance slit, chopping wheel C1 to modulate the light for lock-in detection, filter F1 to exclude the laser line from the monochromator, the grating monochromator itself, and detector D followed by appropriate electronics to process and analyze the signal. The tunable dye laser and chopping wheel C2 shown in dashed outline are auxiliary equipment for luminescence excitation measurements, a related technique. Lamp S and lens L1 allow auxiliary absorption spectroscopy, using the same monochromator and detector. (See Sec. 6.5, General Refs., Lightowlers (1990), fig. 4, p. 138.)

The sample's PL radiation passes through a monochromator and then to a detector, to yield the spectral distribution of intensity versus wavelength or energy. A standard photomultiplier tube is usually employed for visible and near visible applications. Quantum detectors such as germanium and InAs photodiodes are employed for the near infrared. All of these give the best signal-to-noise ratio when cooled to temperatures as low as 77 K for solid-state photodiodes. Improvement in sensitivity comes with the use of an optical multi-channel analyzer such a Si photodiode array. The array has the advantage of providing complete spectra in a short time.

In spectral regions where signal to noise is detector limited, decided improvements in sensitivity and

decreases in measurement times come if the grating monochromator in Fig. 16 is replaced by an Michelson interferometer to carry out Fourier transform spectroscopy. This instrument has already been discussed in the section on infrared spectroscopy.

It is usually necessary to cool the sample below room temperature to observe the best PL spectra. Cooling reduces the thermal broadening of the excited carrier spectrum of the order k_BT, and also reduces the importance of nonradiative de-excitation processes. Cooling to liquid nitrogen temperature is often adequate. The sample can be mounted to a cold finger connected to a liquid nitrogen dewar, and can be held to within a few degrees of 77 K.

When necessary, cooling to liquid helium temperatures can be conveniently obtained by a continuous-flow liquid helium system. With proper shielding and an adequate flow rate of helium (typically 1 L/h to 3 L/h), sample temperatures as low as 6 K to 10 K can be maintained. Temperatures down to −10 K can be reached by mechanical refrigerators. If necessary, temperatures to 4 K can be obtained by immersion in liquid helium or to 2 K by pumped helium methods.

6.4 Illustrative Applications

Figure 17 shows how specific impurities in a semiconductor such as silicon clearly appear in PL spectra. The caption explains the source of each peak. Figure 18 illustrates the conversion of PL data into accurate values for impurity concentrations. Figure 19 shows how two-dimensional PL mapping can help evaluate the homogeneity and quality of a semiconductor wafer, in this case an epitaxial layer of InGaAsP grown on InP. The technique uses the fact that each parameter that describes a PL peak can be related to a sample property. The peak position, for instance, gives the energy gap value, which for an alloy like InGaAsP varies with the proportions of the component elements. Hence, a map of peak PL wavelength correlates well with a map of composition.

Table 6 presents the sensitivities of typical quantities measured by photoluminescence such as composition in III-V and II-VI alloys and the concentration of B, P, As, and Al in Si. The reader should refer to the citations in the table for more specific details.

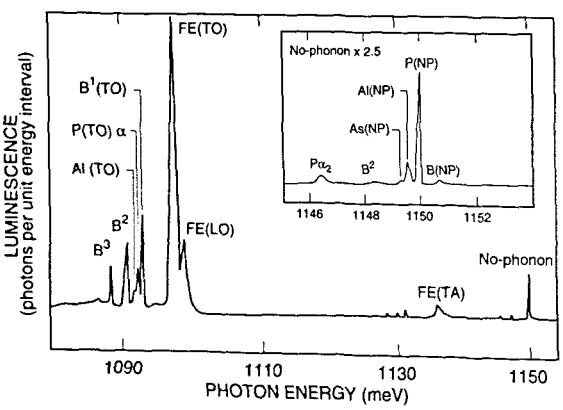

Fig. 17. PL spectrum of high-resistivity (>20 kΩ cm) near-intrinsic silicon showing the presence of the following impurities and their concentrations, in units of 10^{12} cm^{-3}: B, 1.36; P, 1.69; Al, 0.61; and As, 0.14. The fingerprint features for each element are marked. Free-exciton lines are marked FE. Because silicon is an indirect-gap semiconductor, phonon modes must be involved in FE transitions. They are indicated as TO (transverse optical), LO (longitudinal optical), and TA (transverse acoustic). Peaks labeled NP (no phonon) come from bound excitons, which do not require phonon assistance. The technique for deriving quantitative impurity concentration data from such spectra is discussed in the caption for Fig. 18. (See Sec. 6.5, General Refs., Lightowlers (1990), fig. 9, p. 144.)

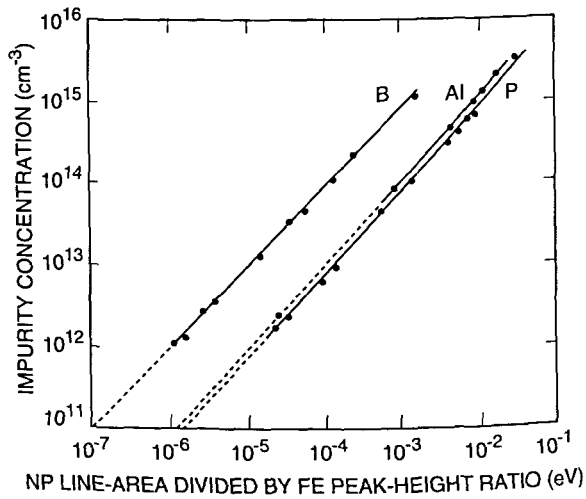

Fig. 18. Calibration chart to convert PL information like that in Fig. 17 into impurity concentration for B, Al, and P in silicon. It is difficult to establish absolute intensity standards for PL, because of differences in laser excitation power and focusing, temperature, and other factors. This chart uses a calibration method which is internal to a given spectrum, and hence avoids many of the problems of absolute calibration, although it was established using careful independent measurements of concentrations, and of temperature and light intensity. The area of the NP peak for the particular impurity is ratioed against the height of the FE(TO) peak in the same spectrum. More recent work has extended the upper limit of the calibration curves to about 10^{17} cm^{-3}. (See Sec. 6.5, General Refs., Lightowlers (1990), fig. 14, p. 148.)

Table 6. Photoluminescence sensitivity. Given are sensitivities for the measurement of substitutional boron, [B_s]; phosphorus, [P_s]; arsenic, [As_s]; and aluminum, [Al_s], in crystalline Si. Sensitivities for determination of ternary composition, x, are given for $Al_xGa_{1-x}As$, $In_xGa_{1-x}As$, and $Zn_xCd_{1-x}Te$. The notations used for the measured quantity column are the boron transverse optical b1 multiexciton peak intensity, $I(B_{TO}b1)$; free exciton intensity, $I(FE)$; phosphorus no-phonon peak intensity, $I(P_{NP})$; arsenic no-phonon peak intensity, $I(As_{NP})$; aluminum no-phonon peak intensity, $I(As_{NP})$; and energy, $h\nu$

Method	Matrix	Quantity	Measured quantity	Conversion	Sensitivity[a]	Ref. (see below)
Exciton intensity ratio	Si	$[B_s]$	$I(B_{TO}b1)/I(FE)$ @4.2 K	$\log[B_s/cm^3] = 1.435\log[I_B/I_{FE}] + 12.81$	$\pm 2\times10^{10}$ cm^{-3}	1
Exciton intensity ratio	Si	$[P_s]$	$I(P_{NP})/I(FE)$ @4.2 K	$\log[P_s/cm^3] = 1.280\log[I_P/I_{FE}] + 12.79$	$\pm 4\times10^{10}$ cm^{-3}	1
Exciton intensity ratio	Si	$[As_s]$	$I(As_{NP})/I(FE)$ @4.2 K	$\log[As_s/cm^3] = 1.049\log[I_{As}/I_{FE}] + 12.76$	$\pm 1\times10^{11}$ cm^{-3}	1
Exciton intensity ratio	Si	$[Al_s]$	$I(Al_{NP})/I(FE)$ @4.2 K	$\log[Al_s/cm^3] = 1.359\log[I_{Al}/I_{FE}] + 13.19$	$\pm 8\times10^{10}$ cm^{-3}	1
Peak energy	$Al_xGa_{1-x}As$	x	$h\nu$ @300 K	$h\nu/eV = 1.424 + 1.247x$ $(0 < x < 0.45)$	$\pm 0.002x$	2
Peak energy	$In_xGa_{1-x}As$	x	$h\nu$ @300 K	$h\nu/eV = 1.424 - 1.337x + 0.270x^2$	$\pm 0.002x$	3
Peak energy	$Zn_xCd_{1-x}Te$	x	$h\nu$ @4.2 K	$h\nu/eV = 1.605 + 0.505x + 0.285x^2$	$\pm 0.0002x$	4

[a] Calculated as the concentration-equivalent-of-noise assuming ±0.02 signal-to-noise ratio for intensity measurements and ±2 meV and ±0.2 meV energy precision at room temperature and 4.2 K, respectively.

References

[1] W. M. Duncan, M. L. Eastwood, and H.-L Tsai, Mat. Res. Soc. Symp. Proc. **69**, 225 (1986).
[2] H. C. Casey and M. B. Panish, Heterostructure Lasers, Part B: Materials and Operating Characteristics, Academic Press, New York (1978), p. 16.
[3] R. E. Nabory, M. A. Pollack, and J. D. DeWinter, J. Appl. Phys. **46**, 775 (1975).
[4] N. Magnea, F. Dal'bo, J. L. Pautrat, A. Million, L. Dicioccio, and G. Feuillet, Mat. Res. Soc. Symp. Proc. **90**, 455 (1987); W. M. Duncan, R. J. Koestner, J. H. Tregilgas, H.-Y. Liu, and M.-C. Chen, Mat. Res. Soc. Symp. Proc. **161**, 39 (1990).

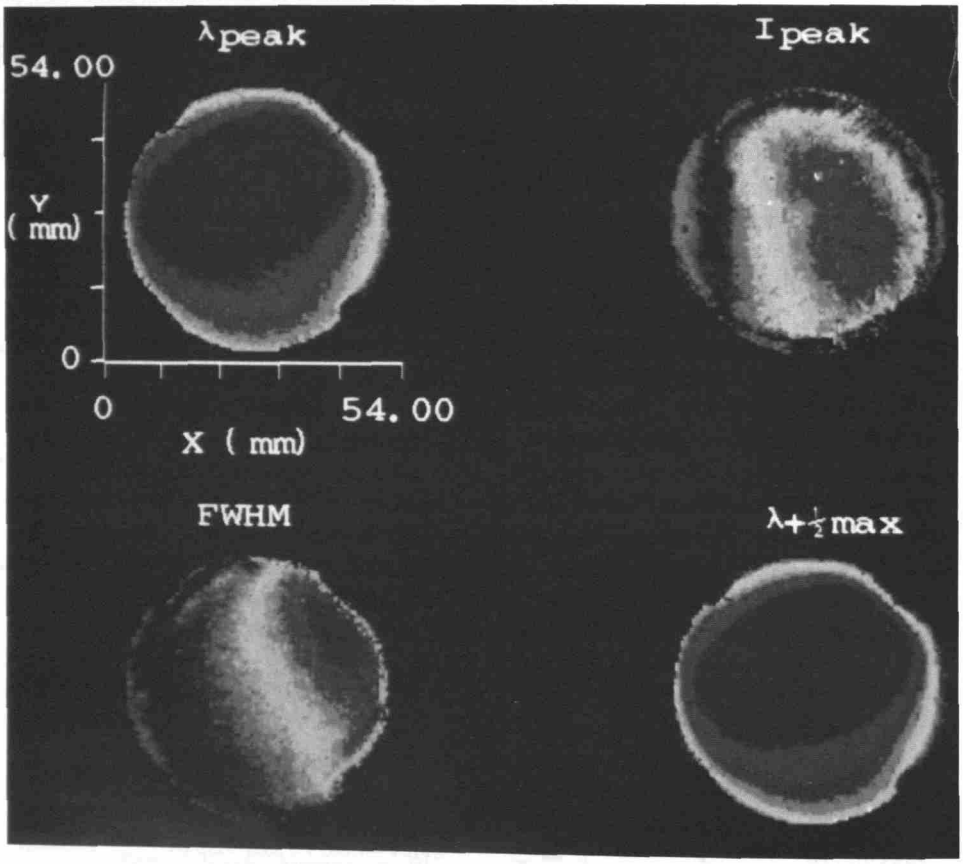

Fig. 19. Two-dimensional maps of PL parameters from a 50 mm wafer of epitaxial InGaAsP grown on InP, obtained using a commercial system with *x-y* scanning capability. Upper left, wavelength of the PL peak, which is related to sample composition; upper right, peak intensity, related to defect density; lower left, peak full width at half maximum (FWHM), related to closeness of the lattice match between layer and substrate; lower right, upper wavelength at which PL intensity falls to 50 % of the peak value, related to sample composition. Spatial variations in all the parameters are clearly seen. (See Sec. 6.5, Applications Refs., Hennessy, Miner, and Moore (1990), fig. 3.)

6.5 References

General

P. Goldberg, Luminescence of Inorganic Solids, Academic, New York (1966).

E. C. Lightowlers, Photoluminescence characterisation, in Growth and Characterization of Semiconductors, R. A. Stradling and P. C. Klipstein, eds., Adam Hilger, Bristol (1990) pp. 135–163.

D. K. Schroder, Semiconductor Material and Device Characterization, John Wiley, New York (1990) pp. 490–494.

M. L. W. Thewalt, M. K. Nissen, D. J. S. Beckett, and K. R. Lundgren, High performance photoluminescence spectroscopy using Fourier transform interferometry, in Impurities, Defects and Diffusion in Semiconductors: Bulk and Layered Structures, Materials Research Society Symposia Proceedings Vol. 163, D. J. Wolford, J. Bernholc, and E. E. Haller, eds., Materials Research Society, Pittsburgh, Pennsylvania (1989) pp. 221–232.

Applications

K. K. Bajaj and D. C. Reynolds, An overview of optical characterization of semiconductor structures and alloys, in Modern Optical Characterization Techniques for Semiconductors and Semiconductor Devices, SPIE Proceedings Vol. 794, O. J. Glembocki, F. H. Pollak, and J. J. Song, eds., SPIE, Bellingham, Washington (1987) pp. 2–10.

S. G. Bishop, Characterization of semiconductors by photoluminescence and photoluminescence excitation spectroscopy, in Optical Characterization Techniques for Semiconductor Technology, SPIE Proceedings Vol. 276, D. E. Aspnes, S. So, and R. F. Potter, eds., SPIE, Bellingham, Washington (1981) pp. 2–10.

M. Bugajaski, K. Nauka, S. S. Rosner, and D. Mars, Photoluminescence studies of annealed GaAs films grown on Si substrates, in Heteroepitaxy on Silicon: Fundamentals, Structure, and Devices, Materials Research Society Symposia Proceedings Vol. 116, H. K. Choi, R. Hull, H. Ishiwara, and R. J. Nemanich, eds., Materials Research Society, Pittsburgh, Pennsylvania (1988) pp. 233-238.

Y. H. Chen and S. A. Lyon, Photoluminescence and diffusivity of free excitons in doped silicon, IEEE J. Quantum Electron. QE-25, 1053–1055 (1989).

H. Conzelmann, Photoluminescence of transition metal complexes in silicon, Appl. Phys. A 42, 1–18 (1987).

W. M. Duncan, M. L. Eastwood, and H-L. Tsai, Fourier transform photoluminescence analysis of trace impurities and defects in silicon, in Materials Characterization, Materials Research Society Symposia Proceedings Vol. 69, N. Cheung and M.-A. Nicolet, eds., Materials Research Society, Pittsburgh, Pennsylvania (1986) pp. 225–230.

J. A. Fouquet, R. R. Saxena, and G. A. Patterson, Near-infrared photoluminescence of high-resistivity epitaxial GaAs and InP and of epitaxial GaAs on Si, IEEE J. Quantum Electron. QE-25, 1025–1034 (1989).

A. Freundlich, G. Neu, A. Leycuras, R. Carles, and C. Verie, Heterogeneous strain relaxation in GaAs on Si (100), in Heteroepitaxy on Silicon: Fundamentals, Structure, and Devices, Materials Research Society Symposia Proceedings Vol. 116, H. K. Choi, R. Hull, H. Ishiwara, and R. J. Nemanich, eds., Materials Research Society, Pittsburgh, Pennsylvania (1988) pp. 251–256.

J. Hennessy, C. Miner, and C. Moore, Photoluminescence mapping in inspection and process control, Photonics Spectra 24, 91–96 (1990).

E. D. Jones and L. R. Dawson, Photoluminescence studies of InGaAlAs quaternary alloys, in Spectroscopic Characterization Techniques for Semiconductor Technology III, Proceedings SPIE Vol. 946, O. J. Glembocki, F. H. Pollak, and F. Ponce, eds., SPIE, Bellingham, Washington (1988) pp. 172–176.

E. S. Koteles, Y. Y. Chi, and R. F. Holmstrom, Low temperature photoluminescence signature of a two-dimensional electron gas, in Modern Optical Characterization Techniques for Semiconductors and Semiconductor Devices, Proceedings SPIE Vol. 794, O. J. Glembocki, F. H. Pollak, and J. J. Song, eds., SPIE, Bellingham, Washington (1987) pp. 61–65.

H. P. Lee, Y-H. Huang, X. Liu, J. S. Smith, E. R. Weber, P. Yu, S. Wang, and Z. Lilienthal-Weber, The photoluminescence and TEM studies of patterned GaAs films on Si substrates grown by molecular beam epitaxy, in Heteroepitaxy on Silicon: Fundamentals, Structure, and Devices, Materials Research Society Symposia Proceedings Vol. 116, H. K. Choi, R. Hull, H. Ishiwara, and R. J. Nemanich, eds., Materials Research Society, Pittsburgh, Pennsylvania (1988) pp. 219–226.

C. J. Miner, Non-destructive, whole wafer assessment of optoelectronic epitaxial materials, Semicond. Sci. Technol. 7, A10–A15 (1992).

C. J. L. Moore and C. J. Miner, A spatially resolved spectrally resolved photoluminescence mapping system, J. Crystal Growth 103, 21–27 (1990).

A. L. Moretti, F. A. Chambers, G. P. Devane, and F. A. Kish, Characterization of GaAs/$Al_xGa_{1-x}As$ structures using scanning photoluminescence, IEEE J. Quantum Electron. QE-25, 1018–1024 (1989).

R. J. Nemanich, D. K. Biegelsen, R. A. Street, B. Downs, B. S. Krusor, and R. D. Yingling, Strain in graded thickness GaAs/Si heteroepitaxial structures grown with a buffer layer, in Heteroepitaxy on Silicon: Fundamentals, Structure, and Devices, Materials Research Society Symposia Proceedings Vol. 116, H. K. Choi, R. Hull, H. Ishiwara, and R. J. Nemanich, eds., Materials Research Society, Pittsburgh, Pennsylvania (1988) pp. 245–250.

T. Nishino, H. Nakayama, J. Katsura, and Y. Hamakawa, Photoluminescence characterization of thermally induced defects in Czochralski-grown Si wafers, Optical Characterization Techniques for Semiconductor Technology, Proceedings SPIE Vol. 276, D. E. Aspnes, S. So, and R. F. Potter, eds., SPIE, Bellingham, Washington (1981) pp. 31–38.

T. Nishino, A new high-sensitivity characterization method of interface stress at heterostructures by Cr-related luminescence, IEEE J. Quantum Electron. QE-25, 1046–1052 (1989).

J. E. Potts, T. L. Smith, and H. Cheng, Photoluminescence studies of donors in molecular beam epitaxy (MBE) grown ZnSe, in Modern Optical Characterization Techniques for Semiconductors and Semiconductor Devices, Proceedings SPIE Vol. 794, O. J. Glembocki, F. H. Pollak, and J. J. Song, eds., SPIE, Bellingham, Washington (1987) pp. 27–33.

D. C. Reynolds and C. W. Litton, Semiconductor materials characterization by high-resolution optical spectroscopy, in Optical Characterization Techniques for Semiconductor Technology, Proceedings SPIE Vol. 276, D. E. Aspnes, S. So, and R. F. Potter, eds., SPIE, Bellingham, Washington (1981) pp. 11–30.

E. K. Riemer, T. G. Stoebe, and A. A. Khan, Scanning photoluminescence, in Modern Optical Characterization Techniques for Semiconductors and Semiconductor Devices, Proceedings SPIE Vol. 794, O. J. Glembocki, F. H. Pollak, and J. J. Song, eds., SPIE, Bellingham, Washington (1987) pp. 20–26.

B. J. Skromme, R. Bhat, H. M. Cox, and E. Colas, Identification of donors in GaAs by resonantly excited high-field magnetospectroscopy, IEEE J. Quantum Electron. QE-25, 1035–1045 (1989).

M. L. W. Thewalt and D. M. Brake, Ultra-high resolution photoluminescence studies of bound excitons and multi-bound exciton complexes in silicon, Materials Science Forum Vols. 65-66 (1990) 187–198.

B. A. Wilson, Novel applications of optical techniques to the study of buried semiconductor interfaces, IEEE J. Quantum Electron. QE-25, 1012-1017 (1989).

S. Zemon, C. Jagannath, S. K. Shastry, W. J. Miniscalco, and G. Lambert, Resonant photoluminescence excitation of annealed GaAs films grown on Si substrates, in Heteroepitaxy on Silicon: Fundamentals, Structure, and Devices, Materials Research Society Symposia Proceedings Vol. 116, H. K. Choi, R. Hull, H. Ishiwara, and R. J. Nemanich, eds., Materials Research Society, Pittsburgh, Pennsylvania (1988) pp. 239–245.

7. Raman Scattering

7.1 Introduction

Raman scattering results when photons interact with optical lattice vibrations (phonons) of a semiconductor crystal lattice. The way in which these phonons appear in a Raman spectrum depends on the crystallinity of a sample and on its crystal orientation. Hence, Raman scattering can determine whether a sample is amorphous or crystalline, and whether the crystal is of good quality or is altered by damage or imperfections. The method is also sensitive to strain effects, which change semiconductor lattice structure and hence phonon frequencies. Since phonon frequencies and amplitudes in an alloy semiconductor like $Al_xGa_{1-x}As$ change with the degree of alloying, Raman scattering can be used to measure composition as well. By changing the wavelength of the light exciting the scattering, the penetration depth can be changed, which gives the capability to probe layered or inhomogeneous structures.

In microprobe Raman scattering, a microscope is coupled to the Raman system, making it possible to probe regions as small as ~ 1 μm across. This allows for the identification of contaminating impurities in extremely small regions of the specimen. In resonance Raman scattering, the scattering process is strengthened when the incoming photon energy matches the energy gap or other higher-order critical point energies in the sample's band structure. This resonance strengthens the inherently weak Raman process and also gives band structure information as well as phonon information.

7.2 Physical Basis

Raman scattering, a two-photon process, is more complex than one-photon optical processes such as photoluminescence. If light impinges on the surface of a semiconductor, a large portion is reflected, transmitted, absorbed, or elastically scattered (Rayleigh scattering), with no change in frequency. A small part of the light interacts inelastically with phonon modes, so that the outgoing photons have frequencies shifted from the incoming values. These are the Raman-scattered photons. Since the photons can either gain energy or lose energy in their phonon interactions, the scattered light can be of higher frequency (anti-Stokes-shifted) or of lower frequency (Stokes-shifted) than the incident light. Because of statistical considerations, the Stokes modes are stronger and are usually the ones observed in Raman measurements at room temperature.

The up-shifted and down-shifted photons can be treated as side bands of the exciting light that come from the nonlinear interaction between the light and the material. This can be seen by examining the crystal polarization P due to the phonons, which is given by

$$P = \alpha E \tag{19}$$

where E is the applied electric field $E_0 \cos\omega t$ and the polarizability α is given by

$$\alpha = \alpha_1 u + \alpha_2 u^2 + \alpha_3 u^3 + \ \ldots\ , \tag{20}$$

where u is the phonon displacement, and α_1, α_2, ... are constants. The first term in Eq. (20) is the dipole approximation, and the other terms represent more complex anharmonic contributions. If the phonon vibrates at frequency Ω, u is of the form $u = u_0 \cos(\Omega t)$ and Eq. (19) becomes

$$P = E_0 [\alpha_1 u_0 \cos(\omega t)\, \cos(\Omega t) + \alpha_2 u_0^2 \cos(\omega t)\, \cos^2(\Omega t) + \ \ldots\ ]\,. \tag{21}$$

From standard trigonometric identities, Eq. (21) can be rewritten as expressions that contain $\cos(\omega + \Omega)t$, $\cos(\omega \pm 2\Omega)t$ ..., $\cos(\omega + n\Omega)t$. The leading term $\cos(\omega \pm \Omega)t$ represents the fundamental Raman-shifted bands at frequency $\omega + \Omega$ (so-called anti-Stokes lines) and $\omega - \Omega$ (Stokes lines), and the others represent the interaction of the photon with multiple phonons ($n = 2, 3, \ldots$).

This simple development of the theory gives the shift in photon frequency, that is, where the Raman bands lie relative to the exciting wavelength. However, the intensity and line shape of the Raman bands are more difficult to calculate. Although some appropriate theory exists, it is not easy to apply to specific semiconductors. In general, Raman scattering is a weak process, and the higher order terms in Eq. (20) generally contribute weakly. Beyond these qualitative trends, line-shape analysis of Raman spectra of semiconductors is not well developed. However, it is true that smaller half-widths correlate with higher levels of sample crystalline perfection.

When carried out in detail, the calculation of the Raman intensity depends strongly on the orientation and polarization of the exciting light relative to the crystal axes, since such geometric considerations determine how the field and the polarization interact. Hence, the Raman spectrum from a given crystal depends on its orientation, with various "allowed" and "forbidden" Raman modes for different orientations.

An exception to the statement that Raman scattering is weak occurs in resonant Raman scattering. If the energy of the exciting photon is chosen to match a fundamental feature in the semiconductor band structure, such as the energy gap or higher order critical points in the band structure, the amount of energy imparted to the lattice increases dramatically, and so does the strength of the Raman modes.

7.3 Experimental and Technical Details

The overriding consideration in Raman scattering is the weakness of the signal, and the difficulty of separating it from unavoidable accompanying spectral information. Weak Raman peaks usually must be measured in the immediate neighborhood of intense Rayleigh scattering, which occurs at the energy of the exciting photon. Raman measurements require the strongest possible light sources that will not damage the sample, special optical methods to filter out the Rayleigh peak, and sensitive detection schemes to capture the few emerging Raman-shifted photons.

Any monochromatic light source can act as a Raman source. Most often, lasers operating at visible frequencies are employed to provide the necessary power. To give flexibility in varying the penetration depth, and some capability to excite resonance Raman scattering, it is better to use lasers that can be tuned over several powerful lines in the visible. Argon-ion and krypton-ion lasers are good choices; they are powerful, commercially available, and easily tunable, one from the ultraviolet to the green, the other toward the red end of the spectrum. For maximum flexibility in tuning, say for exact resonant coincidence, a tunable dye laser is the best choice. With the range of available dyes, these lasers can be tuned through the energy gaps of most semiconductors. The power is much lower than that of ion lasers but the increased signal due to the resonant effect more than compensates for this.

The optical arrangement for Raman spectroscopy is similar to that for photoluminescence (fig. 16), but with one important exception: a single monochromator is usually inadequate to separate the Raman signal from the strong accompanying Rayleigh light. A double monochromator is standard, consisting of two tandem gratings turning together and sequentially dispersing the light. In recent years, holographic notch filters have matured sufficiently that they can be used to eliminate the Rayleigh signal and allow the use of a single monochromator. Triple monochromators are sometimes used.

Raman scattering excited in the visible or ultraviolet can be detected by visible or ultraviolet detectors, so photomultiplier tubes (PMT) and array detectors work well. The PMTs should be chosen to give broad spectral coverage and to display a low dark count for maximum sensitivity. Cooled operation to reduce dark count is also important. As in photoluminescence work, it is possible to use Fourier methods to enhance Raman sensitivity or to reduce data collection time.

7.4 Illustrative Applications

The sensitivity of Raman scattering to phonon modes makes it possible to distinguish between amorphous and crystalline semiconductors. Figure 20 illustrates the direct way in which Raman spectra follow the increasing presence of crystalline silicon, as annealing proceeds on amorphous material.

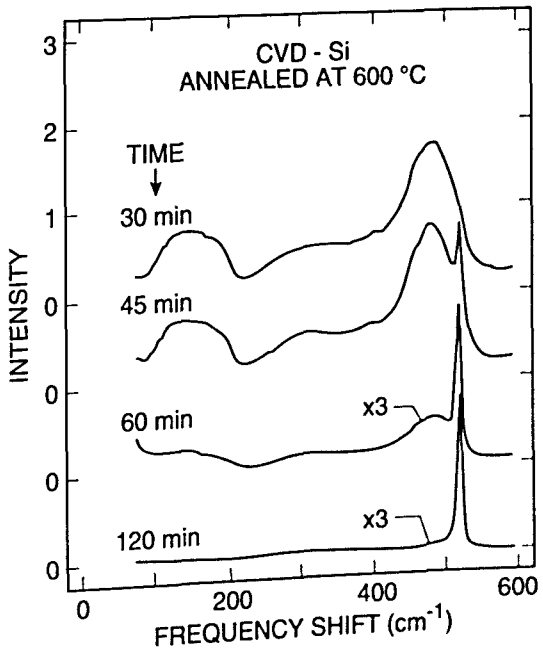

Fig. 20. Raman spectra of silicon grown by chemical vapor deposition, showing change in the character of the silicon after annealing. The top spectrum, taken after 30 min of annealing, is virtually the same as from as-grown material. It shows only broad peaks coming from amorphous silicon. After annealing for 45 min, a sharp line appears at 520 cm^{-1}, which comes from the optical phonon characteristic of crystalline silicon. The broad structure continues to decrease with annealing time, until after 120 min, the spectrum indicates that little or no amorphous silicon remains. (See Sec. 7.5, General Refs., Nemanich (1986), fig. 1, p. 26.)

Figure 21 shows how strain in a semiconductor appears in a Raman spectrum. The Raman peak for epitaxial GaAs grown on a silicon substrate shifts relative to that for bulk GaAs, because the epilayer lattice spacing changes under the strain induced by the mismatch between film and substrate. Microprobe Raman analysis can be helpful for examining contamination by small particles or for examining thin films, as illustrated in Fig. 22.

Table 7 gives the sensitivities of typical quantities measured by Raman spectroscopy such as stress, impurity concentrations of C and Zn in GaAs, alloy composition, and temperature. For more specific details, the reader should refer to the citations in the table.

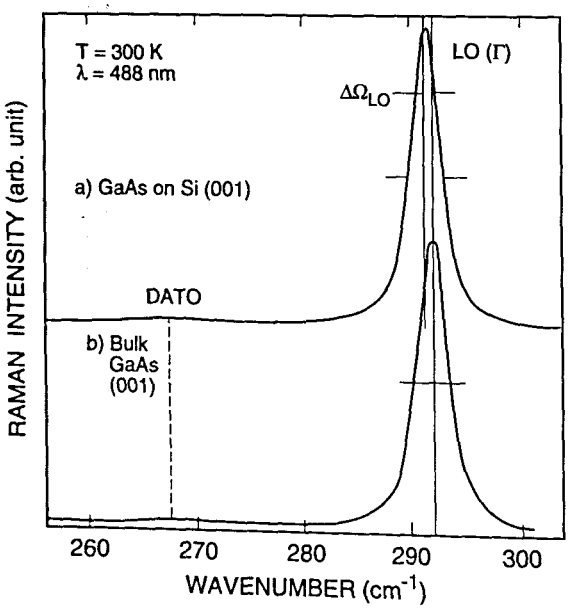

Fig. 21. Raman spectra of bulk (100) GaAs (lower curve) compared to that from a GaAs film 2 μm thick grown on (100) silicon (upper curve). The main peak near 292 cm^{-1} comes from the longitudinal optical (LO) phonon. Peak halfwidths are the same in both curves, indicating similar sample quality. The barely visible disorder-activated transverse optical (DATO) peak remains equally small in both spectra, also indicating that there is no significant disorder. However, the peak position for the film is 0.7 cm^{-1} lower than for the bulk sample, because the epilayer is stressed. Raman methods can easily detect and measure such small changes in peak position. (See Sec. 7.5, Applications Refs., Freundlich, Neu, Leycuras, Carles, and Verie (1988), fig. 1, p. 252.)

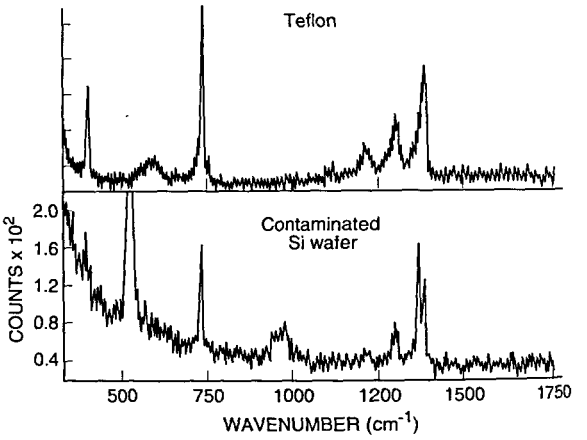

Fig. 22. Raman microprobe spectrum of a silicon wafer with surface contamination (lower plot) compared to the Raman spectrum of polytetrafluorethylene or teflon (upper plot). The peaks in the lower spectrum at 520 cm^{-1} and 950 cm^{-1} are known phonon modes for silicon. The additional peaks arise from the contaminant. They resemble the teflon spectrum and suggest that the contamination came during wafer processing, which included polishing in a slurry containing organic solvents, and etching in a CF_4/H_2 plasma. Polymer could have been deposited on the wafer either as teflon from a container holding the slurry, or during the plasma etch. (See Sec. 7.5, Applications Refs., Adar (1986), fig. 2, p. 234.)

General

Light Scattering in Solids I. Introductory Concepts, M. Cardona, ed., Springer-Verlag, Berlin (1983).

Light Scattering in Solids II. Basic Concepts and Instrumentation, M. Cardona and G. Guntherodt, eds., Springer-Verlag, Berlin (1982).

G. J. Exarhos, Molecular characterization of dielectric films by laser Raman spectroscopy, in Characterization of Semiconductor Materials, G. E. McGuire, ed., Noyes, Park Ridge, New Jersey (1989) pp. 242–288.

J. Geurts and W. Richter, Raman scattering from interface regions; structure, composition, and electronic properties, in Semiconductor Interfaces: Formation and Properties, G. Le Lay, J. Derrien, and N. Boccara, eds., Springer-Verlag, Berlin (1987) pp. 328–334.

R. J. Nemanich, Raman spectroscopy for semiconductor thin film analysis, in Materials Characterization, Materials Research Society Symposia Proceedings Vol. 69, N. Cheung and M-A. Nicolet, eds., Materials Research Society, Pittsburgh, Pennsylvania (1986) pp. 23–37.

J. Sapriel, Raman characterization of semiconductor superlattices, in Spectroscopic Characterization Techniques for Semiconductor Technology III, Proceedings SPIE Vol. 946, O. J. Glembocki, F. H. Pollak, and F. Ponce, eds., SPIE, Bellingham, Washington (1988) pp. 136–145.

Table 7. Raman spectroscopy sensitivity. Given are sensitivities for the measurement of stress; σ; crystallinity; surface damage; boron 11 concentration, [B^{11}]; temperature; composition; substitutional carbon concentration, C_s; substitutional zinc concentration, Zn_s; built-in potential, V_{bi}; and composition, x. The notations used for the measured quantity column are frequency of the LO phonon, ω_{LO}; frequency of the TO phonon, ω_{TO}; crystallite diameter, L; intensity at a given energy, $I(2000\ cm^{-1})$; frequency, (ω), frequency shift, $\Delta\omega$; intensity of the two LO mode, I(2LO); intensity of the TO mode, I_{TO}; intensity of the LO mode, I_{LO} or I(LO); intensity of the L^- plasmon branch, $I(L^-)$; intensity of the anti-Stokes peak, I_{AS}; and intensity of the Stokes peak, I_S

Method	Matrix	Quantity	Measured quantity	Conversion	Sensitivity[a]	Ref. (see below)
RS	Si	Stress	ω_{LO}	$\sigma = (2.49\times10^{10}\ Pa^{-1})\times\Delta\omega$	$\pm 1\times10^{7}$ Pa	1
RS	Si	Crystallinity	L @300 K	Ref. 2		2
RS	Si	Surface damage	$I(2000\ cm^{-1})$	Ref. 3		3
RS	Si	[B^{11}]	$I(620\ cm^{-1})$	Ref. 4		4
RS	Si	Temperature	ω and $\Delta\omega$	Ref. 5		5
RS	Si_xGe_{1-x}	x	ω	Ref. 6		6
RS	GaAs	Crystallinity	L @300 K	Ref. 7		7
RS	GaAs	Crystallinity	I(2LO)/I(540) @300 K	Ref. 8		8
RS	GaAs	Crystallinity	I_{TO}/I_{LO} @300 K	Ref. 9		9
ERS	GaAs	C_s, Zn_s	$I(148\ cm^{-1})$, $I(174\ cm^{-1})$ 6 K	Ref. 10	$<1\times10^{15}\ cm^{-3}$	10
RS	GaAs	V_{bi}	I(LO)/$I(L^-)$	Ref. 11	± 0.2 V	11
RS	$Al_xGa_{1-x}As$	x	ω_{LO}	$(\omega_{LO}/2\pi c)/cm^{-1} = 292.4 + 70.8x - 26.8x^2 - 41.13x^3$	$\pm 0.01x$	12
RS	GaAs	Temperature	ω_{LO}, ω_{TO}	I_{AS}/I_S	± 20 °C	13

[a] Calculated as the concentration-equivalent-of-noise or uncertainty in frequency.

References

[1] Th. Englert, G. Abstreiter, and J. Pontcharra, Solid-State Electronics **23**, 31 (1980).
[2] H. Richter, Z. P. Wang, and L. Ley, Solid State Commun. **39**, 625, 1981; E. Bustarret, M. A. Hachicha, and M. Brunel, Appl. Phys. Lett. **52**, 1675 (1988).
[3] J. C. Tsang, G. S. Oehrlein, I. Haller, and J. S. Custer, Appl. Phys. Lett. **46**, 589 (1985).
[4] P. T. T. Wong and M. Simard-Normandin, J. Electrochem. Soc. **132**, 980 (1985).
[5] H. Tang and I. P. Herman, Phys. Rev. **B43**, 2299 (1991).
[6] W. J. Brya, Solid State Commun. **12**, 253 (1973); J. B. Renucci, M. A. Renucci, and M. Cardona, Solid State Commun. **9**, 1651 (1971).
[7] K. K. Tiong, P. M. Armitharaj, F. H. Pollak, and D. E. Aspnes, Appl. Phys. Lett. **44**, 122 (1983); P. Parayanthal and F. H. Pollak, Phys. Rev. Lett. **52**, 1822 (1984).
[8] J. Wagner and Ch. Hoffman, Appl. Phys. Lett. **50**, 682 (1987); J. Wagner and H. Seelewind, J. Appl. Phys. **64**, 2761 (1988).
[9] W. M. Duncan, R. J. Matyi, and H.-Y. Liu, Appl. Phys. Lett. **57**, 163 (1990).
[10] J. Wagner, H. Seelewind, and U. Kaufmann, Appl. Phys. Lett. **48**, 1054 (1986).
[11] L. A. Farrow, C. J. Sandroff, and M. C. Tamargo, Appl. Phys. Lett. **51**, 1931 (1987).
[12] O. K. Kim and W. G. Spitzer, J. Appl. Phys. **50**, 4362 (1979); S. Adachi, J. Appl. Phys. **58**, R1 (1985).
[13] J. R. Shealy and G. W. Wicks, Appl. Phys. Lett. **50**, 1173 (1987).

B. Schrader, Possibilities and limitations of FT-Raman spectroscopy, in Practical Fourier Transform Infrared Spectroscopy, J. R. Ferraro and K. Krishnan, eds., Academic Press, San Diego, California (1990) pp. 167–202.

Applications

F. Adar, Application of the Raman microprobe to analytical problems of microelectronics, in Microelectronic Processing: Inorganic Materials Characterization, ACS Symposia Series 295, L. A. Casper, ed., American Chemical Society, Washington, DC (1986) pp. 230–239.

F. Adar, Developments of the Raman microprobe instrumentation and applications, Microchemical Journal **538**, pp. 50–79 (1988).

P. M. Amirtharaj, K-K. Tiong, and F. H. Pollak, Raman scattering in $Hg_{0.8}Cd_{0.2}Te$, J. Vac. Sci. Technol. A1, 1744 (1983).

S. J. Chang, M. A. Kallel, K. L. Wang, and R. C. Bowman, Strain distribution of MBE grown GeSi/Si layers by Raman scattering, in Spectroscopic Characterization Techniques for Semiconductor Technology III, Proceedings SPIE Vol. 946, O. J. Glembocki, F. H. Pollak, and F. Ponce, eds., SPIE, Bellingham, Washington (1988) pp. 163–168.

Z. C. Feng, S. Perkowitz, and O. Wu, Raman and resonant Raman scattering from the HgTe/CdTe superlattice, Phys. Rev. B **41**, 6057–6060 (1990).

Z. C. Feng, S. Perkowitz, T. S. Rao, and J. B. Webb, Raman characterization of InSb/GaAs grown by metalorganic magnetron sputtering, in Layered Structures: Heteroepitaxy, Superlattices, Strain, and Metastability, Materials Research Society Symposia Proceedings Vol. 160, B. D. Dodson, L. J. Schowalter, J. E. Cunningham, and F. H. Pollak, eds., Materials Research Society, Pittsburgh, Pennsylvania (1990) pp. 739–744.

Z. C. Feng, S. Perkowitz, T. S. Rao, and J. B. Webb, Resonance Raman scattering from epitaxial InSb films grown by metalorganic magnetron sputtering, J. Appl. Phys. 68, 5363–5365 (1990).

A. Freundlich, G. Neu, A. Leycuras, R. Carles, and C. Verie, Heterogeneous strain relaxation in GaAs on Si (100), in Heteroepitaxy on Silicon: Fundamentals, Structure, and Devices, Materials Research Society Symposia Proceedings Vol. 116, H. K. Choi, R. Hull, H. Ishiwara, and R. J. Nemanich, eds., Materials Research Society, Pittsburgh, Pennsylvania (1988) pp. 251–256.

J. Gonzalez-Hernandez, D. Martin, and R. Tsu, Raman study of strain and microadhesion in silicon, in Spectroscopic Characterization Techniques for Semiconductor Technology, Proceedings SPIE Vol. 452, F. H. Pollak and R. S. Bauer, eds., SPIE, Bellingham, Washington (1983) pp. 44–50.

D. Kirillov, P. Ho, and G. A. Davis, Raman scattering study of mixing of GaAs/AlAs superlattices by ion implantation and rapid thermal annealing, in Materials Characterization, Materials Research Society Symposia Proceedings Vol. 69, N. Cheung and M.-A. Nicolet, eds., Materials Research Society, Pittsburgh, Pennsylvania (1986) pp. 185–190.

D. S. Knight and W. B. White, Characterization of diamond films by Raman spectroscopy, J. Mater. Res. **4**, 385–393 (1989).

P. Lao, W. C. Tang, A. Madhukar, and P. Chen, Alloy disorder effects in molecular beam epitaxially grown AlGaAs examined via Raman and Rayleigh scattering and near edge luminescence, in Spectroscopic Characterization Techniques for Semiconductor Technology III, Proceedings SPIE Vol. 946, O. J. Glembocki, F. H. Pollak, and F. Ponce, eds., SPIE, Bellingham, Washington (1988) pp. 150–154.

J. Menendez, A. Pinczuk, J. P. Valladares, L. N. Pfeiffer, K. W. West, A. C. Gossard, and J. H. English, Resonance Raman scattering in short period GaAs-AlAs superlattices, in Spectroscopy of Semiconductor Microstructures, G. Fasol, A. Fasolino, and P. Lugli, eds., Plenum Press, New York (1989) pp. 157–164.

S. Nakashima and M. Hangyo, Characterization of semiconductor materials by Raman microprobe, IEEE J. Quantum Electron. **QE-25**, 965–975 (1989).

R. J. Nemanich, D. K. Biegelsen, R. A. Street, B. Downs, B. S. Krusor, and R. D. Yingling, Strain in graded thickness GaAs/Si heteroepitaxial structures grown with a buffer layer, in Heteroepitaxy on Silicon: Fundamentals, Structure, and Devices, Materials Research Society Symposia Proceedings Vol. 116, H. K. Choi, R. Hull, H. Ishiwara, and R. J. Nemanich, eds., Materials Research Society, Pittsburgh, Pennsylvania (1988) pp. 245–250.

R. J. Nemanich, R. W. Fiordalice, and H. Jeon, Raman scattering characterization of titanium silicide formation, IEEE J. Quantum Electron. **QE-25**, 997–1002 (1989).

G. D. Pazionis, H. Tang, and I. P. Herman, Raman microprobe analysis of temperature profiles in CW laser heated silicon microstructures, IEEE J. Quantum Electron. **QE-25**, 976–987 (1989).

L. S. Plano and F. Adar, Raman spectroscopy of polycrystalline diamond films, in Raman and Luminescence Spectroscopy in Technology, Proceedings SPIE Vol. 822, J. E. Griffiths and F. Adar, eds., SPIE, Bellingham, Washington (1987) pp. 52–56.

C. J. Radens, B. Roughani, H. E. Jackson, J. T. Boyd, and R. D. Burnham, Raman microprobe analysis of strain induced by patterned dielectric films on GaAlAs structures, IEEE J. Quantum Electron. **QE-25**, 989–992 (1989).

B. Roughani, J. J. Jbara, J. T. Boyd, T. D. Mantei, and H. E. Jackson, Reactive ion etching of MBE GaAs; a Raman scattering study, in Spectroscopic Characterization Techniques for Semiconductor Technology III, Proceedings SPIE Vol. 946, O. J. Glembocki, F. H. Pollak, and F. Ponce, eds., SPIE, Bellingham, Washington (1988) pp. 146–149.

B. Roughani, H. E. Jackson, J. J. Jbara, T. D. Mantei, G. Hickman, C. E. Stutz, K. R. Evans, and R. L. Jones, Raman scattering studies of reactive ion-etched MBE (100) n-type GaAs, IEEE J. Quantum Electron. **QE-25**, 1003–1007 (1989).

J. C. Tsang and S. S. Iyer, Raman spectroscopy and the characterization of buried semiconductor layers, IEEE J. Quantum Electron. **QE-25**, 1008–1011 (1989).

J. Wagner and M. Ramstener, Raman spectroscopic assessment of Si and Be local vibrational modes in GaAs layers grown by molecular beam epitaxy, IEEE J. Quantum Electron. QE-25, 993–996 (1989).

About the authors: *Sidney Perkowitz is a Charles Howard Candler Professor of Condensed Matter Physics at Emory University and Walter M. Duncan is a senior member of the Technical Staff at Texas Instruments. David G. Seiler is Leader of the Materials Technology Group in the Semiconductor Electronics Division of the NIST Electronics and Electrical Engineering Laboratory. The National Institute of Standards and Technology is an agency of the Technology Administration, U.S. Department of Commerce.*

Volume 99, Number 5, September–October 1994
Journal of Research of the National Institute of Standards and Technology

[J. Res. Natl. Inst. Stand. Technol. 99, 641 (1994)]

Critical Issues in Scanning Electron Microscope Metrology

Volume 99 | Number 5 | September–October 1994

Michael T. Postek

National Institute of Standards and Technology, Gaithersburg, MD 20899-0001

During the manufacturing of present-day integrated circuits, certain measurements must be made of the submicrometer structures composing the device with a high degree of repeatability. Optical microscopy, scanning electron microscopy, and the various forms of scanning probe microscopies are major microscopical techniques used for this submicrometer metrology. New techniques applied to scanning electron microscopy have improved some of the limitations of this technique and time will permit even further improvements. This paper reviews the current state of scanning electron microscope (SEM) metrology in light of many of these recent improvements.

Key words: accuracy; backscattered electron; field emission; metrology; scanning electron microscope; secondary electron.

Accepted: July 22, 1994

1. Introduction

During the manufacturing of present-day integrated circuits, certain measurements must be made of the submicrometer structures composing the device with a high degree of repeatability.[1] These measurements of minimum feature sizes known as critical dimensions (CD) are made in order to ensure proper device operation. For example, the current version of the Intel Pentium[2] microprocessor operates at 66 MHz; it is reported that by reducing the CD from its current dimensions to 0.6 μm the speed of the microprocessor can be increased to 100 MHz or more [32]. The CD and other dimensions must be monitored during manufacture. Optical microscopy, scanning electron microscopy and the various forms of scanning probe microscopies are major microscopical techniques used for this submicrometer metrology. Optical microscopy, undeniably the oldest form of microscopy of the three, has been available for over 300 years. During that time, a substantial amount of maturation has gone into the methodology of optical microscopy. But, even with this time and research devoted to the development of this technique there are limitations to optical submicrometer metrology [72]. These are physical limitations based upon the properties of light. Once some of these limitations became recognized it was thought that the scanning electron microscope would then become the metrology tool of choice for submicrometer metrology. Unfortunately, limitations

[1] The term repeatability is used in this paper in place of the more commonly used term by the semiconductor industry—precision. This is because NIST has adopted the ISO definitions for metrology and its approach to measurement uncertainty [153, 154].

[2] Certain commercial equipment, instruments, or materials are identified in this paper to foster understanding. Such identification does not imply recommendation or endorsement by the National Institute of Standards and Technology, nor does it imply that the materials or equipment identified are necessarily the best available for the purpose.

also exist using this technique [86, 137]. These limitations are based upon the interaction of the electron beam with the sample. Scanning probe microscopy was then considered the "heir apparent" to the submicrometer metrology "throne." But, under scrutiny, limitations to this technique were also soon encountered [29,30,41]. These limitations include tip bending during the measurement scan, hysteresis and the need for tip characterization [29, 31]. But, are all these criticisms based upon actual limitations to the tools or are they only limitations to the knowledge of the tool? Are we only looking for a quick answer in the desperation of keeping up with a rapidly moving technology and not looking beyond? Clearly, even with over 300 years of research and development, optical microscopy remains a viable tool in the submicrometer region. Recent modifications and improvements to the optical techniques for near-field microscopy, interference and confocal scanning microscopy, have helped to extend optics further into the submicrometer measurement regime than predicted even 5 years ago. New techniques applied to the field of scanning electron microscopy have improved some of the limitations of this technique and time will permit even further improvements. The field is still open to the scanning probe instruments. Although there may appear to be physical limitations to a particular technique, clever new innovations can help to overcome the shortcomings *once they have been identified* and help to extend the applicability of the technique even further. Eventually, for each of these techniques, an insurmountable wall, based on fundamental physics, must be reached. However, none of these measurement techniques have necessarily reached this wall in the submicrometer measurement region and so all of these techniques continue to have their niche in the measurement of submicrometer structures. In many ways, they are all complementary to each other and each will remain useful for some time to come. In some instances, the strengths of two (or more) of these techniques can be combined to provide a powerful metrology tool. For example, an optical microscope has been combined with an SEM resulting in a dedicated, in-line measurement tool which is designed to accomplish rapid low magnification wafer positioning and pattern recognition optically. Then, once the wafer is properly positioned, the instrument automatically switches to the high resolution electron beam for the subsequent measurement. The combination of the SEM with a scanned probe instrument is also possible. Consequently, there is no single solution to the submicrometer metrology issue. Similarly, there is no panacea to the measurement of submicrometer structures since one instrument may work better for some applications than others [1]. Each instrument operates on physically different principles and so differences should be expected and anticipated. None of these instruments can be used blindly with the anticipation that good results will happen just because an expensive instrument has been purchased.

This review and a related paper [80] focuses exclusively on current aspects of scanning electron microscope metrology. The state-of-the-art of scanning electron microscope metrology has, in many ways, changed substantially since the topic was reviewed by this author in 1987 [86]. Scanning electron microscopy can still be viewed as a rapidly evolving field in many areas. Unfortunately, this field has also remained somewhat idle in many other ways. It is this contrast that will be reviewed in this paper. But, even as this review is being written, it should be clearly noted that, since this is a very progressive field, new technology is being developed and perhaps employed to improve this instrumentation even further.

2. SEM Specifications and Current Capabilities

The SEM is used in a number of applications inside and outside of the wafer fabrication facility (fab). These include: stepper setup [5], stepper lens characterization [129], overlay [109], inspection [55, 124], process control [100], particle analysis [26], as well as, CD metrology [4,28,58,114,119,122, 138]. The SEM is often used as the tool to which all other techniques are compared. Because of the diversity of instrument use, no universal set of specifications satisfying all needs can be defined. Some of the current, *desired* specifications for in-line and inspection SEM instrumentation are found in Table 1. This table should be considered to be somewhat generic and not specific to any particular organization. These specifications may be under or over specified depending upon SEM application (production vs development) and demands for a specific facility. This Table is also relatively consistent with specifications established by three major European IC manufacturers in collaboration with the Joint European Submicron Silicon Initiative (JESSI) [37]. The following is a discussion of *some* of the major points of Table 1.

Table 1. Typical scanning electron microscope metrology instrument specifications

Minimum predicted feature size	0.1 μm
Image resolution (@ 1.0 kV)	<8.0 nm
Accelerating voltage range	General purpose 0.5 kV to 30 kV In-Line 0.5 kV to ~2.5 kV
Magnification	100× to 300 000×
Wafer size capabilities (in mm)	100, 125, 150, 200
Cleanliness	<2 particles added/pass
Mean time between failure	>1500 h
Availability	>95 %
3*S* Repeatability (lines and spaces)	Static <5 nm Dynamic <10 nm
3*S* Repeatability (contact holes and vias)	Static <10 nm Dynamic <20 nm
Wafer throughput	>20/h
Stage speed	>50 mm/s
Pattern recognition—probability of detection	>99 %
Pattern recognition—position uncertainty	±0.2 μm

2.1 Minimum Feature Size

The minimum feature size generally specified, by most companies, for a comparison such as that found in Table 1 is 0.1 μm. Most fabrication facilities have not achieved this dimension in production. Thus, there is no need to specify for smaller structures. This does not mean that this is the smallest feature measurable by an SEM metrology instrument, *but* the minimum feature predicted to be fabricated during the life of the specified instrument. The ability of an SEM to view and measure sample structure, as small as or smaller than about 70 nm at low (1 kV) accelerating voltage is shown in Fig. 1a and at high accelerating voltage (30 kV) in Fig. 1b. Anything that can be imaged acceptably having a good signal-to-noise ratio can be, in principle, measured. Figure 1c shows a measurement of the new SEM low accelerating voltage standard prototype SRM 2090. Note that the 0.2 μm nominal linewidth is easily measured at 100 000× magnification. The accuracy and the repeatability of such a measurement are issues discussed later in Sec. 4.1 and also by Larrabee and Postek [53]. Competing technologies often cite that the SEM cannot measure below this 0.1 μm minimum feature size, but this is clearly not the case.

2.2 SEM Resolution

The achievable resolution of the SEM has improved substantially over the past 5–10 years. Improvements in electron sources, lenses and electronics have contributed greatly to this advancement, as discussed below. The resolution attainable relates to many factors other than just the instrument capabilities including the composition of the specimen being observed or measured [44,46,78,86]. As shown in Table 2, achievable resolution also depends upon the type and design of the instrumentation being discussed. In recent years, instrument design has gone through a rapid evolution. Generally, an in-line metrology instrument should have 8 nm resolution (or better) at 1 kV accelerating voltage. The European initiative [37] has gone even further and set the goal to be 6 nm at 1 kV accelerating voltage. The determination and maintenance of this performance level is an issue that will be discussed further in Sec. 4.3.2.

2.3 SEM Accelerating Voltage Range

Nondestructive SEM operation [64,58,83] generally restricts the metrology instrument accelerating voltage to an arbitrary range from about 0.5 kV to about 2.5 kV. Several dedicated in-line metrology instruments are restricted, by design, to this or a slightly higher range. For special purposes, the accelerating voltage can go higher and if a device will not be damaged or charged the higher accelerating voltage can yield higher signal and instrument resolution. Many laboratory and some on-line SEM instruments routinely operate throughout the accelerating voltage range of 0.5 kV to 30 kV (or even 50 kV). What is important is performance in the nondestructive region of the accelerating voltage range for a particular device and not necessarily the specification listed in Table 2, as this can be very instrument and application specific and so the wider range is also listed in Table 2.

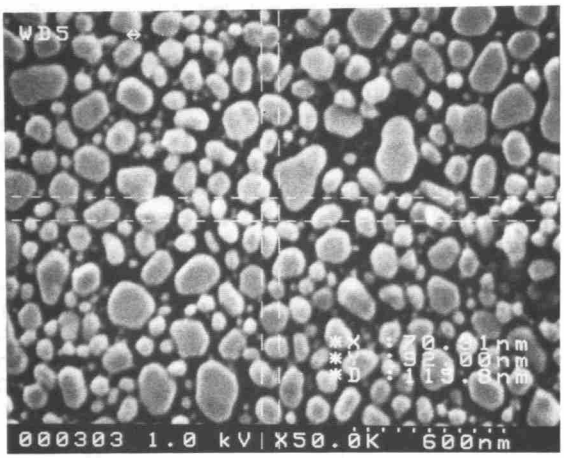

a

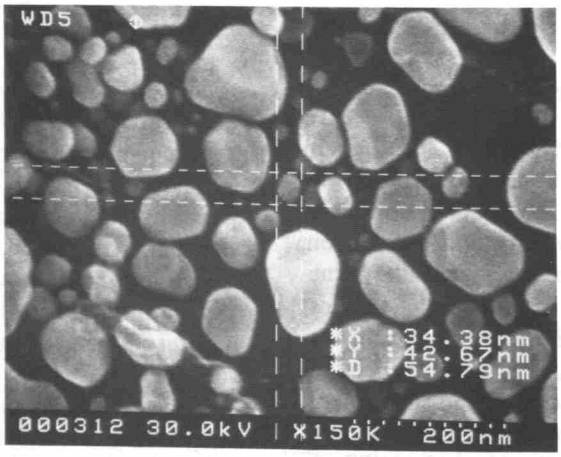

b

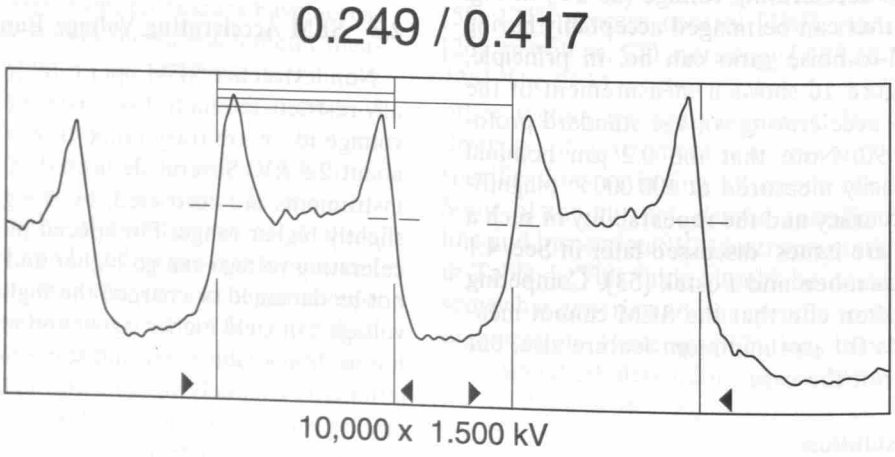

c

Fig. 1. SEM resolution and measurement capabilities. (a) High magnification, low accelerating voltage (1.0 kV) image showing the measurement of a 70.3 nm gold structure at 50 000× magnification; (b) high magnification high accelerating voltage (30 kV) image showing the measurement of a 34.38 nm gold structure at 150 000× magnification; (c) measurement of a 0.2 μm nominal line (0.249 μm width, 0.417 μm pitch) with the new NIST SRM 2090 prototype sample from the SEM interlaboratory study with a field emission measurement instrument (courtesy of AMRAY, Inc.).

Table 2. SEM achievable resolution

Detector position	Accelerating voltage	In-Lens FE	Extended field FE	Post-Lens FE	Post-Lens LaB_6	Post-Lens tungsten
Upper	30.0 kV	0.7 nm	1.5 nm			
	1.0 kV	3.5 nm	4.5 nm			
Lower	30.0 kV			1.5 nm	2.5 nm	3.5 nm
	1.0 kV			5.0 nm	7.5 nm	10.0 nm

2.4 Magnification

Metrology, in an SEM, is fundamentally done by identifying two picture elements or pixels in a digitized image and then determining the distance between them. The lateral resolution of the measurement system is fixed by the number of pixels comprising the digital electronics (see Sec. 3.2). Calibration of the SEM magnification effectively determines a known column scan (see Sec. 4.3.1) in both the X and the Y directions. The scan width divided by the number of pixels of the measurement system yields the pixel width or measurement unit. In instruments with a fixed number of pixels (i.e., 512 or 1024), the higher the magnification (relative to the micrograph), the smaller the area on the sample this pixel represents. It is therefore advantageous to make measurements at the highest magnification possible in order to obtain the smallest measurement unit and thus the most sensitive measurement (where the measurement system is concerned). In order for the measurement be meaningful, the pixel size must be less than the required repeatability (Table 1) in order for the instrument to be sensitive to the measurement and that the measure of instrumental repeatability be meaningful [53]. For example, at 50,000× magnification (on a typical micrograph) the pixel width is equal to about 2.25 nm on the sample for a 1024 digital measurement system; twice that size for a 512 digital measurement system. Furthermore, the SEM must also have the resolution, and thus the sensitivity, to detect structural differences at that magnification, or the result is just empty or useless magnification and insensitive measurements (see Sec. 4.3.2).

2.5 Measurement Repeatability

The 3 standard deviation or 3S repeatability [52, 53] of measurements made with the metrology instrument is generally specified to be at least 1 % of the feature width. This also implies that the feature being measured has a structure variation less than the instrument's repeatability so that the data is sensitive to instrument repeatability and not the converse [53]. One interesting factor that one must consider when comparing the repeatability of an optical metrology tool to that of the SEM metrology tool is that each instrument is unique in the measurement process. An optical tool can average as much as 1 μm to 2 μm along a line in a single measurement scan depending upon the instrument design. In contrast, a single SEM measurement scan obtains information from as little as only a few tens of nanometers. It would take multiple SEM line scans to average the same sample area. Therefore, any variability of the sample, along the line, is averaged more in the optical measurement than in a typical SEM measurement. Consequently, on the surface it would appear that SEM measurements were less repeatable than optical microscope measurements, but only because the SEM measurements were more sensitive to changes in the sample [53]. Many factors influence the measurement repeatability of the SEM. A number of these factors have been discussed previously [86] and others are discussed in later sections of this paper. One factor that has *not* been fully explored that might improve measurement repeatability is data oversampling. One difficulty automated measurement systems have is the reproducible determination of edge position. Having more data points available in the proximity of the edge improves the repeatability of the determination of the location of the edge and thus the measurement. The concept of data oversampling was shown to be highly successful in an earlier study on x-ray lithographic masks [92, 93]. Unfortunately, obtaining more data may impact throughput which leads to the age old question: "Is the goal to obtain good data or fast data?"

2.6 Throughput

Rapid processing of wafers through an instrument provides a financial advantage to the user. Clearly, one of the main driving forces for the specifications in Table 1 is throughput. Cost-of-owner-

ship modeling [10, 50] has placed a great deal of emphasis on wafer throughput and thus a great deal of engineering effort has been spent on this facility [132]. It must be emphasized that the ideal number of 20 wafers per hour listed in the Table depends greatly upon the sampling plan employed. It should also be noted that an instrument with high throughput but poor overall resolution or measurement sensitivity provides no advantage at all.

2.7 Availability and Mean Time to Failure

Availability or uptime of a metrology tool for most production fabs is required to be greater than 95 %. This should also be expected for any modern laboratory instrument, not just those in the wafer fabs. If the instrument is unavailable due to a failure, maintenance, or lack of availability of parts, the instrument is considered to be down and unavailable for use by some definitions. If an instrument cannot do its assigned job function, money is lost since the production line is delayed. Similarly, in a laboratory situation a down instrument may cost the facility money due to delayed work or lost revenue from canceled laboratory appointments, providing embarrassment to both the user and the instrument manufacturer or service organization. Such a broken instrument or a "hard down" situation (e.g., a filament failure) is obvious and easily determined. But what about a subtle down condition when the instrument is apparently functioning normally, but the measurement data generated is marginal because of a resolution, or sensitivity loss? How and at what frequency is this checked? More on this topic is presented in Sec. 4.3.2.

2.8 Particles

Particle metrology and characterization is now becoming a growing field. Particles are a bane of semiconductor processing [3, 74]. The SEM has numerous moving parts. Each can generate particles through wear mechanisms. As the wafer is transferred into and out of the system, particles can be generated from contact with the wafer transfer machinery. Movement of the wafer into and out of the vacuum causes some degree of turbulence which can mobilize particles possibly depositing them on the wafer surface. Particles can also be formed by temperature and pressure changes during the sample exchange process leading to water vapor condensation, droplet formation and liquid-phase chemical reactions [52]. Modern SEM instrument design minimizes particle generation [74]. Specifications found in Table 1 indicate that the inspection instrumentation should induce fewer than two particles per wafer pass. Clearly, the size of the wafer, as well as the size of the particles, must also be considered in such a specification in order to make it meaningful to a specific process. Reduction of particle generation is also important to the performance of the instrument since a charged particle landing on a sensitive portion of the instrument can rapidly compromise the resolution of the SEM, especially at low accelerating voltages.

2.9 Measurement Scan Linearity

Historically, the SEM does not necessarily do flat field scanning [107]. It is imperative that any measurements made with this instrument be made in the center of the scan field. It is also imperative that little or no scan shift be used (unless fully tested) for the same reason. This ensures that the measurement is done in the most linear part of the scan. Desired European specification indicates a scan linearity of 10 nm ($3S$) as measured on 7 points on the SEM monitor [37]. However, it should be clearly noted that it is not the display monitor scan linearity that metrologists should be concerned with, but the measurement scan linearity.

3. Instrumentation Improvements

The scanning electron microscope metrology instrument has undergone a number of design improvements during the past few years. Many of these improvements have been generally applicable across the board in the field of scanning electron microscopy and some of them have been specific to semiconductor processing applications. Improvements in: electron sources, digital imaging, lens designs and electron detectors are four areas where fundamental design improvements have been instrumental in improving submicrometer SEM metrology, as well as the entire field of scanning electron microscopy.

3.1 Improved Electron Sources

In 1987, when the first review of the topic was done by the author [86], the predominant electron sources were the thermionic emission type cathodes, especially tungsten and lanthanum hexaboride (LaB_6). Lanthanum hexaboride filaments became more prevalent for low accelerating voltage applications because of the increased brightness

and decreased source diameter in comparison to tungsten filaments (Table 3). Cerium hexaboride (CeB_6) is a new innovation which is similar in performance to the lanthanum hexaboride filament [12]. Point-cathode electron sources or field emission instrumentation were available for semiconductor processing, but the concept was still in its infancy at the time of the earlier review and few commercial instruments were available with that capability. Today, a wide variety of both laboratory-type and in-process type instruments are commonly available with field emission technology. For most in-line semiconductor processing applications, only the field emission instruments provide the high resolution necessary for this type of work, especially at the low accelerating voltages needed for nondestructive inspections (Table 2). In the near future other electron sources, such as nanometer-sized field emission tips, may also become available [96,97,120,121].

Table 3. Comparison of pertinent electron source characteristics

	Unit	Tungsten filament	LaB_6 filament	CeB_6 filament	Cold field emission filament	Schottky field emission filament
Reference number		99	14, 76	12	75,99,134 136, 143	75,99,125 126, 134 135, 136 139
Angular current intensity	mA/sr	n/a	n/a	n/a	<0.1	0.1 to 1.0
Source brightness	A/(cm²·sr)	10^6	10^7	10^7	10^9	10^8 to 10^9
Emitting surface area	μm²	>>1	>1	>1	0.02	0.2
Crossover or virtual source diameter	nm	$>10^4$	$>10^3$	$>10^3$	3 to 5	15 to 25
Energy spread	eV	1 to 3	1 to 1.5	1 to 1.5	0.2 to 0.3	0.3 to 1.0
Source temperature	K	2500 to 2900	1800	1800	300	1800
Work function	eV	4.5	2.6	2.4	4.5	2.8
Operating vacuum	Pa	10^{-4}	10^{-6}	10^{-6}	10^{-9} to 10^{-11}	10^{-8} to 10^{-9}
RMS short term beam current stability	%	<1	<1	<1	4 to 6	<1
Typical service life	h	40 to 100	1000	>1500	>2000	>2000

3.1.1 Point-Cathode Electron Source Types There are two basic categories of point-cathode electron source types used in the current SEM metrology instruments: Cold cathode Field Emission (CFE) and Thermally-assisted Field Emission cathodes (TFE). Although the concept of field emission can be traced to the early work of Wood [150] and was used in early instrumentation by Zworykin et al. [152], it was not until the late 1960s that Crewe and his coworkers [15] developed a successful cold cathode field emission source that was later introduced into commercial instrumentation [145,146]. CFE has had a relatively long history in scanning electron microscopy and SEM metrology and was the first type of field emission cathode to be applied to semiconductor processing instrumentation. Thus, CFE dominates the field by sheer numbers of instruments.

For many applications, such as analytical microscopy and microfabrication, the CFE was not capable of producing the high currents and large spot sizes needed [59,75]. Work to develop a high current thermally assisted field emission cathode with relaxed vacuum and environment requirements was then begun [127,128,133,147]. There have been several designs of thermally assisted field emission cathodes developed. The two major types are: the Tungsten <100> built-up Emitter (TE) and the ZrO/W <100> cathode Shottky Emitter (SE). At the current time, the ZrO/W is the more commonly used of the two types of thermally assisted field emission source in modern laboratory and SEM-based metrology instruments.

Instruments utilizing either CFE or SE currently populate the SEM metrology field. Each type has its advantages and disadvantages. It is up to the informed user to test and to determine the type of source that suits the application. The characteristics of the various electron sources, as they are currently understood, including CFE and SE, are summarized in Table 3 and are briefly discussed below.

Field Emission Cathodes

Cold field emission cathodes, developed for use in the scanning electron microscope by Crewe and co-workers [15], have an advantage of providing a relatively high-current electron probe having a low energy spread, high brightness, and a small virtual source diameter, especially at low accelerating voltages. The CFE source diameter is sufficiently small that the electron gun alone (as shown in Fig. 2) without any additional condenser lenses is capable of producing a 10 nm probe [17, 18]. From Table 2 it can be observed that depending upon the type of instrument design, better than 1 nm resolution may be reached with an instrument equipped with a field emission electron source. The overall advantages afforded by CFE are offset somewhat by the rigorous requirements for ultra-high gun vacuum (Table 3) and some fluctuation (flicker) in the emission current. The emission current fluctuation is readily compensated for by constant beam monitoring and feedback control [13,115,116], and also (with the newer instruments) through digital frame averaging, and in general, is not an issue of concern.

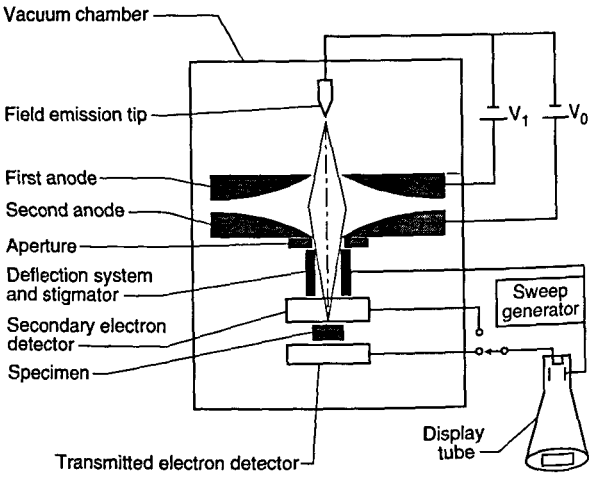

Fig. 2. Cold field emission electron microscope column of the design of Crewe et al. (redrawn from Crewe et al., 1969).

Schottky Emission

The second basic category of point-cathode electron sources is the thermally assisted field emission cathode. In this mode of operation, the cathode is heated and thus vacuum requirements are reduced and the emission current is relatively stable [134]. Because of its lower work function, the use of the Schottky point emitter (SE), such as the Zirconiated/tungsten <100> (ZrO/W) point cathode [134], is preferred. This source can produce a high current electron beam with a slightly poorer energy spread. This differs from cold field emission by an amount as small as about 8 % to 10 % depending upon how evaluation criteria are established [134, 136]. Since this source is currently being used for a number of different applications, the operational characteristics and parameters of the source are quite varied. Thus it is quite difficult to tabulate a direct comparison of source characteristics. For SEM metrology applications the SE source is generally operated with conditions resulting in the lowest energy spread (0.3 eV) possible for that type of

source. Under these conditions using test samples, comparable resolution (as related to image sharpness as discussed in Sec. 4.3.2) to similarly equipped CFE instruments has been obtained (Fig. 3). Unlike the CFE, the larger source diameter characteristic of this type of electron source requires the use of an extra condenser lens in the electron microscope column in order to increase the source demagnification. The need for increased demagnification also provides a positive secondary effect since it also results in increased demagnification of external noise such as vibration and fields affecting the source.

3.2 Improved Digital Image Storage and Image Analysis

Another of the major advancements applied to SEM metrology during the past few years has been the incorporation of digital imaging technology. Advancements in semiconductor technology, notably the availability of less expensive, high-density memory chips and the development of inexpensive high speed analog-to-digital converters, mass storage, and high performance central processing units, have fostered this revolution. Today, most modern SEM metrology instruments have digital electronics as a standard feature. These instruments generally have 8 bit or 256 gray levels, with *at least*, 512 pixel by 512 pixel density operating at TV rate. Many of the more modern metrology instruments operate at either 1024 by 1024 or higher pixel density and at least 10 bit or higher gray levels [87]. In addition, current slow-scan commercial frame-grabber cards, directly applicable to the SEM, can have upwards of 12 bit to 14 bit lateral resolution, which permits image acquisition and measurement at 4096 by 4096 resolution or greater [87]. Pre-digital electronics metrology SEMs were plagued by the problem of having a poor signal-to-noise ratio, especially at low accelerating voltages and TV scan rates. Recent developments in field emission filament technology improved that situation, but parallel development of the modern digital imaging technology brought both of these technologies together into an extremely powerful tool with exceptional flexibility. Some of the advantages afforded by digital imaging include:

3.2.1 Pattern Recognition Rapid transfer of the wafers within an in-line instrument requires a rapid, accurate, pattern recognition system for high throughput. Depending upon the system design, the pattern recognition process can be accomplished either with an optical system, the electron beam system, or both in conjunction. In actual use, the

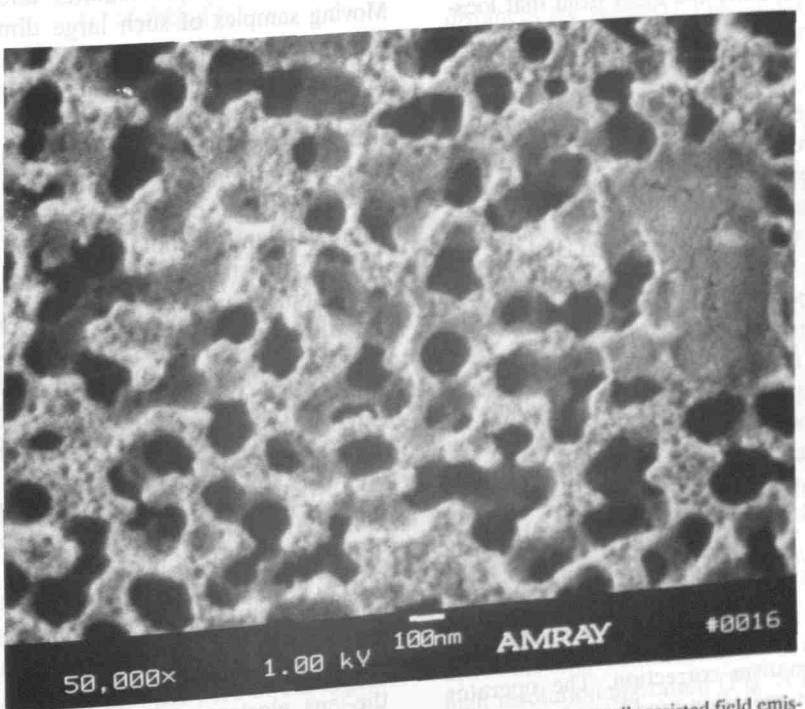

Fig. 3. High resolution low accelerating voltage imaging using a thermally assisted field emission electron source (courtesy of AMRAY, Inc.).

probability of detection is often highly substrate dependent. For current metrology instruments, this leads to one of the major causes of measurement variability (Table 1).

3.2.2 TV Rate Scanning TV rate scanning is not new to SEM, but previously this type of operation had to be done at increased beam currents and thus reduced resolution in many instruments. Today, essentially the "slow scan" presentation of the SEM is gone and is replaced with a flicker-free, real-time TV image. Digital integration of poorer signal-to-noise images is transparently accomplished by frame buffering and frame averaging of the video signal. TV rate scanning has also been shown to be useful in the reduction of charging on many samples [146].

3.2.3 Digital Image Storage Image archiving of the digital images, either to floppy disk or hard disk, provides a permanent record that is inexpensive and easy to retrieve. Image quality is identical to the originally stored image. Standardized file storage such as the TIFF (or other) file format can enable importation of the images into desk-top computers, particularly statistical analysis and word processing programs (see Sec. 4.7).

3.2.4 Paperless Image Transmission The image and measurement data can be transmitted via data lines to remote locations. It is conceptually possible to view the SEM image from a remote location and actually operate the SEM from that location in real-time. Today, the production engineer does not have to be suited-up in the wafer fabrication facility in front of the instrument to view the wafers or measurement results, or for that matter to operate the instrument.

3.2.5 Real-Time Image Analysis/Processing Digital enhancement of the image can be done transparently, as the image is acquired, and the image and data can be processed at the SEM console. It should be noted that in many laboratory and metrology instruments the signal undergoes some processing as it is transported through the video chain. The operator may not even be provided with the ability to view the "raw" data. Blindly allowing the image or data to be processed should be approached with caution and raw data should always be able to be obtained from a metrological instrument.

3.2.6 Optimization of Operating Conditions Digital SEMs can automatically optimize the operating conditions, such as the brightness, contrast, focus, and astigmatism correction. The operator can save optimum operating conditions for a particular sample class, then reload them as needed. Many of the instrument parameters that need to be changed when instrument conditions are altered can be changed automatically through look-up tables.

Until a few years ago, digital imaging was severely limited by the power, memory, and cost of the computer systems available, and, therefore, much of the digital imaging was done externally through interfacing to a powerful minicomputer coupled to an x-ray microanalysis system. Today, many desktop computers have computing capabilities surpassing these early minicomputers. Computer systems are now small and inexpensive enough to be directly incorporated into the SEM electronics console as a standard component by the SEM manufacturer. This concept presents a major advantage because the digital architecture of modern SEMs now permits the application of a whole host of peripheral technologies associated with, and being developed for, the personal computer industry to be readily applied to the SEM and SEM metrology.

3.3 Improved Lens Design

The semiconductor wafer samples being viewed in the scanning electron microscope metrology and inspection instruments are by their nature quite large. Instruments are being designed to accommodate up to 200 mm diameter and larger wafers. Moving samples of such large dimensions rapidly within the specimen chamber, in vacuum, has been a difficult engineering problem. Not only did specimen chambers and stages need to be increased in size and travel, but also final lens technology required improvement.

At the time of the earlier review [86], flat "pinhole" lens technology predominated (Fig. 4a). This was the state-of-the art of the instrumentation at that time. Later, 45° and 60° conical lens technology with improved low-accelerating voltage performance began to improve the manipulation and viewing of the wafer within the specimen chamber (Fig. 4b and Fig. 4c). However, these were still pinhole-type lenses and limitations imposed by the sample/lens geometry on the instrument resolution remained. For example, even a 60° conical lens having a broad front face would still be restricted to rather long working distances with highly tilted samples. Two improvements in lens design directly applicable to the in-line wafer instrumentation were introduced. The first improvement was through-the-lens electron detection and the second was extended-field lens technology.

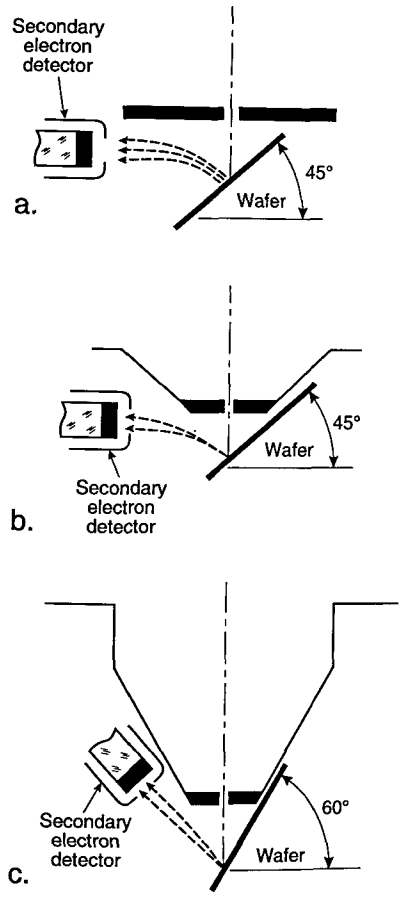

Fig. 4. Drawing of the comparison between different types of "pinhole" lenses. (a) Early version flat lens; (b) 45° conical lens; (c) 60° conical lens.

3.3.1 Through-The-Lens Electron Detection The term "through-the-lens detection" relates to the fact that signal electrons are transported back through the lens that focused the primary electron beam on the sample; this concept has been reviewed by Kruit [49]. Pinhole lenses have always been restricted in that the space between the lens and the sample had to be shared by the electron detector (Fig. 5a). Therefore, in typical SEM applications, some open working distance between the final lens and the sample surface is required to permit electron collection. Scanning transmission electron microscopes have, for many years, been able to place specimens directly into the bore of the objective lens, effectively immersing the sample into the lens field at essentially very short working distances. Unfortunately, the space in the lens is quite small and restricts the size of the specimen to be viewed to a few millimeters. The immersion lens concept and the through-the-lens electron collection technique was adapted into ultra-high resolution scanning electron microscopes (Fig. 5b). In this configuration, secondary electrons were caught in the field of the lens and drawn upward to be collected by the detector placed above the lens. However, the sample size restriction remained. Opening up the bore of the final lens and placement of the electron detector into the space above the lens also improved this geometry for normal SEM operation. In some instances, a small sample could even be carefully raised into the final lens bore for higher resolution (Fig. 5c). These solutions allowed shorter working distances, even for larger samples, and thus higher source demagnification and attainable instrument resolution. This approach proved to be very successful for in-line wafer metrology instruments since there is no need for sample tilting; thus the wafers could be viewed at short working distance with high resolution and signal collection. Many in-line metrology instruments are based upon this concept (Fig. 6).

3.3.2 Extended-Field Lens Technology It is well known that to obtain the highest resolution in scanning electron microscopy, the shortest working distances are required. Placing the sample into the bore of the final lens near the principal plane of the lens is another alternative (as discussed above), but such an approach is limited to very small samples. Mulvey [67] proposed the design of a new type of lens, referred to as a snorkel lens, where the imaging magnetic field of the lens extends entirely beyond the lens structure. In essence, rather than placing the specimen into the bore of the lens, the lens extends the field toward the sample. Employing an inverted snorkel or extended-field type lens as the final lens of the scanning electron microscope enables a large sample to be essentially immersed in the field of the lens external to the bulk of the lens (Fig. 7). Because of the very short working distance resulting from this lens concept, high resolution is possible, especially if through-the-lens electron collection is also employed (Table 2). For laboratory and inspection instruments, a secondary electron detector could be placed in the sample chamber as in the conventional design (Fig. 5a) and also placed above the lens for extremely short working distance, high resolution operation (Fig. 5c). Either detector

could be used depending upon the need. Fig. 8, shows a graphical comparison of a field emission laboratory-type instrument with "pinhole" lens technology to one having extended field lens technology (with two detectors – upper and lower – as described previously). Apparent in the graph is the substantial improvement in resolution possible with this technology, which approaches that of the ultra-high resolution in-lens instrument. Effectively, instruments with this technology can now resolve as well at low accelerating voltage (1.0 kV) as instruments equipped with lanthanum hexaboride can resolve at high accelerating voltage (Fig. 9).

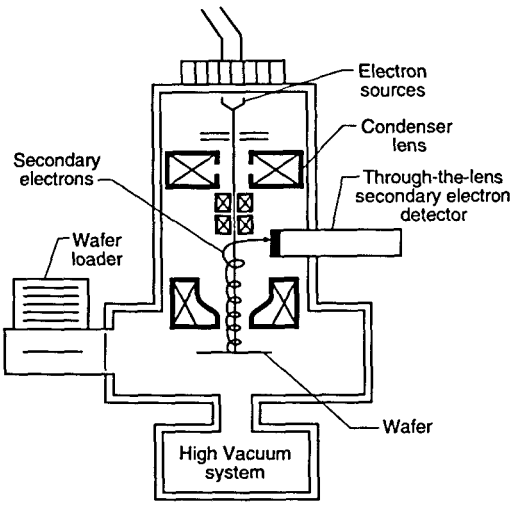

Fig. 6. Drawing of a typical metrological SEM with "through-the-lens" electron detection (redrawn after Hitachi).

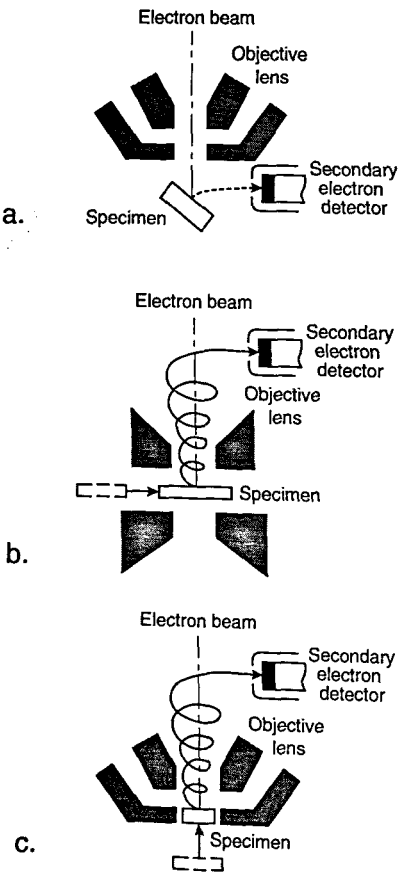

Fig. 5. Comparison of SEM final lens design. (a) Conventional flat lens technology; (b) in-lens SEM technology showing the detector above the lens; (c) conventional SEM with in-lens capability.

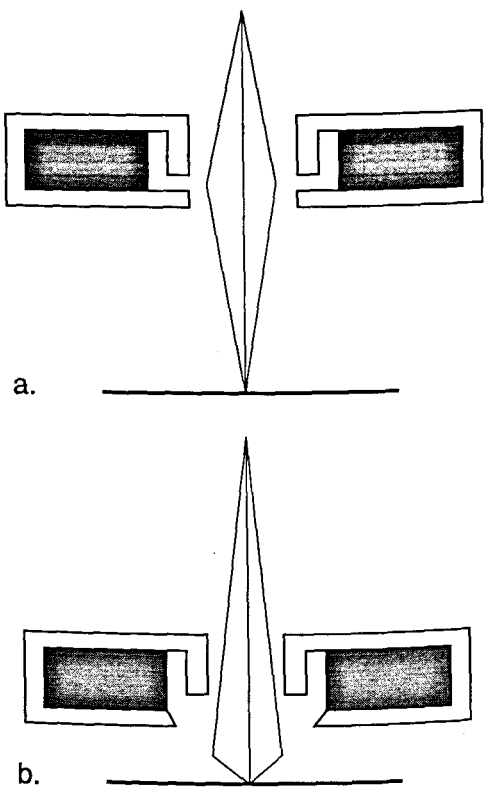

Fig. 7. Extended-field lens technology. (a) Standard lens technology; (b) extended-field lens technology where the focusing field is extended beyond the bulk of the lens, thus permitting short working distances with large samples.

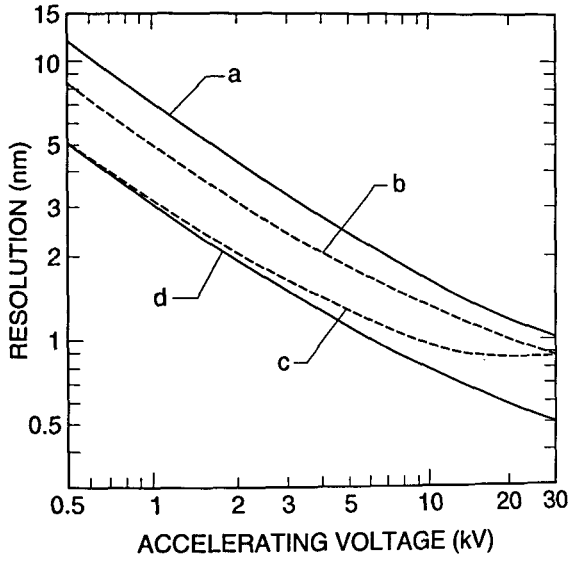

Fig. 8. Graphical comparison of the calculated resolution capabilities of different designs and applications of field emission scanning electron microscopes. (a) Standard "pinhole" type final lens with the secondary electron detector in the "normal" location within the specimen chamber; (b) extended-field lens with the electron detector in the "normal" location; (c) extended-field lens with the detector positioned above the lens; (d) in-lens ultra-high resolution instrument (courtesy of Hitachi Scientific Instruments).

3.4 Improved Electron Detection Capabilities

At the time of the first review of SEM metrology [86], most of the scanning electron microscopes used the common Everhart/Thornley (E/T) detector [25], or a variation, as the main detection system for secondary electron imaging. The original detector had a positively biased grid for the collection of secondary electrons, and this design has served well for over 25 years for general purpose SEM operation. Unfortunately, this detector design is generally quite large and intrusive in the specimen chamber (Figs. 4 and 5). Furthermore, the varied applications of the modern scanning electron microscope have, in many ways, been expanded beyond the capabilities of this detector system, especially for low accelerating voltage studies and for SEM metrology. When the picoampere beam currents characteristic of nondestructive, low accelerating voltages are used, the performance of the E/T detector degrades and yields a poor signal-to-noise ratio. The E/T detector also suffers from alignment difficulties, often because of its non-coaxial mounting position with respect to the sample and the electron beam, or the uneven distribution of the collection field. It is imperative to metrology that the signal being measured be symmetric. Asymmetric signal collection is especially troublesome where linewidth measurements of microcircuit patterns are being made [73, 113]. These limitations, and others, have led recent investigators to reconsider secondary electron collection mechanisms and detectors. In order to improve the electron collection geometry, Volbert and Reimer [140] and Suganuma [123] proposed using two opposed E/T detectors to improve signal collection efficiency and symmetry. Other workers have placed the electron detector on-axis with the electron beam in the tilt plane in an effort to improve collection symmetry [73]. Schmid and Brunner [117] developed a quadruple electron detector for use as a high efficiency electron detector for low accelerating voltages. Other workers [88,89,112,113,114] proposed using microchannel-plate (MCP) type detectors (Fig. 10a) and this detector proved to be quite successful. Since that time, MCP detectors have been used extensively in many SEM metrology applications. As shown in Figs. 10b and 10c, these detectors can be used to collect the "secondary" electron image or the backscattered electron image (see Sec. 3.4.1). The MCP detector can be placed above the sample in the specimen chamber or even into the microscope column as an in-lens detector [66].

3.4.1 Backscattered Electron Detection Technology, Collection, and Measurement The "secondary" electron signal, usually collected and measured in the SEM, is composed not only of those secondary electrons generated from initial interaction of the electron beam as it enters the sample (SE-1), but also of secondary electrons generated by the escape of elastically and inelastically scattered electrons when they leave the sample surface (SE-2 and SE-3). The emitted backscattered electrons (BSE) can interact singly or multiply with other structures on the sample or other internal instrument components and generate more secondary electrons; they can also be collected as a component of the secondary electron image if their trajectory falls within the solid angle of collection of the electron detector [22, 79].

A fourth contribution of secondary electrons (SE-4) to the signal results from the interaction of the primary electron beam with internal column components (i.e., apertures). The magnitude of the SE-4 contribution is generally small and is instrument specific. It has been calculated that the number of remotely generated electrons (i.e., energy less than 50 eV) is much larger than those generated from the primary electron beam interaction by a factor greater than three [118]. Peters [79] has measured the components of the secondary

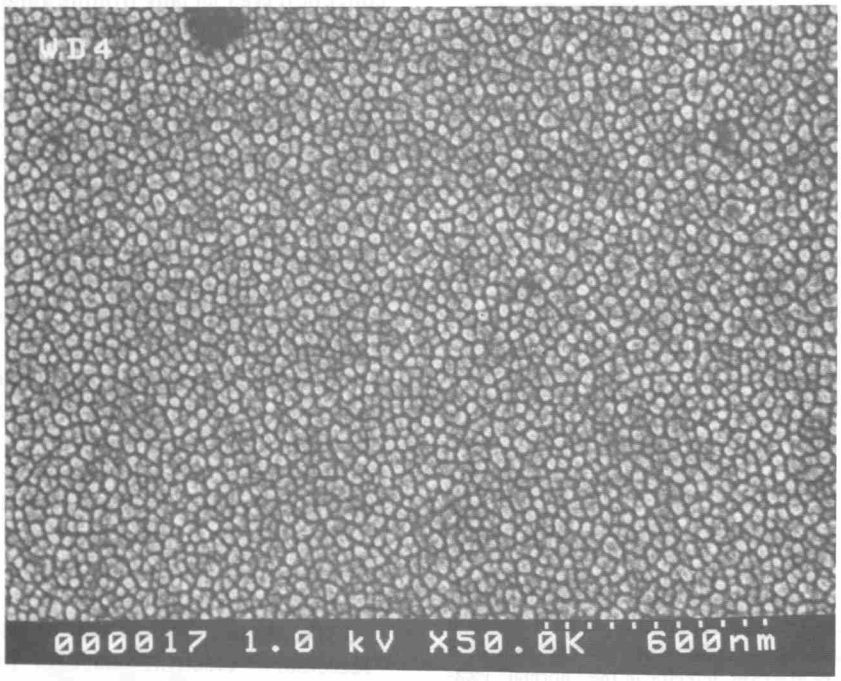

a

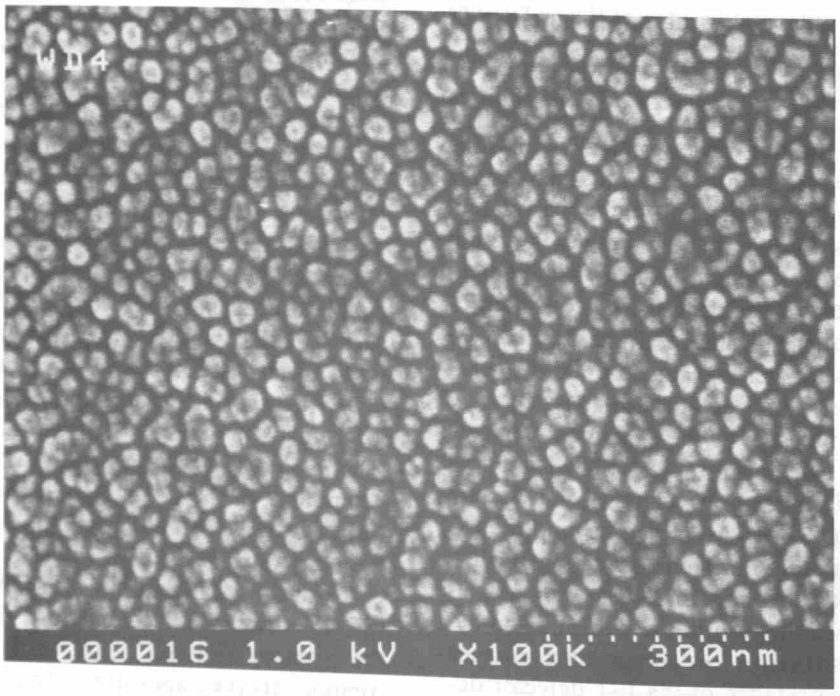

b

Fig. 9. Low accelerating voltage (1.0 kV), high resolution image using an instrument with extended field technology the sample is "grass" on a silicon wafer, (a) Lower magnification image taken at 50 000× and (b) higher magnification image taken at 100 000×. (Courtesy of Hitachi Scientific Instruments.)

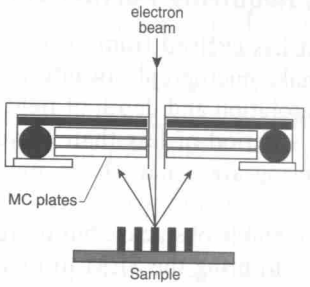

a

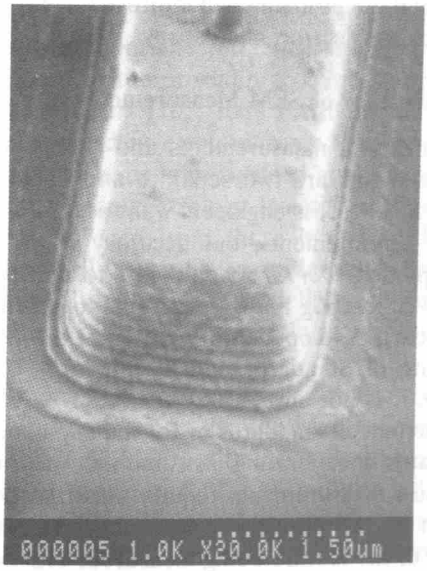

b

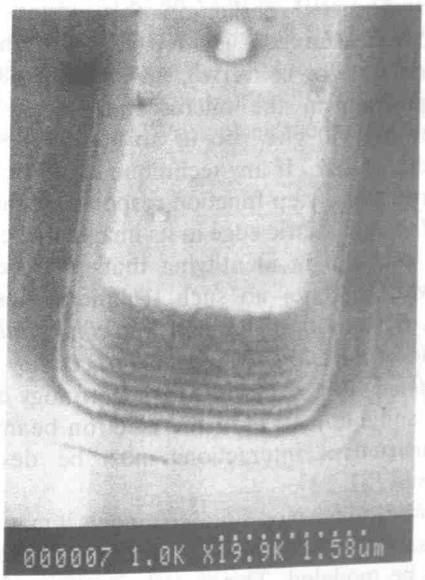

c

Fig. 10. Microchannel-plate electron detector. (a) Drawing of the detector showing its coaxial placement above the sample; (b) secondary electron image; (c) backscattered electron image.

electron signal from gold crystals and has found that, depending upon the sample viewed, the contribution of the SE-2 is approximately 30 % and the contribution to the image of the SE-3 electrons is approximately 60 % as compared to the approximately 10 % of the image contributed by the SE-1 derived signal. The standard Everhart/Thornley type secondary electron detector does not discriminate between these variously generated electrons and thus the collected and measured secondary electron signal is composed of a combination of all these signal forming mechanisms. The difficulties in interpreting this composite signal can lead to measurement errors that can be highly variable and that have a strong dependence upon sample composition, sample geometry, and to a lesser or greater extent (depending on instrument design), upon other physical factors such as an instrument's internal geometry that induces anomalies in the detector collection field (i.e., stage motion). Furthermore, since this signal is highly variable and often instrument specific, it is extremely difficult to model.

Relative to the pure backscattered electrons, early workers with the SEM were concerned mainly with imaging and not metrology. Metrological applications often require a different way of thinking and operation. These workers considered all the signal derived from the backscattered electrons to be low in resolution, generally providing only atomic number information and background to the image. Wells [148, 149], using the low-loss method for several classes of materials (including photoresist), demonstrated that this concept was inaccurate, and that high-resolution imaging of backscattered electrons could be done under specific conditions. The behavior of the backscattered electrons has also been modeled by Murata [68, 69], who showed that there is a predominant component of the backscattered signal that is unscattered and high in energy and is therefore believed to carry high resolution information. The high resolution potential of the backscattered electron signal was also later experimentally demonstrated using the converted backscattered secondary electron (CBSE) technique at high accelerating voltages [65,66,101,141]. Later, using field emission instrumentation at low accelerating voltages, the CBSE technique was used successfully by Postek et al. [91] to obtain high resolution images, low accelerating voltage backscattered electron images of uncoated photoresist (and other samples). The concept of the high resolution nature of the backscattered electron image is further supported by the work of Joy [45] who demonstrated that the relative nature of the secondary

electrons and backscattered electrons can be inverted at low accelerating voltages. In low atomic weight samples such as photoresist or polyethylene, the depth of information represented in the backscattered electron image is about 0.3–0.5 times the electron range [43], while the secondary electron image corresponds to about three times the mean secondary electron escape depth [45]. This results in a potential loss of surface detail in the secondary electron image, due to the longer escape length of the secondary electrons at low accelerating voltages relative to that of the backscattered electrons. This can also result in measurement variability. Differences between measurements using the backscattered electron signal and the secondary electron signal have also been demonstrated [87, 90]. In one instance, on a nominal 2.5 μm silicide on silicon line at 30 keV accelerating voltage, measurement broadening associated with a width measurement of the standard secondary electron signal was shown to be 0.2 μm larger than the backscattered electron signal derived from the same sample under similar conditions. It was also demonstrated, in that same study, that under the experimental conditions chosen, the measured backscattered electron signal was less prone to random variations, thus improving its measurement repeatability compared to the secondary electrons. With the microchannel-plate electron detector, Postek [81] demonstrated that backscattered electrons derived from a low accelerating voltage electron beam could be collected and measured. Comparison measurements of the secondary and the backscattered electron images using the same MCP detector showed results similar to the earlier study [90]. Again, the measured values of the structures using the backscattered electron signal were smaller and had less variability. The backscattered electron signal did not demonstrate the measurement broadening effect shown by the collection of the secondary electrons. Backscattered electron measurement capabilities have been recently been adopted in in-line metrology instruments for linewidth measurement and the measurement of contact holes [66]. To date, the use of the backscattered electron signal has yet to be fully implemented in SEM metrological applications largely because of the weak signal generated at low accelerating voltages. However, the distinct advantage presented by this mode of operation, in contrast to the "secondary" electron detection mode, is its ability to be readily modeled, thus providing the potential for accurate metrology (see Sec. 4.1.1).

4. Areas Requiring Further Improvement

The SEM has evolved from an instrument used mainly to make micrographs of interesting samples with high resolution and depth of field to a metrology tool in a period of less than 10 years. During this time, many areas have been improved; however, others still require work. These problems are not insurmountable obstacles, but do require attention in order to bring the SEM to its full potential as an accurate metrological tool. As with the previous improvements found in Sec. 3, attention to many of these problems will improve the entire field of scanning electron microscopy.

4.1 Accuracy of SEM Measurements

Accuracy of measurements and repeatability of measurements are two separate and distinct concepts [53]. Process engineers want accurate dimensional measurements, but accuracy is an elusive concept that everyone would like to deal with by simply calibrating their measurement system using a standard developed and certified at the National Institute of Standards and Technology. Unfortunately, it is not always easy for NIST to calibrate submicrometer standards or for the engineer to use standards in calibrating instruments. Accurate feature-size measurements require accurate determination of the position of *both* the left and right edges of the feature being measured. The determination of edge location presents difficulties for all current measurement technologies because of the reasons discussed earlier in this paper. Since linewidth measurement is a left-edge-to-right-edge measurement (or converse), an error in absolute edge position in the microscopic image of an amount ΔL will give rise to an additive error in linewidth of $2\Delta L$. If any technique could be found that produces a step-function response at the location of the geometric edge in its image, there would be no problem in identifying that edge position. However, to date, no such technique has been found. *Without an ability to know with certainty the location of the edges, measurement accuracy cannot be claimed.* For accurate SEM metrology to take place, suitable models of the electron beam/specimen/instrument interactions must be developed and used [52, 53].

In order to develop suitable models it may also be necessary to modify the SEM design to make it easier to be modeled. This was done successfully for the metrology of x-ray masks [92, 93] and may be equally successful for the backscattered electron image (see below).

4.1.1 Improved Electron Beam Modeling

Using current SEM design philosophy, meaningful electron beam modeling is very complicated to do on the current SEM designs. This is because numerous factors contribute to the derivation of the image and thus to the model. It is necessary to model not only the electron beam/specimen interaction, but also the contribution of the specimen chamber, detector geometry, detector sensitivity, electron collection fields, amplification bandwidth, as well as other factors. A great deal of fundamental information needs to be known about each particular instrument. The electron beam model must also take into account the influence on the measurement posed by the proximity to other structures or underlying layers [107, 108]. Proximity effects are well recognized in electron beam lithography and they must be equally recognized as a complication to electron beam metrology. Isolated lines present a different linescan from those in a nested array. Modeling will help us to understand this phenomenon. Electron beam modeling is currently an area of active interest for metrology and other SEM applications.

The most common approach to electron beam modeling has been to use the Monte Carlo technique [19,40,42,51,70], although other approaches have been considered [71, 142]. These other approaches include the use of transport equation theory [103] and the use of a cylindrical envelope model [33]. Electron beam modeling has been done on both the secondary and the backscattered electron images [34,42,56,57,71,86,110]. Unfortunately, since there are so many contributions to the normal secondary and even the broadband backscattered electron image, it is very difficult to isolate individual contributions. Work using the transmitted electron detection (TED) mode on a unique sample, such as the mask used for x-ray lithography, demonstrated that by restricting the contributing factors, a great deal of information could be obtained from the theoretical and the experimental data [92, 93]. Using the transmitted electron image, a relatively rapidly changing intensity in the vicinity of the true edge position is identifiable. It can, therefore, be made inherently less sensitive than the conventional secondary electron based SEM modes to this source of error in linewidth measurements. The TED technique is not inherently more or less accurate than other SEM modes for pitch measurements because pitch measurements are not subject to this type of error as long as the two lines in question have similarly shaped left and right edges.

Lithography Masks as a Model System for the Development of other Accurate SEM Standards

The x-ray lithography mask provides a unique sample for the development of future accurate dimensional SEM standards. Accurate electron beam modeling has been developed for transmission electron detection for this type of sample and accurate measurements have been made [92, 93]. The development of the model for the transmitted electrons also encompassed the simultaneous development of a model for the backscattered electrons. During this research, it was predicted by the model that both the transmitted electron signal and the backscattered electron signal contained important information about specimen characteristics, especially edge location and wall angle (Fig. 11a). These predictions were confirmed experimentally (Fig. 11b). Comparison work between experimentally obtained data and the computed data of both the TED and the BSE images is currently underway at NIST and

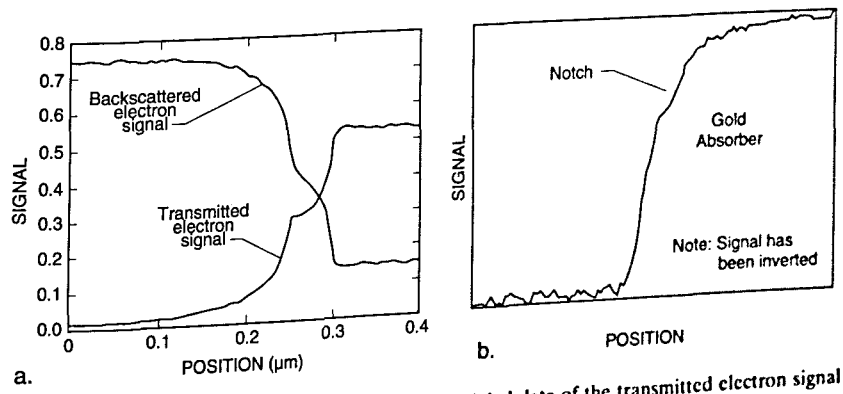

Fig. 11. X-ray mask metrology. (a) Monte Carlo modeled data of the transmitted electron signal and the backscattered electron signal showing the appearance of the characteristic notch in both modes of electron collection; (b) digitized field emission SEM micrograph of the transmitted electron signal demonstrating the presence of the notch in the experimental data.

continued model development to include the secondary electron image is also planned. Further, comparison of the experimental and theoretical data relative to portions of the x-ray mask not etched to the thin support membrane will also be instructive and is in progress.

4.2 SEM Measurement of Depth, Height and Wall Angle

One of the common criticisms of the scanning electron microscope is the perceived inability of the SEM to provide depth measurement. This is a misconception based upon the lack of full development of this facility for general use, as well as metrology. Real-time TV-rate stereo scanning electron microscopy has been available for many years and numerous papers using stereo microscopy have been published, especially in the biological sciences [7,8, 9,11]. Depth measurements of the stereo image has been applied to the metallurgical sciences. Lee and Russ [54] applied digital image processing, stereomatching, and parallax measurements to measure surface height, slope, and wall angles [54], while Thong and Breton [130] applied the technique to three dimensional mapping of semiconductor devices. Kayaalp and Jain [47] investigated wafer pattern topography with a stereo SEM and, as described earlier, Postek et al [92, 93], demonstrated that when the electron beam modeling was compared to experimental data, wall slope information of gold absorber lines of an x-ray mask can be obtained from both the transmitted and backscattered electron images with a high degree of sensitivity. There is no reason why this facility cannot be developed and utilized further. One characteristic of the SEM is the large depth-of-field, but this is a variable, user-controllable parameter that can be manipulated to provide more data.

4.3 Development of SEM Standards

Currently, the need has been identified for three different standards for SEM metrology. The first need is for the accurate certification of the magnification of a nondestructive SEM metrology instrument (see Sec. 4.3.1); the second is for the determination of the instrument sharpness (see Sec. 4.3.2); and the third is an accurate linewidth measurement standard (see Sec. 4.3.3).

4.3.1 Magnification Certification Currently, the only certified magnification standard available for the accurate calibration of the magnification of an SEM is NIST Standard Reference Material (SRM) 484. SRM 484 is composed of thin gold lines separated by layers of nickel providing a series of pitch structures ranging from nominally 1 to 50 μm. Newer versions have a 0.5 μm nominal minimum pitch. This standard is still very viable for many SEM applications. Certain limitations (e.g., size, low kV performance, etc.) presented by this standard for the particular needs of the semiconductor industry have been published previously [82] and NIST has been attempting to develop new standards designed to circumvent these limitations [94, 95]. During 1991–1992, an interlaboratory study was held using a prototype of the new low accelerating voltage SEM magnification standard. This standard, identified as NIST SRM 2090, is currently being fabricated.

Definition and Calibration of Magnification

In typical scanning electron microscopy, the definition of magnification is essentially the ratio of the area scanned in both the X and Y directions on the specimen by the electron beam to that displayed in both the X and the Y directions on the photographic CRT. Because the size of the photographic CRT is fixed, by changing the size of the area scanned in both X and Y directions on the sample, the magnification is either increased or decreased. Today, where SEM metrology instruments are concerned, the goal is not only to calibrate the magnification as previously defined and discussed, but to calibrate the size of the pixels in both the X and the Y directions of the digital measurement system. For in these instruments, it is the measurement and not the micrograph that is important. Since, in most modern integrated metrology instruments, the digital storage and measurement system is common to the imaging, the "magnification" is also calibrated. It should be noted that because of the aspect ratio of the SEM display screen the number of pixels in X may differ from the number in Y, but the size of the pixel must be equal in both X and Y. This is an important concept, because in order for a sample to be measured correctly in both X and Y the pixel must be square. Such an X and Y measurement might be done on a structure such as a contact hole viewed normal (0° tilt) to the electron beam. The concept of pixel calibration and magnification calibration is essentially identical and pitch measurements can be used to adjust either [82,94, 95]. A pitch is the distance from the edge of one portion of the sample to a similar edge some distance away from that first edge (Fig. 12). Adjustment of the calibration of the magnification should not be done using a width measurement [38,39,82,94,95]. A pitch is the distance from the edge of one portion of the sample to a similar edge

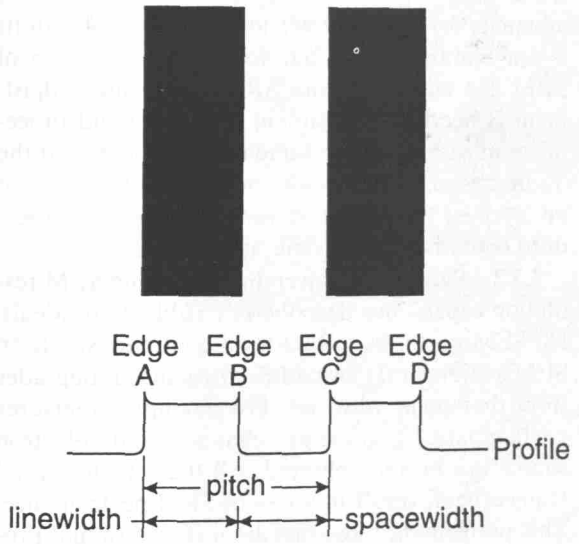

Fig. 12. Graphic comparison between the measurement of pitch and width. Measurement of A to C or measurement of B to D defines the pitch of the sample. Measurement of A to B or C to D defines the linewidth of the sample and measurement of B to C defines the spacewidth.

some distance away from that first edge (Fig. 12). Adjustment of the calibration of the magnification should not be done using a width measurement [38,39,82,94,95]. This is because width measurements are especially sensitive to electron beam/specimen interaction effects and other perturbing influences (see below and Sec. 4.1). This fact cannot be ignored or calibrated away especially if accurate SEM metrology is desired. Fortunately, it can be minimized by the use of a pitch type magnification calibration sample, such as SRM 484 [2], or the new SEM magnification calibration standard SRM 2090 [94, 95] when it is issued (Fig. 13). These standards are both based on the measurement of "pitch." In a pitch standard, that distance is certified and it is to that certified value that the magnification calibration of the SEM is set. Under these conditions the beam scans a calibrated field width in both X and Y. That field width is then divided by the number of pixels making up the measurement system, thus defining the measurement unit or the pixel width. If we consider two lines separated by some distance, the measurement of the distance from the leading edge of the first line to the leading edge of the second line defines the pitch. Many systematic errors included in the measurement of the pitch are equal on both of the leading edges; these errors, including the effect of the specimen beam interaction, cancel. This form of measurement is therefore self-compensating. The major criterion for this to be a successful measurement is that the two edges measured must be similar in all ways. SEM pixel/magnification calibration can be easily and accurately calibrated to a pitch.

The measurement of a width of a line, as discussed earlier, is complicated in that many of the errors (vibration, electron beam interaction effects, etc.) are now additive. Therefore, errors from both edges are included in the measurement. The SEM magnification should not be calibrated to a width measurement since these errors vary from specimen to specimen due to the differing electron beam/

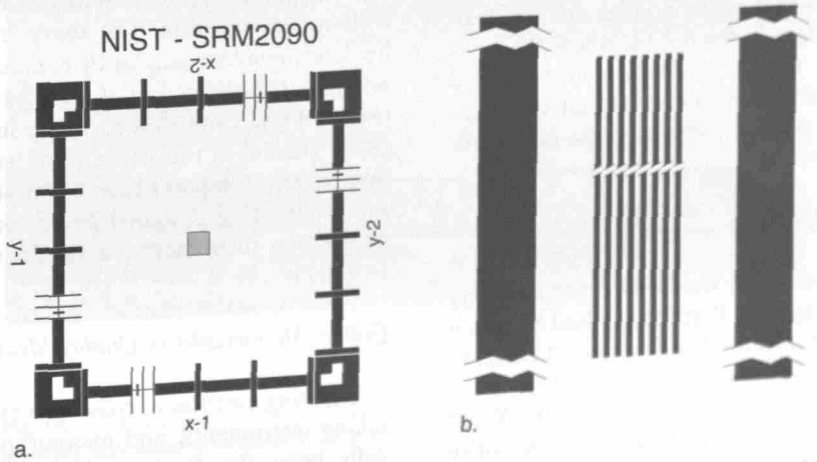

Fig. 13. SRM 2090 artwork. (a) Low magnification of the 1 mm low magnification pattern; (b) higher magnification pattern showing eight of the nominal 0.1 μm width lines having a 0.2 μm pitch.

sample interaction effects, as well as other factors [38,39,82,94,95]. Effectively, with this type of measurement, we do not know the accurate location of an edge in the video image; more importantly, it changes with instrument conditions. Postek et al. [94, 95], in an interlaboratory study of 35 laboratories, demonstrated that the width measurement of a 0.2 μm nominal linewidth varied substantially among the participants. Many factors contributed to this variation including instrument measurement conditions and measurement algorithms used [94, 95]. Calibration based on a width measurement requires the development of electron beam modeling, as described previously. This is the ultimate goal of the program at NIST and recently has been shown to be successful for special samples such as x-ray masks measured in the SEM (see below).

The dedicated "linewidth measurement" instruments or those with linewidth measurement computer systems often have an additional pixel calibration offset added to the magnification calibration in the software of the measurement function. This places a user defined "offset" or "correction" factor into the system. The measurement offset should be in *addition* to the magnification calibration and not in place of it. This offset can be determined from the measurement of an internal standard, NIST standard, or even the pitch of the actual device. Unfortunately, this offset does not usually affect the actual column scans or any of the above mentioned calibrations – only the "computer" measurement made directly with that system. Therefore, digital measurements made with the computer system may be relatively correct, but micrographs taken with that system may be out of (magnification) calibration by several percent. This software adjustment is really a *point calibration* in that it is usually done in the decade where the measurement is to be made. Erroneous results can also occur if the magnification is changed from that "calibrated" decade without rechecking the point calibration for that new decade.

Magnification Adjustment

The data obtained in the NIST interlaboratory study [94, 95] suggested that the method by which the magnification of the SEM is adjusted needs to be reengineered in many instruments. This is because the potentiometers used for setting the X and Y magnification calibration are often too insensitive or the calibration software step-size is too coarse for the repeatability required by today's semiconductor industry needs. Such coarse adjustment was adequate for the older version of SRM 484 with its 1 μm nominal pitch, but for the new version of SRM 484 and the future SRM 2090, finer adjustment is needed. Adjustment sensitivity and procedures must also be the same in both the X and the Y directions. Today, with computer integration at all levels of the SEM electronics, this entire procedure could readily become automated.

4.3.2 Sharpness Determination The SEM resolution capabilities described in Table 2 are ideals. No SEM performs at that level continuously. If an SEM achieves that level of performance it degrades from that point with use. For example, apertures contaminate, alignments change, and electron source tips become blunted. All these factors (and many others) result in a loss of SEM performance. This performance loss may be a slow, gradual process as contamination builds up or may occur rapidly if a charged particle leaves the sample and is deposited in a sensitive location. Procedures for checking the performance level of the SEM need to become standardized and standard test samples need to be developed. Many of the basic criteria established for such a sample for use in an in-line instrument are similar to those described for the low accelerating voltage SEM magnification standard [82]. A sample developed for this type of work has been used successfully by NIST for the determination of the low accelerating voltage performance of laboratory SEM instrumentation (Fig. 3 and Fig. 14). This sample is based on the concept of the determination of sharpness and not "resolution." Resolution determination implies a knowledge of the diameter of the electron beam. Whereas the concept of sharpness only requires an establishment of a sharpness criterion. The sharpness criterion can be determined visually or by computer using image analysis. The evaluation of samples similar to those used in Figs. 3 and 14 is currently in process for the establishment of this concept, as well as the development of a computer based analysis program. This sample is being designed to be readily applied to production instruments, as well as laboratory instruments.

Quality Micrographs vs Quality Measurements

Scanning electron microscopes evolved as picture taking instruments, and micrographs have historically been the final product. Modern scanning electron microscope metrological tools are data taking instruments and numbers are the final product.

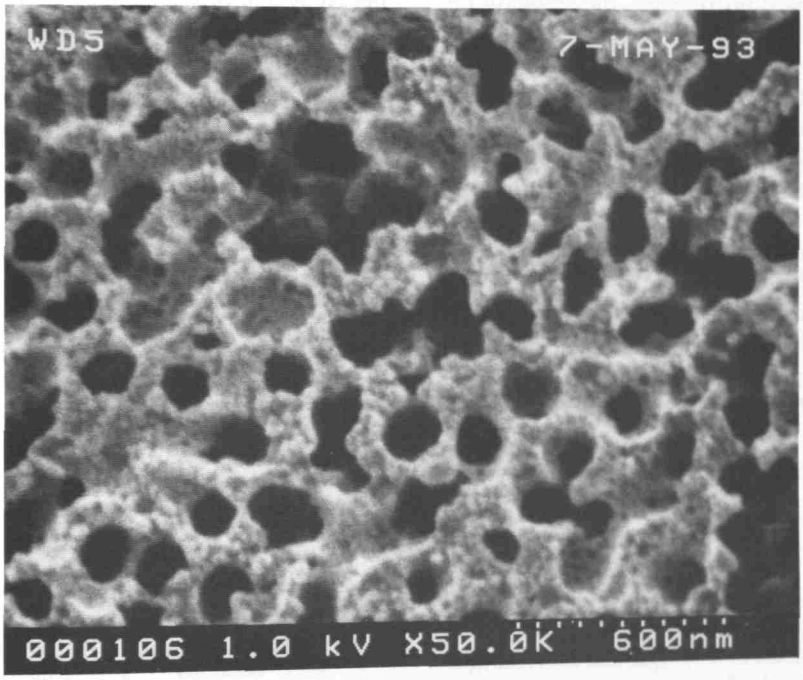

a

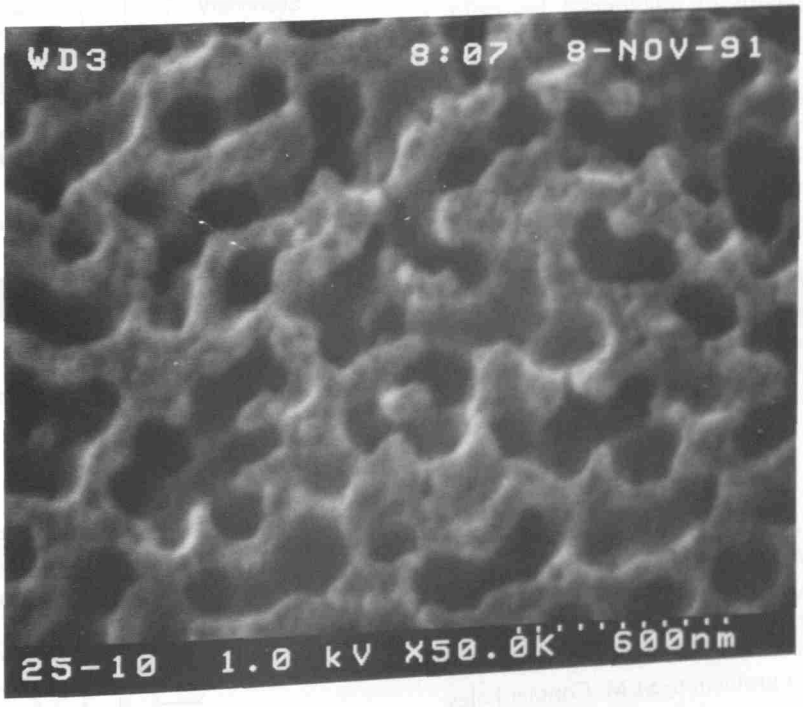

b

Fig. 14. SEM sharpness comparison using a special etched and coated biphasic glass specimen. (a) Instrument demonstrating good low accelerating voltage resolution; (b) instrument demonstrating poorer resolution.

In many metrological instruments, the emphasis on the production of micrographs is minimized or even eliminated. However, both laboratory and in-line SEM instruments are similar in their general anatomy and design. The latter is generally more elaborately outfitted for rapid wafer transport, but, both operate on essentially the same principles and are subject to the same limitations. With the de-emphasis of the recording of images, especially photographically, it is often felt that the image of the sample is less important than the numbers obtained. Yet, the only tie to the quality of the numbers obtained is the image or an analysis of the image. High quality image recording is primary to the quality of the data obtained and some "checks and balances" must be retained. Using the sample shown in Fig. 14, evaluation of the performance of the SEM can be visually determined from the micrographs or stored data. However, automated computer analysis is currently being investigated at NIST.

4.3.3 Accurate Linewidth Standard Accurate SEM linewidth standards are highly desired by the semiconductor industry. This industry is especially interested in standards for photoresist linewidth measurements. The knowledge of how to develop and measure an accurate linewidth standard for other materials such as masks used in x-ray lithography is already known and an accurate measurement has been accomplished [92, 93]. Building upon this knowledge, the generalized modeling necessary to develop other accurate linewidth-type standards may be able to be accomplished, as discussed above. But, until a flexible and accurate electron beam sample interaction model has been developed and tested, accurate linewidth standards cannot be issued.

4.4 Metrology of Contact Holes and Vias

The metrology of contact holes and vias has become very important in recent years. It is important that contact holes and vias be inspected to see if they are properly etched and cleaned out and that they are fabricated in the proper dimensions. The inspection and metrology of contact holes has always presented a problem to SEM. Contact holes can be considered as being essentially small Faraday cups. Electrons entering the contact hole have a great difficulty leaving the hole again to be collected as a signal (Fig. 15). Workers have attempted to develop methods for looking into the contact holes. Postek et al. [91] demonstrated that by applying a positive or negative bias to a sample, the collection of secondary electrons from contact holes can be enhanced or reduced. Sample biasing is not easily implemented where large samples or wafer-transfer instruments are concerned; thus Hitachi (personal communication) has used a biasing technique referred to as "field control" to influence the collection of the electrons leaving the contact hole (Fig. 16). With the field control off, the contact hole has no detail (Fig. 17a) and with the field control, on detail becomes visible (Fig. 17b). Mizuno et al. [61] used high accelerating voltage to penetrate the photoresist in order to view the holes. Alternatively, Monahan et al. [66] have shown that the backscattered electron signal can be used to image the bottom of the contact holes (Fig. 18).

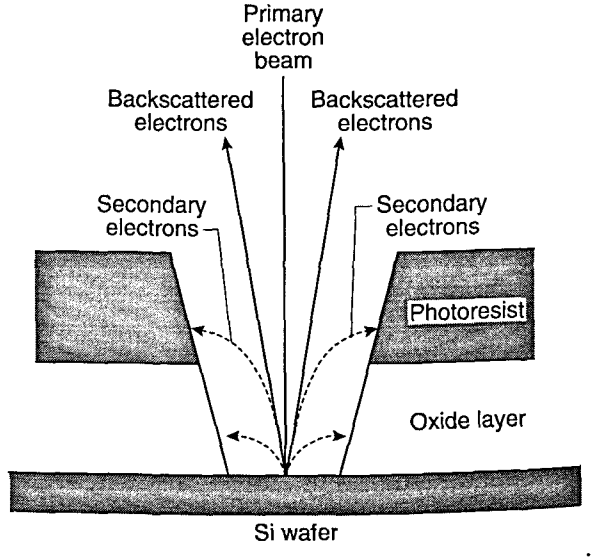

Fig. 15. Drawing showing a contact hole and the problem with electron collection.

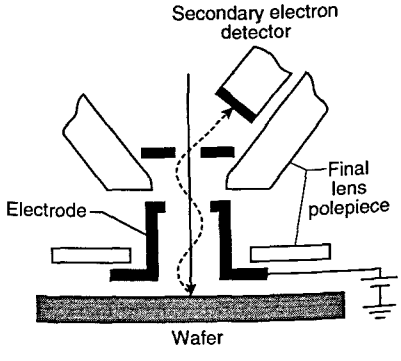

Fig. 16. Drawing describing the field control concept (redrawn from Hitachi).

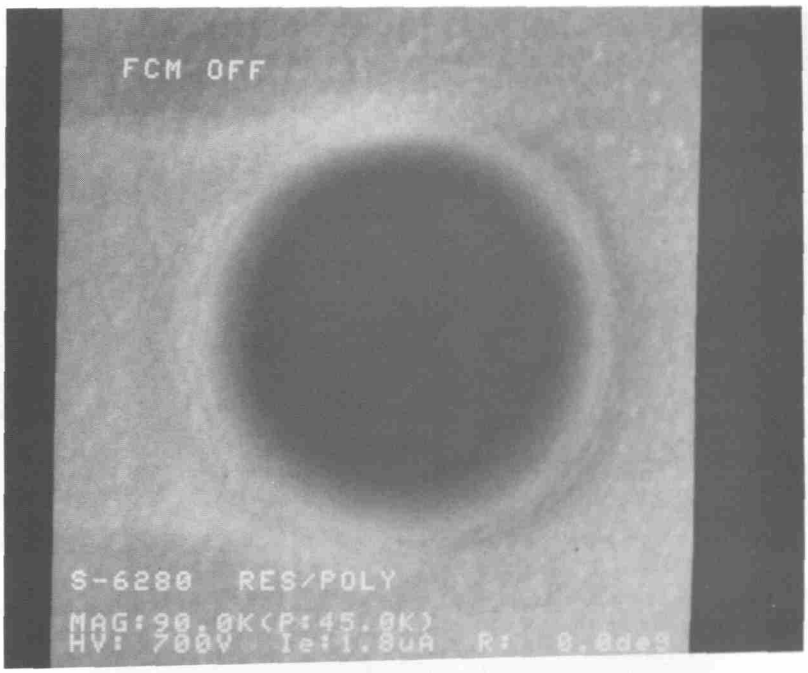

a

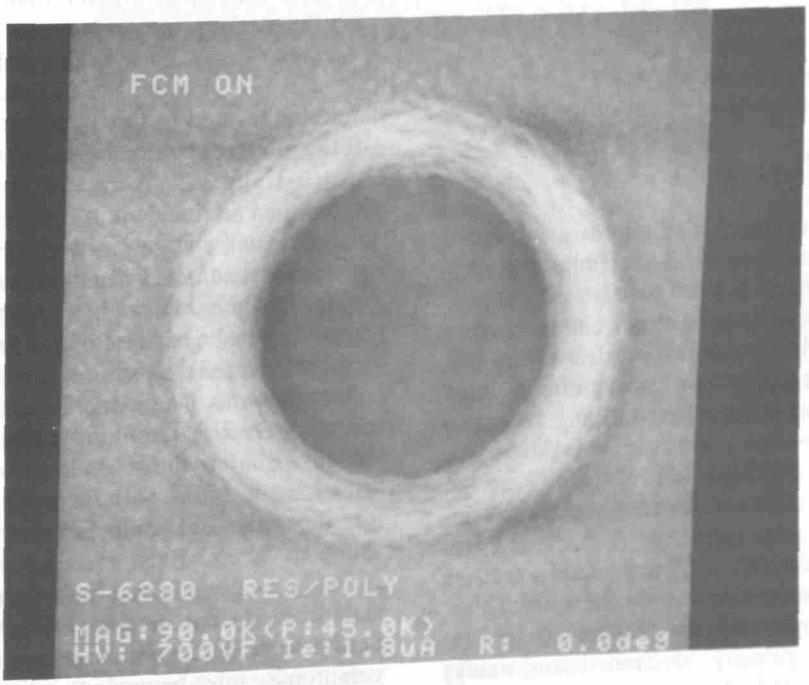

b

Fig. 17. Enhancement of electron collection from a contact hole using the field control method. (a) Field control off; (b) field control on.

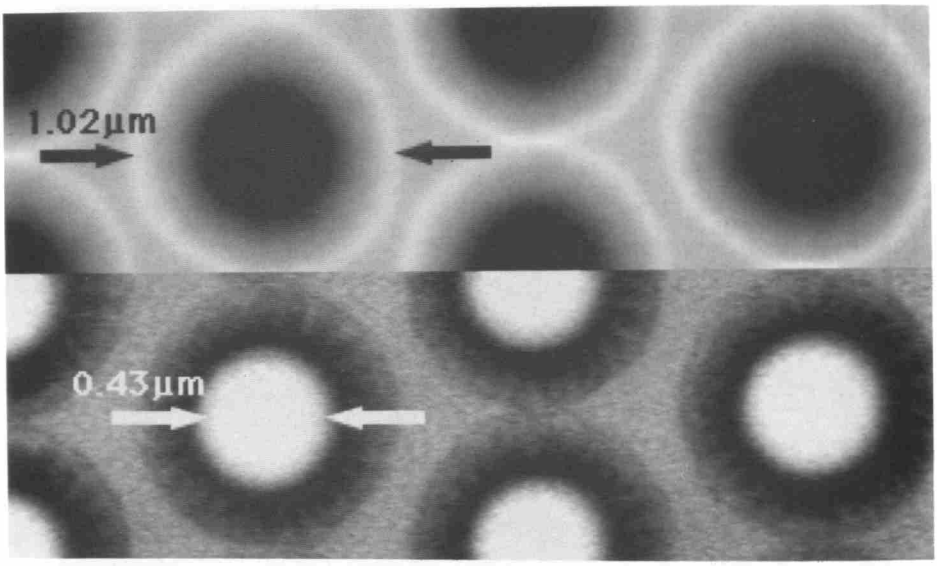

Fig. 18. Micrographs showing contact holes viewed with dual microchannel-plate electron detectors. (a) Normal wide-angle collection; (b) high angle electron collection.

This was accomplished by using two MCP backscattered electron detectors to collect the signal from the contact holes. The first detector, with a wide angle of collection, optimized the image from the top of the specimen while a narrow angle detector collected the image from the bottom of the hole.

4.5 Specimen Charging

Accumulation of charge on photoresist and other samples can result in nonreproducible and nonlinear measurement results. Therefore, the behavior of the total number of electrons emitted from a sample for each beam electron is extremely significant to nondestructive low accelerating voltage operation and metrology [65,83,85,86]. The two points where the total electron emission curve crosses unity (i.e., the E-1 and E-2 points) are the points where no net electrical charging of the sample is thought to occur [48]. During irradiation with the electron beam, an insulating sample such as photoresist or silicon dioxide can collect beam electrons and develop a negative charge causing a reduction in the primary electron beam energy incident on the sample. In principle, this could then also have a detrimental effect on the SEM magnification computation, as well as result in electron beam deflection. This charging can also have other detrimental effects on the primary electron beam and degrade the observed image. Backscattered electron collection has been successfully used to avoid the "obvious" charging effects on imaging and metrology using the secondary electrons. However, if charge build up is greater than a few electron volts, the backscattered electrons can also be affected. Few studies on charging at low accelerating voltage have been done and a great deal more work should be devoted to this issue.

If the primary electron beam energy is chosen between E-1 and E-2, there will be more electrons emitted than are incident in the incident beam, and the sample will charge positively. Positive charging is not as detrimental as negative charging, since this form of charging is thought to be only limited to a few electron volts because of the barrier it presents to the continued emission of the low energy secondary electrons. The reduction in the escape of the secondary electrons resulting from positive charging reduces signal as the secondary electrons are now lost to the detector. The closer the operating point is to the unity yield points E-1 and E-2, the less the charging effects. Each material component of a specimen being observed has its own total emitted electron/keV curve, and so it is possible that in order to completely eliminate sample charging, a compromise must be made to adjust the voltage for both materials. For most materials used in the present semiconductor processing, a beginning accelerating voltage in the neighborhood of 1.0 kV is sufficient to reduce charging and to minimize device damage (Fig. 19). It is clear that any accurate electron beam-specimen interaction model include the potential effects of sample charging.

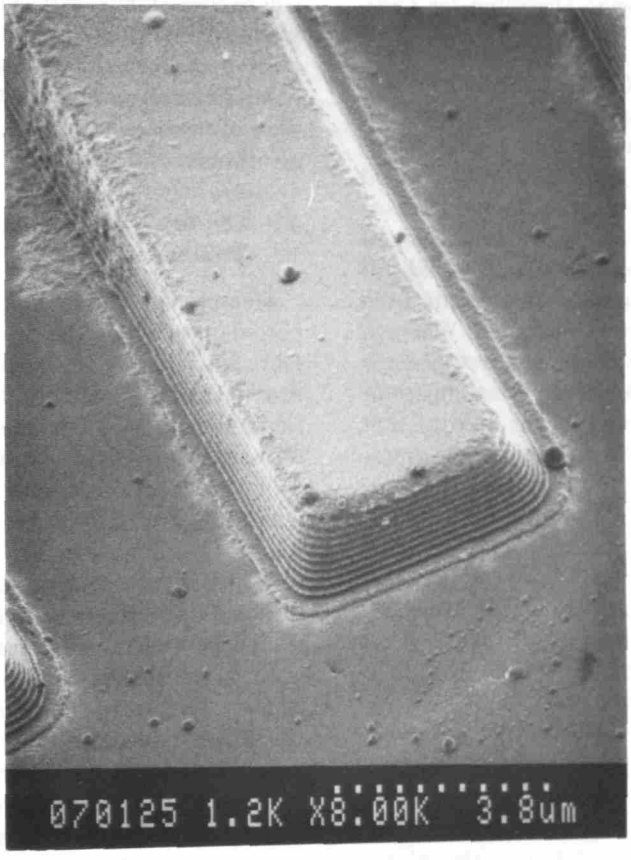

Fig. 19. SEM micrograph of uncoated photoresist taken at 1.2 keV accelerating voltage showing a lack of sample charging.

Although operation at low beam energies is useful for the inspection of semiconductor samples with a minimum of sample damage and charging, a detrimental result is a reduction in the beam current available from the electron source (as compared with high voltage operation). The net result is that the signal-to-noise ratio is poorer. This leads to a loss in apparent sample detail. High brightness filaments and digital frame storage techniques for multiscan signal integration, or slow scan rates coupled with photographic or electronic integration, help to overcome this problem. The more abiding problem with low accelerating voltage operation is the lower resolution (as compared to the higher beam energy operation) characteristic of this mode of operation. It is also extremely important to continue to monitor the image sharpness to ensure that the instrument performance is up to specification (see Sec. 4.3.2).

4.5.1 Environmental SEM Specimen charging can be dissipated at poor vacuum pressure. "Environmental" scanning electron microscopes have been introduced in several areas of general SEM applications in order to look at samples generally prone to charging. Low chamber vacuum for semiconductor processing has two consequences: the first is on throughput and the second is on specimen charging. For many years, scanning electron microscopy has routinely been done at relatively high vacuum in the specimen chamber. For metrological applications, this initially posed a complication because of the reduction in throughput that the pumpdown of the wafers from atmospheric pressure to the working chamber pressure posed. One solution developed was to cache wafers in a prepumping chamber, then move them individually into the specimen chamber when needed for viewing. The alternative is to view the wafers in poor vacuum in a specialized environmental SEM metrology instrument. Environmental SEM is relatively new to the overall SEM field and a great deal of work is being done to understand the mechanisms of operation. The reader is directed to the work of Danilatos for further information [20, 21].

4.6 Universal Measurement Algorithm for Comparison

Each metrological SEM has had developed for it a set of measurement algorithms. These algorithms are commonly manufacturer and sometimes instrument specific. Many of these algorithms are based upon instrumental convenience or in some cases experimental observation [60, 151]. The matching of data from various instruments is desirable [98], but often difficult to undertake where instruments from different manufacturers are concerned. Where a pitch measurement is concerned, the type of measurement algorithm employed is not as important because of the self compensating nature of that measurement. However, when a linewidth measurement is employed, the measurement is not self-compensating and errors are additive. In this case, the choice of algorithm becomes extremely important [94, 95]. Different samples may also require different data analysis techniques [106, 107]. No measurement algorithm based upon accurate electron beam modeling currently exists. Therefore, none exists in commercial instrumentation. However, the x-ray mask modeling results (described earlier) could lead to one [92, 93]. For instrument testing and comparison purposes a common algorithm and data handling techniques should be adopted. This would include known data processing (smoothing, etc.) and measurement procedures. *Raw (unprocessed) data should always be able to be obtained from a measurement system.* This will readily permit the comparison of the experimental data to modeled data. A common algorithm should also be transportable and capable of being used to compare instruments. The need for this was clearly pointed out in the SEM interlaboratory study [94, 95], where data from several different types of instruments were compared. In that study, no viable comparison of linewidth measurement data could be obtained because of the differences between handling of the data in the various instruments and the algorithms involved (Fig. 20).

4.7 Universal Measurement Data Storage and Transmittal

Measurement data and images need to be transported throughout the laboratory and the wafer fabrication facility. Instruments of many different manufacturers may be used for different purposes. In some cases different models of instruments from the same manufacturer cannot even communicate with each other. This problem was clearly pointed out during the SEM interlaboratory study [94, 95], when data supplied to NIST on disk could not be used. Issues regarding compatibility with existing software, accurate data representation, data compactness on disk, and rates of data transfer have been raised and standard formats suggested [23]. A common data transfer and storage format should be established and adopted for *all* metrological instruments and adhered to so that image files or data can be easily transported from any instrument to personal computers and back again, as needed.

4.8 Lens Hysteresis/Compensation Correction

Many in-line scanning electron microscopes always operate under the same operating parameters day-after-day. Other instruments operate through a range of instrumental conditions. The electromagnetic lenses comprising the column of the SEM may exhibit the effects of lens hysteresis following

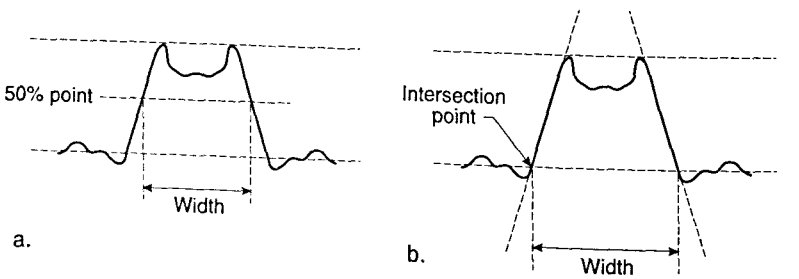

Fig. 20. Diagrammatic comparison of the difference between two common measurement algorithms on the reported "width" measurement. (a) Threshold crossing algorithm; (b) linear regression algorithm. Please note the difference in measurement result possible between the two algorithms.

changes in instrument operating conditions (i.e., especially during accelerating voltage changes) [86]. This limitation on metrology became quite apparent in many instruments during the SEM interlaboratory study [94, 95]. Many metrological instruments have some form of lens hysteresis/compensation correction, but some do not. This capability should be checked by each user of the instrument to determine if it is present in their instrument and that it functions properly.

4.9 Specimen Contamination/Specimen Damage

The effects of the electron beam on the sample can be two-fold: first, the beam can generate specimen contamination from its interaction with hydrocarbons, either in the specimen surface or from the instrument; second, it can induce damage to the actual devices.

4.9.1 Contamination Sample contamination is inevitable in all but the fully dry-pumped SEM in-line instruments. Contamination results from sample handling, the environment, and the instrument. Hydrocarbons interact with the electron beam and form a layer on the surface. The speed at which this deposition occurs varies with the amount of hydrocarbon (or other contaminant) available to interact, as well as the operational conditions of the instrument (i.e., beam current) and electron beam dwell-time on the sample [27,35,36]. Dry nitrogen purging and backfilling is helpful in reducing contamination. Subsequent post processing with oxygen plasma can often clean off this contamination from the wafer [94, 95].

4.9.2 Damage Irradiation damage of some devices viewed in an SEM at higher accelerating voltages has been reported [102, 131]. Tocci et al. [102] found damage in MOSFET devices irradiated at 2 keV accelerating voltage. Erasmus [24] observed that photoresist can change dimension under electron beam inspection. However, it was also found by that author that an optimum dose can be identified where no damage occurs. Both Van Asselt [138] and Robb [105] detected no damage when the accelerating voltage was restricted to below 3 kV and the inspection was followed by a high temperature anneal. Bhattacharya [6] reported no significant radiation-induced gate insulator damage with an exposure of 1 keV electrons. It was further concluded by these authors that SEM examination of finished devices could be accomplished with no radiation damage below 7 keV accelerating voltage. It is currently felt that it is safe to inspect most devices in an SEM during production.

4.10 Reduced Sensitivity to External Noise

The SEM metrology tool is expected to perform in a relatively "hostile" environment [64, 86]. Vibration from numerous sources and stray fields are quite common in the wafer fabrication facility. Some field emission instruments are exceptionally sensitive to stray electromagnetic fields. In some instances of high field intensity, mu-metal enclosures had to be built to completely surround the SEM column. In other instances the instrument itself has been found to be the source of the perturbing field. Regardless of the source, these instruments must be designed better to better handle the "hostile" environment in which they work.

5. Conclusions

Scanning electron microscope metrology is a dynamically changing field. The needs of the semiconductor industry have driven numerous improvements in the instrumentation. These improvements have been felt throughout the SEM field and have enabled a great deal of progress to be made in all applications of this instrument. In this paper, several areas of misconception regarding instrument performance and capabilities have been clarified. Clearly, further effort is needed in fundamental areas of scanning electron microscopy metrology. Many of these areas will be dealt with in future years resulting in even further improved instrumentation.

Acknowledgments

The author would like to thank the following for assistance during the preparation of this manuscript: Dr. Robert Larrabee, Dr. Dale Newbury, and Dr. Andras Vladar for their comments and review of the manuscript; Mr. Ray Mele of the NIST Program Office for his assistance in preparing the graphics and Ms. Marylyn Bennett for her assistance in generating the specifications tables and for her cogent manuscript review. The author also thanks Mr. Samuel Jones of NIST; AMRAY, Inc.; Hitachi Scientific Instruments; and Metrologix Inc., for the use of some of the data and figures appearing in this paper.

6. References

[1] T. Ahmed, S.-R. Chen, H. M. Naguib, T. A. Brunner, and S. M. Stuber, Low voltage metrology for pilot line applications, SPIE Proceedings 775 (1987) pp. 80–88.

[2] D. B. Ballard, A procedure for calibrating the magnification of a scanning electron microscope using NBS SRM 484, NBSIR 77-1248 (1977) pp. 1–9.
[3] M. H. Bennett, Particle metrology for microelectronics, SPIE Critical Review 52 (1993), in press.
[4] M. H. Bennett and G. E. Fuller, In-process inspection and metrology of semiconductor wafers with the use of an automated low-voltage SEM, Microbeam Anal. 649–652 (1986).
[5] J. P. H. Benschop, K. M. Monahan, and T. A. Harris, High-speed stepper setup using a low voltage SEM, SPIE Proceedings 1464 (1991) pp. 62–70.
[6] P. K. Bhattacharya, S. K. Jones, and A. Reisman, A study of electron damage effects during low voltage SEM metrology, SPIE Proceedings 1087 (1989) pp. 9–16.
[7] A. Boyde, A stereo-plotting device for SEM micrographs and a real time 3-D system for the SEM, SEM/1974/I IITRI Chicago, Il (1974) pp. 93–100.
[8] A. Boyde, Photogrammetry of stereo pair images using separate measurements from two images, SEM/1974/I IITRI Chicago, Il (1974) pp. 101–108.
[9] A. Boyde, S. J. Jones, and J. B. Pawley, Some practical applications of real time TV speed stereo SEM in hard tissue research, SEM/1974/I IITRI Chicago, Il (1974) pp. 109–116.
[10] R. Carnes and M. Su, Long term cost of ownership: Beyond purchase price, Proc IEEE/SEMI Int. Semiconductor Manufacturing Science Symposium (1991) pp. 39–43.
[11] E. J. Chatfield, J. More, and V. H. Nielsen, Stereoscopic scanning electron microscopy at TV scan rates, SEM/1974/I IITRI Chicago, Il (1974) pp. 117–124.
[12] L. A. Christman, G. A. Schwind, and L. W. Swanson, A comparison of CeB_6 and LaB_6 thermionic cathodes, Proc. EMSA, G. W. Bailey and E. Hall, eds., San Francisco Press, San Francisco, CA (1991) pp. 46–347.
[13] J. R. A. Cleaver and K. C. A. Smith, Optical characteristics of a field emission scanning microscope, Scanning Electron Microsc. Sys. Appl. 18, 6–11 (1973).
[14] C. K. Crawford, Mounting methods and operating characteristics for LaB_6 cathodes, SEM/1979/I SEM, Inc., AMF O'Hare, Il (1979) pp. 19–30.
[15] A. V. Crewe, D. N. Eggenberger, J. Wall, and L. M. Welter, Electron gun using a field emission source, Rev. Sci. Instrum. 39, 576–583 (1968).
[16] A. V. Crewe and M. Isaacson, The use of field emission tips in a scanning electron microscope, Proc. EMSA, G. W. Bailey, ed. (1968) pp. 359–360.
[17] A. V. Crewe, M. Isaacson, and D. Johnson, A simple scanning electron microscope, Rev. Sci. Instr. 40, 241–246 (1969).
[18] A. V. Crewe, D. Johnson, and M. Isaacson, An electron gun scanning microscope, Proc. EMSA, G. W. Bailey, ed. (1968) pp. 360–361.
[19] Z. Czyzewski and D. C. Joy, Fast method for simulating electron scattering in solids, J. Microsc. 156(3), 285–291 (1989).
[20] G. D. Danilatos, Introduction to the ESEM Instrument, Microsc. Res. Tech. 25, 354–361 (1993).
[21] G. D. Danilatos, Foundations of environmental scanning electron microscopy, Adv. Electronics Electron Phys. 71, 109–250 (1988).
[22] H. Drescher, L. Reimer, and H. Seidel, Rückstreukoeffizient und Sekundärelektronen-Ausbeute von 10–100 keV-Electronen und Beziehungen zur Raster-Elektronenmikroskopie, Z. Angew. Phys. 29, 331–336 (1970).
[23] R. F. Egerton, D. S. Bright, S. D. Davilla, P. Ingram, E. J. Kirkland, M. Kundmann, C. E. Lyman, P. Rez, E. Steele, and N. J. Zaluzek, Standard formats for the exchange and storage of image data, MSA Proceedings, G. W. Bailey and C. L. Reider, eds. (1993) pp. 220–221.
[24] S. J. Erasmus, Damage to resist structures during scanning electron microscope inspection, J. Vac. Sci. Technol. B. 5(1), 409–413 (1987).
[25] T. E. Everhart and R. F. M. Thornley, Wideband detector for micro-microampere low-energy electron currents, J. Sci Instrum. 37, 246–248 (1960).
[26] T. T. H. Fu, M. H. Bennett-Lilley, and R. A. Bowling, Particle generation mechanisms in vacuum processing tools, SPIE Proceedings 1673 (1992) pp. 526–533.
[27] R. M. Glaeser, Radiation damage with biological specimens and organic materials, Introduction to Analytical Electron Microscopy, J. J. Hren, J. I. Goldstein, and D. C. Joy, eds., Plenum Press, New York (1979) pp. 423–426.
[28] P. W. Grant, Use of a scanning electron microscope for critical dimension measurements on a semiconductor production line, SPIE Proceedings 565 (1985) pp. 169–172.
[29] J. E. Griffith and D. A. Grigg, Dimensional metrology with scanning probe microscopes, J. Appl. Phys. 74(9), R83–R109 (1993).
[30] J. E. Griffith, D. A. Grigg, G. P. Kochanski, M. J. Vasile and P. E. Russell, Metrology with Scanning Probe Microscopes, in: The Technology of Proximal Probe Lithography, C. K. Marrian, ed., SPIE Inst. for Adv. Technol. (1993) in press.
[31] D. A. Grigg, P. A. Russell, J. E. Griffith, M. J. Vasile, and E. A. Fitzgerald, Probe characterization for scanning probe metrology, Ultramicroscopy 42-44, 1616–1620 (1992).
[32] J. Haystead, The power behind Pentium, EDN 38 (10A), (1993) p. 7, p. 54.
[33] T. Hatsuzawa, A cylindrical envelope projection model for estimation of secondary electron intensity distribution at micro-steps, Meas. Sci. Technol 4, 842–845 (1993).
[34] G. G. Hembree, S. W. Jensen, and J. F. Marchiando, Monte Carlo simulation of submicrometer linewidth measurements in the scanning electron microscope, Microbeam Analysis, San Francisco Press, San Francisco, CA (1981) pp. 123–126.
[35] L. W. Hobbs, Radiation effects in analysis of inorganic specimens by TEM, Introduction to Analytical Electron Microscopy, J. J. Hren, J. I. Goldstein, and D. C. Joy, eds., Plenum Press, New York (1979) pp. 437–480.
[36] J. J. Hren, Barriers to AEM: Contamination and etching, Introduction to Analytical Electron Microscopy, J. J. Hren, J. I. Goldstein, and D. C. Joy, eds., Plenum Press, New York (1979) pp. 481–505.
[37] J. Jackman, E-beam metrology – the European Initiative, SPIE Proceedings 1464 (1991) pp. 71–80.
[38] S. Jensen, Planar Micrometrology in the SEM. Microbeam Analysis, San Francisco Press, San Francisco, CA (1980) pp. 77–84.
[39] S. Jensen and D. Swyt, Sub-micrometer length metrology: problems, techniques and solutions, Scanning Electron Microscopy I (1980) pp. 393–406.
[40] S. Johnson and N. C. MacDonald, A program for Monte Carlo simulation of electron energy loss in nanostructures, J. Vac. Sci. Technol. B 7(6), 1513–1518 (1989).

[41] D. C. Joy, The future of scanning electron microscopy and fundamental measurements of electron-solid interaction, Microbeam Anal. 1, 19–27 (1992).
[42] D. C. Joy, An introduction to Monte Carlo simulations, Scanning Microscopy 5(2), 329–337 (1991).
[43] D. C. Joy, Low voltage scanning electron microscopy, Inst. Phys. Conf. Ser. No. 90, Ch. 7, EMAG 1987 (1987) pp. 175–180.
[44] D. C. Joy, Resolution in low voltage scanning electron microscopy, J. Microsc. 140(3), 283–292 (1985).
[45] D. C. Joy, Beam interactions, contrast and resolution in the SEM, J. Microsc. 136(2), 241–258 (1984).
[46] D. C. Joy and J. B. Pawley, High-resolution scanning electron microscopy, Ultramicroscopy 47, 80–100 (1992).
[47] A. E. Kayaalp and R. C. Jain, Using SEM stereo to extract semiconductor wafer pattern topography, SPIE Proceedings 775 (1987) pp. 18–26.
[48] M. Knoll, Aufladepotential und Sekundäremission elektronenbestrahlter Körper, Z. Tech. Phys. 16, 467–475 (1935).
[49] P. Kruit, Magnetic through-the-lens detection in electron microscopy and spectroscopy, part 1, Adv. Optical Electron Microsc. 12, 93–137 (1991).
[50] S. M. Kudva and R. W. Potter, Cost analysis and risk assessment for metrology applications, SPIE Proceedings 1673 (1992) pp. 2–13.
[51] D. F. Kyser, Monte Carlo Simulation in analytical electron microscopy, Introduction to Analytical Electron Microscopy, J. J. Hren, J. I. Goldstein, and D. C. Joy, eds., Plenum Press, New York (1979) 199–221.
[52] B. Y. H. Liu, How particles form during vacuum pump down, Semiconductor Intl. 3, 75–80 (1994).
[53] R. D. Larrabee and M. T. Postek, Precision, accuracy, uncertainty and traceability and their application to submicrometer dimensional metrology, Solid-State Elec. 36(5), 673–684 (1993).
[54] J.-H. Lee and J. C. Russ, Metrology of microelectronic devices by stereo SEM, J. Computer-Assisted Microsc. 1, 79–90 (1989).
[55] K. L. Lee and M. Ward, Low voltage backscattered electron collection for package substrates and integrated circuit inspection, J. Vac. Sci. Technol. B 9(6), 3590–3596 (1991).
[56] D. Levy and L. Hendler, A model for electron beam metrology algorithm, SPIE Proceedings 1673 (1992) 104–116.
[57] S. Lou and D. C. Joy, Monte Carlo calculations of secondary electron emission, Scanning Microsc. 2(4), 1901–1915 (1988).
[58] K. S. Maher, Techniques for low voltage scanning electron microscopy linewidth measurements, Scanning Microsc. 7(1), 65–86 (1993).
[59] G. L. R. Mair and T. Mulvey, High brightness sources for electron and ion beam microscopy and micro-lithography, Ultramicroscopy 15, 255–260 (1984).
[60] M. Miyoshi, M. Kanoh, H. Yamaji, and K. Okumura, A precise and automatic very large scale integrated circuit pattern linewidth measurement method using a scanning electron microscope, J. Vac. Sci. Technol. B, Vol. 4(2), 493–499 (1986).
[61] F. Mizuno, S. Yamada, A. Miura, and H. Todokoro, Observation of deep holes using new technique, SPIE Proceedings 1926, 347–356 (1993).
[62] S. H. Moll, F. Healey, B. Sullivan, and W. Johnson, A high efficiency nondirectional backscattered electron detection mode for SEM, SEM/1978/I SEM, Inc., AMF O'Hare, IL (1978) pp. 310–330.
[63] S. H. Moll, F. Healey, B. Sullivan, and W. Johnson, Further developments of the converted backscattered electron detector, SEM/1979/II SEM Inc., AMF O'Hare, IL (1979) pp. 149–154.
[64] K. M. Monahan and D. S. Lim, Nanometer-resolution SEM metrology in a hostile laboratory environment, SPIE Proceedings 565 (1985) pp. 173–179.
[65] K. M. Monahan, J. P. Benschop, and T. A. Harris, Charging effects in low-voltage SEM metrology, SPIE Proceedings 1464 (1991) pp. 2–9.
[66] K. M. Monahan, G. Toro-Lira, and M. P. Davidson, A new low-voltage SEM technology for imaging and metrology of submicrometer contact holes and other high-aspect-ratio structures, SPIE Proceedings 1926 (1993) pp. 336–346.
[67] T. Mulvey, Mini-lenses and the SEM. SEM/1974/I, IITRI Chicago, IL (1974) pp. 43–50.
[68] K. Murata, Monte Carlo calculations on electron scattering and secondary electron production in the SEM, SEM/1973 IITRI, Chicago, IL (1973) pp. 267–275.
[69] K. Murata, Spatial distribution of backscattered electrons in the scanning electron microscope and electron microprobe, J. Appl. Phys. 45(9), 4410–4416 (1974).
[70] D. E. Newbury and R. L. Myklebust, Performance of a "conventional" Monte Carlo program at low-beam energy, Microbeam Analysis, Newbury, ed., San Francisco Press, San Francisco, CA (1988) pp. 139–142.
[71] D. Nyyssonen, A new approach to image modeling and edge detection in the SEM, SPIE Proceedings 921 (1988) pp. 48–63.
[72] D. Nyyssonen and R. D. Larrabee, Submicrometer linewidth metrology in the optical microscope, J. Res. Natl. Bur. Stand. (U.S.) 92(3), 187–204 (1987).
[73] D. Nyyssonen and M. T. Postek, SEM-based system for calibration of linewidth SRMs for the IC industry, SPIE Proceedings 565 (1985) pp. 180–186.
[74] T. Ohtaka, S. Saito, T. Furuya and O. Yamada, Hitachi S-6000 field emission CD-measurement SEM, SPIE Proceedings 565 (1985) pp. 205–208.
[75] J. Orloff, Thermal field emission for low voltage scanning electron microscopy, J. Microsc. 140(3), 303–311 (1985).
[76] J. Orloff, A comparison of lanthanum hexaboride, cold field emission and thermal field emission electron guns for low voltage scanning electron microscopy, Electron Optical Systems, SEM Inc., AMF O'Hare (1984) pp. 149–162.
[77] J. Orloff, L. W. Swanson, and J.-Z. Li, The prospects of field emission for e-beam inspection, J. Vac. Sci. Technol. B. 3(1), 224–226 (1985).
[78] J. B. Pawley, Low voltage scanning electron microscopy, J. Microsc. 136, 45–68 (1984).
[79] K.-R. Peters, Working at higher magnifications in scanning electron microscopy with secondary and backscattered electrons on metal coated biological specimens and imaging macromolecular cell membrane structures, Scanning Electron Microscopy/1985/IV SEM Inc., AMF O'Hare, IL (1985) pp. 1519–1544.
[80] M. T. Postek, Scanning Electron Microscopy Metrology, SPIE Critical Rev. 52 (1994) in press.
[81] M. T. Postek, Low accelerating voltage SEM imaging and metrology using backscattered electrons, Rev. Sci. Instrum. 61(12), 3750–3754 (1990).

[82] M. T. Postek, Scanning electron microscope-based metrological electron microscope system and new prototype SEM magnification standard, Scanning Microsc. 3(4), 1087–1099 (1989).
[83] M. T. Postek, Nondestructive submicron dimensional metrology using the scanning electron microscope, Review of Progress in NDE 6(b) (1987) pp. 1327–1338.
[84] M. T. Postek, Electron detection modes and their relation to linewidth measurement in the scanning electron microscope, Proceeding Joint Annual Meeting EMSA/MAS, G. W. Bailey, ed. (1986) pp. 646–649.
[85] M. T. Postek, Low accelerating voltage inspection and linewidth measurement in the scanning electron microscope, SEM/1984/III, SEM Inc. (1984) pp. 1065–1074.
[86] M. T. Postek and D. C. Joy, Submicrometer microelectronics dimensional metrology: scanning electron microscopy, J. Res. Natl. Bur. Stand. (U.S.) 92(3), 205–228 (1987).
[87] M. T. Postek and A. E. Vladar, The bright future of digital imaging in scanning electron microscopy, MSA Proceedings, G. W. Bailey and C. L. Reider, eds. (1993) pp. 768-769.
[88] M. T. Postek, W. J. Keery, and N. V. Frederick, Low-profile high-efficiency microchannel-plate detector system for scanning electron microscopy applications, Rev. Sci. Instrum. 61(6), (1990) pp. 1648–1657.
[89] M. T. Postek, W. J. Keery, and N. V. Frederick, Development of a low-profile microchannel-plate electron detector system for SEM imaging and metrology, Scanning 12, I-27–28 (1990).
[90] M. T. Postek, W. J. Keery and R. D. Larrabee, The relationship between accelerating voltage and electron detection modes to linewidth measurement in an SEM, Scanning 10, 10–18 (1988).
[91] M. T. Postek, R. D. Larrabee, and W. J. Keery, Specimen biasing to enhance or suppress secondary electron emission from charging specimens at low accelerating voltages, Scanning 11, 111–121 (1989).
[92] M. T. Postek, J. R. Lowney, A. E. Vladar, W. J. Keery, E. Marx, and R. D. Larrabee, X-ray lithography mask metrology: use of transmitted electrons in an SEM for linewidth measurement, J. Res. Natl. Inst. Stand. Technol. 98(4), 415–445 (1993).
[93] M. T. Postek, J. Lowney, A. Vladar, W. J. Keery, E. Marx, and R. Larrabee, X-ray mask Metrology: The development of linewidth standards for x-ray lithography, SPIE Proceedings 1924 (1993) pp. 435–449.
[94] M. T. Postek, A. E. Vladar, S. Jones, and W. J. Keery, The NIST low accelerating voltage SEM magnification standard interlaboratory study, J. Res. Natl. Inst. Stand. Technol. 98(4), 447–467 (1993).
[95] M. T. Postek, A. E. Vladar, S. Jones, and W. J. Keery, Report on the NIST low accelerating voltage SEM magnification standard interlaboratory study, SPIE Proceedings 1926, 268–286 (1993).
[96] W. Qian, M. R. Scheinfein, and J. C. H. Spence, Brightness measurements of nanometer-sized field-emission-electron sources, J. Appl. Phys. 73(11), 7041–7045 (1993).
[97] W. Qian, W., M. R. Scheinfein, and J. C. H. Spence, Electron optical properties of nanometer field emission electron sources, Appl. Phys. Lett. 62(3), 315–317 (1993).
[98] T. W. Reilly, Metrology algorithms for machine matching in different CD SEM configurations, SPIE Proceedings (1992) pp. 48–56.
[99] L. Reimer, Image Formation in Low-Voltage Scanning Electron Microscopy, SPIE Tutorial Text TT 12, 144 (1993).
[100] J. Reimer, Problem solving by SEM in IC wafer fabrication, Scanning Electron Microsc. 1, 167–176 (1977).
[101] L. Reimer and B. Volbert, Detector system for backscattered electrons by conversion to secondary electrons, Scanning 2, 238–248 (1979).
[102] A. Reisman, C. Merz, J. Maldonado, and W. Molzen, Low energy x-ray and electron damage to IGFET gate insulators, J. Electrochem. Soc. 131, 1404–1409 (1984).
[103] P. Rez, A transport equation theory of beam spreading in the electron microscope, Ultramicroscopy 12, 29–38 (1983).
[104] E. Ritz, Progress in the theory of electron-beam deflection, Electron Optical Systems for Microscopy, Microanalysis and Microlithography, SEM Inc., AMF O'Hare, IL (1984) pp. 97–108.
[105] F. Robb, In-process linewidth measurement of polysilicon gates using a scanning electron microscope, SPIE Proceedings 775 (1987) pp. 89–97.
[106] M. G. Rosenfield, Measurement techniques for submicron resist images, 32nd International Symp. Elect. Ion & Photon Beams (1988) pp. 1–25.
[107] M. G. Rosenfield, Analysis of linewidth measurement techniques using the low voltage SEM, SPIE Proceedings 775 (1987) pp. 70–79.
[108] M. G. Rosenfield, Analysis of backscattered electron signals for x-ray mask inspection, SEM/1985/II SEM Inc., AMF O'Hare, IL (1985) pp. 605–615.
[109] M. G. Rosenfield and A. Starikov, Overlay measurement using the low voltage scanning electron microscope, Microelectronic Eng. 17, 439–444 (1992).
[110] J. C. Russ, B. W. Dudley, and S. K. Jones, Monte-Carlo modelling of scanning electron signals from heterogeneous specimens with non-planar surfaces, SPIE Proceedings 1464 (1991) pp. 10–21.
[111] P. E. Russell, Low-voltage SEM for metrology and inspection, Microbeam Analysis (D. E. Newbury, ed.) San Francisco Press, San Francisco, CA (1988) pp. 463–465.
[112] P. E. Russell, Microchannel-plates as specialized scanning electron microscopy detectors. Electron Optical Systems, SEM Inc., AMF O'Hare, IL (1984) pp. 197–200.
[113] P. E. Russell and J. F. Mancuso, Microchannel-plate detector for low voltage scanning electron microscopes, J. Microsc. 140, 323–330 (1985).
[114] P. E. Russell, T. Namae, M. Shimada, and T. Someya, Development of SEM-based dedicated IC metrology system, SPIE Proceedings 480 (1984) pp. 101–108.
[115] S. Saito, T. Nakaizumi, H. Mori, and T. Nagatani, A FE SEM controlled by microprocessor, EUREM 1, 379–380 (1982).
[116] S. Saito, T. Nakaizumi, T. Nagatani and H. Todokoro, Microprocessor control of a field-emission scanning electron microscope (Model S-800), Proceedings EMSA, G. W. Bailey, ed., San Francisco Press, San Francisco, CA (1983) 410–411.
[117] R. Schmid and M. Brunner, Design and application of a quadruple detector for low voltage scanning electron microscopy, Scanning 8, 294–299 (1986).
[118] H. Seiler, Einige aktuelle Probleme der sekundärelektronenemission, Z. Angew. Phys. 22(3), 249–263 (1967).

[119] D. G. Seiler and D. V. Sulway, Precision linewidth measurement using a scanning electron microscope, SPIE Proceedings 480 (1984) pp. 86–93.
[120] M. R. Scheinfein, W. Qian, and J. C. H. Spence, Aberrations of emission cathodes: nanometer diameter field-emission electron sources, J. Appl. Phys. 73(5), 2057–2068 (1993).
[121] M. R. Sheinfein, W. Qian, and J. C. H. Spence, Brightness measurements of nanometer-sized field-emission tips, MSA Proceedings, G. W. Bailey and C. L. Reider, eds. (1983) pp. 632–633.
[122] B. Singh and W. H. Arnold, Linewidth measurement by low voltage SEM, SPIE Proceedings 921 (1988) pp. 16–21.
[123] T. Suganuma, Measurement of surface topography using SEM with two secondary electron detectors, J. Elec. Microsc. 34(4), 328–337 (1985).
[124] N. Sugiyama, S. Ikeda, and Y. Uchikawa, Low voltage inspection of micro electronic devices, J. Electron. Microsc. 35(1), 9–18 (1986).
[125] L. W. Swanson, Field emission source optics, Electron Optical Systems, SEM Inc., AMF O'Hare, IL (1984) pp. 137–147.
[126] L. W. Swanson, Comparative study of the zirconiated and built-up W thermal-field cathode, J. Vac. Sci. Technol. 12(6), 1228–1233 (1975).
[127] L. W. Swanson and L. C. Crouser, Angular confinement of field electron and ion emission, J. Appl. Phys. 40(12), 4741–4749 (1969).
[128] L. W. Swanson and N. A. Martin, Field electron cathode stability studies: Zirconium/tungsten thermal-field cathode, J. Appl. Phys 46(5), 2029–2050 (1975).
[129] M. Tipton, M. H. Bennett, J. Pollard, J. Smith, and R. Jackson, Stepper lens characterization using a field emission SEM, SPIE Proceedings 921 (1988) pp. 64–70.
[130] J. T. L. Thong and B. C. Breton, In situ topography measurement in the SEM, Scanning 14, 65–72 (1992).
[131] L. Tocci, M. McNutt, and R. Johnson, Threshold voltage shift due to low energy electrons used in SEM voltage contrast testing, IEEE Electron Devices Lett. EDL-4 (1983) p. 175.
[132] G. L. Toro-Lira, Techniques for high speed SEM wafer inspection for production applications, SPIE Proceedings 1087 (1989) pp. 17–29.
[133] D. W. Tuggle and L. W. Swanson, Emission characteristics of the ZrO/W thermal field electron source, J. Vac. Sci. Technol. B 3(1), 220–223 (1985).
[134] D. W. Tuggle and S. G. Watson, A low-voltage field-emission column with a Schottky emitter, Proceedings EMSA, G. W. Bailey, ed., San Francisco Press, San Francisco, CA (1984) pp. 455–457.
[135] D. W. Tuggle, L. W. Swanson and J. Orloff, Application of a thermal field emission source for high resolution, high current e-beam microprobes, J. Vac. Sci. Technol. 16(6), 1699–1703 (1979).
[136] D. W. Tuggle, J. Z. Li, and L. W. Swanson, Point cathodes for use in virtual source electron optics, J. Microsc. 140 (3), 293–301 (1985).
[137] S. G. Utterback, Semiconductor dimensional metrology using the scanning electron microscope, Review of Progress in Quantitative Nondestructive Evaluation (1988) pp. 1141–1151.
[138] R. L. Van Asselt, H. Becker and E. C. Douglas, Development of accurate linewidth measurement techniques to support fabrication of devices with structures 1 μm and less, SPIE Proceedings 921 (1988) pp. 22–32.
[139] K. D. Van Der Mast, Field emission, developments and possibilities, J. Microsc. 130(3), 309–324 (1983).
[140] B. Volbert and L. Reimer, Advantages of two opposite Everhart-Thornley detector on SEM, SEM/1986/IV SEM Inc., AMF O'Hare Chicago, IL (1985) pp. 1–10.
[141] B. Volbert and L. Reimer, Detector system for backscattered electrons by conversion to secondary electrons, Scanning 2, 238–248 (1979).
[142] X. Wang and D. C. Joy, A new high-speed simulation method for electron-beam critical dimension metrology profile modeling, J. Vac. Sci. Technol. B 9(6), 3573–3577 (1991).
[143] L. M. Welter, Application of a field emission source to SEM in: Principles and Techniques of Scanning Electron Microscopy, Vol. 3. M. A. Hayat (ed.), 195-220 (1975).
[144] L. M. Welter and V. J. Coates, High resolution scanning electron microscopy at low accelerating voltages, SEM/1974/I IITRI, Chicago, IL (1974) pp. 59–66.
[145] L. M. Welter and V. J. Coates, A compact field emission scanning electron microscope, Proc. EMSA, C. J. Arceneaux, ed. (1971) pp. 32–33.
[146] L. M. Welter and A. N. McKee, Observations on uncoated, nonconducting or thermally sensitive specimens using a fast scanning field emission source SEM, Scanning Electron Microscopy/1972/I IITRI, Chicago, IL (1972) pp. 161–168.
[147] J. E. Wolfe, Operational experience with zirconiated T-F emitters, J. Vac. Sci. Technol. 16(6), 1704–1708 (1979).
[148] O. C. Wells, Low loss electron images of uncoated photoresist in the scanning electron microscope, Appl. Phys. Lett. 49(13), 764–766 (1986).
[149] O. C. Wells, Low loss image for surface scanning electron microscope, Appl. Phys. Lett. 19(7), 232–235 (1979).
[150] R. W. Wood, A new form of cathode discharge and the production of x-rays, together with some notes on diffraction, Phys. Rev. 5(1), 1–10 (1897).
[151] H. Yamaji, M. Miyoshi, M. Kano, and K. Okumura, High accuracy and automatic measurement of the pattern linewidth on very large scale integrated circuits, Scanning Electron Microsc. 97–102 (1985).
[152] V. A. Zworykin, J. Hillier, and R. L. Snyder, A scanning electron microscope, ASTM Bull. 117 (1942) pp. 15–23.
[153] ISO, Guide to the Expression of Uncertainty in Measurement, 1st Edition, Geneva (1993).
[154] ISO, International Vocabulary of Basic and General Terms in Metrology, 2nd Edition, Geneva (1984).

About the author: Michael T. Postek is the Leader of the Microelectronics Dimensional Metrology Group of the Precision Engineering Division at NIST and the Project Leader for scanning electron microscope metrology. His main interests are the industrial applications of scanning electron microscope metrology and the development of dimensional standards for the scanning electron microscope. The National Institute of Standards and Technology is an agency of the Technology Administration, U.S. Department of Commerce.

Volume 99, Number 5, September–October 1994
Journal of Research of the National Institute of Standards and Technology

[J. Res. Natl. Inst. Stand. Technol. 99, 673 (1994)]

Conference Report

QUEST FOR EXCELLENCE VI Gaithersburg, MD February 7–9, 1994

Report prepared by

Cheryl Parrott and
Robert E. Chapman

Office of Quality Programs,
National Institute of Standards and Technology,
Gaithersburg, MD 20899-0001

1. Introduction

As part of the national quality improvement campaign, industry and government have joined together to establish the Malcolm Baldrige National Quality Award. Created by public law in 1987, the Award promotes an understanding of quality excellence, greater awareness of quality as a crucial competitive element, and sharing of information and strategies. There are three categories in which companies may compete: manufacturing, service and small business. Although up to two Awards may be given annually in each of the three categories, and each year many companies apply, to date the maximum number of Baldrige Awards granted in one year is five. In 1989 and 1993, only two companies received the honor. While the criteria against which companies assess their quality programs evolve, the standards for judging and winning the Award are exceedingly high.

Each year the Quest for Excellence provides quality-seeking businesses the opportunity to listen and question the winning companies, and to learn their strategies for adapting and implementing total quality management (TQM) into their professional lives. In his keynote address, Deputy Secretary of Commerce David J. Barram noted that quality management, as exemplified by the Baldrige Award winners, has a measurable effect, not only on the winners, but on the nation's economy. The two most recent winners, Eastman Chemical Company and Ames Rubber Corporation, are in the vanguard of companies which have moved to reshape U.S. competitiveness. Barram remarked that the economic effects of quality management have been so dramatic that President Clinton was proposing a 4-million-dollar initiative to extend the scope of the Baldrige Award to the fields of health care and education. Secretary of Commerce Ron Brown and President Clinton had made it clear, Barram said, that this administration, both pro-business and avowed steward of the environment, would, "... urge all U.S. business to follow the models of Eastman and Ames in the combat of the global marketplace ... where they take no prisoners."

The companies that apply for the Malcolm Baldrige National Quality Award each year write extensive descriptions of their business practices, showing the Board of Examiners for the Award how they have implemented the philosophy and techniques of total quality management to meet the stringent criteria of the Baldrige Award. This Conference Report, a summary of the comments by representatives of the winning companies, is organized much as the presentations themselves were. Plenary sessions based on the Baldrige Award criteria are: Leadership (Sec. 2.); Infor-

mation and Analysis (Sec. 3.); Strategic Quality Planning (Sec. 4.); Human Resource Development and Management (Sec. 5.); Management of Process Quality/Quality and Operatonal Results (Sec. 6.); and Customer Focus and Satisfaction (Sec. 7.). In addition, there were special sessions on Public Responsibility and Corporate Citizenship (Sec. 8.) and on the role of Quality in Research and Development (Sec. 9.). The final section, a Conference Summary, is a synopsis of comments by Dr. Joseph M. Juran, a renowned expert in quality management since 1924. Dr. Juran founded the Juran Institute, dedicated to providing education, training, and consulting in quality to organizations worldwide.

2. Leadership

In the experience of Earnest Deavenport, Chairman and Chief Executive Officer of Eastman, and of Joel Marvil, Ames' President and Chief Executive Officer, success in applying the concept of total quality management is impossible without the strong commitment, involvement, and personal support of an organization's senior management team.

For Eastman, according to Deavenport, the journey began with a wake-up call in the late 1970s, when his company of over 17,000 employees was losing market share in a major product line, one that it had invented, patented, and licensed others to make. They saved the product line, making a conscious decision to adopt the tools and techniques of quality, and soon learned that integrated processes and systems and the social aspects of quality are critical for a world-class company.

Founded in 1949, Ames supplies elastomeric rollers, such as those used in typewriters, to office equipment manufacturers. To meet the demands of a marketplace changing from typewriters to computers, photocopiers, and printers, Ames had a choice of extinction or evolution. Its evolution, however, was insufficient to maintain a competitive stance with offshore companies. In the 1980s, Ames sought a new culture; the company used more innovative design, more efficient manufacturing techniques, and most importantly, it expanded the involvement of its 450 employees through training programs and built a teamwork philosophy.

Both companies, realizing that their survival hung in the balance, chose long-term solutions, not quick fixes. Ames inherited its quality principles and training from Xerox Corporation Business Products and Systems, a 1989 Baldrige Award winner. Ames, a key supplier to Xerox, requested and received training for its Executive Committee in 1987. The smaller company quickly modified the Xerox "Leadership Through Quality" process to fit Ames' size and culture (see Fig. 1). Marvil and his senior management devoted eight months to formulating strategy for the Ames Total Quality Process. When they were ready to apply their new process, the "Teammates" at Ames owned it, believed in it, and were determined to implement it.

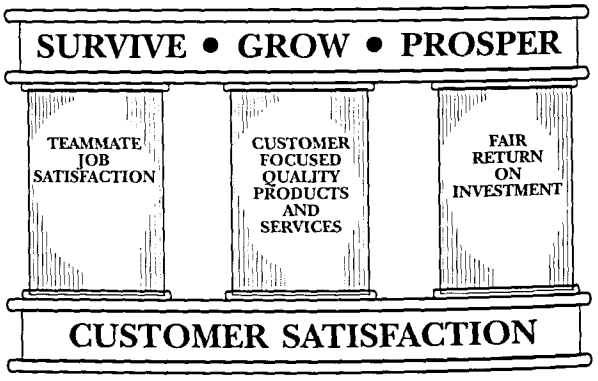

By insuring that our customers are satisfied - We will meet our goals:

- To Survive, Grow and Prosper in the changing business environment.
- To provide customer focused quality products and services to our customers.
- To provide all Teammates with continuous employment, a healthy environment, fair treatment, wages and benefits, open communication, and job satisfaction.
- To provide a fair return to our investors.

Fig. 1. The Ames Team "Excellence Through Total Quality".

Eastman, too, was prepared to commit time and financial and human resources to developing a Quality Policy and its Quality Management Process. CEO Deavenport understood that TQM could not be a pilot project of 6 months or even 6 years duration; it had to become a way of life. He provided a vision, and communicated it to his employees, along with the thought that as new measures were implemented to effect the new vision, employees had input. They could bring about thoughtful and continuous change. Empowered employees became more creative, energetic, enthusiastic, and productive, as management learned to, in Deavenport's words, "stand back and let them do their jobs."

Yet, with the strikingly positive results that both Ames and Eastman derived from their conversions to TQM, both emphasize that TQM is not *what* they do, but the *way* they do it. Both responded to customers, market demand, and, as the success of their new cultures of quality grew, so did their businesses.

3. Information and Analysis

Up-to-the-minute, accurate information and insightful analysis of that information makes a competitive-edge difference in today's world marketplace. Benchmarking and competitive comparisons are ways in which businesses can set "stretch" goals for themselves to attain superior results.

Eastman considers itself "data-driven," noting that information and analysis drive everything that follows—strategic planning, human resource management, operational results. Good information and analysis help Eastman to determine: i) whether the company's processes are working, ii) if those processes are the best possible for Eastman, and iii) whether the processes are in concert with one another and contributing to success.

Access to information is also crucial in Eastman's communications network of PCs, mid-range and mainframe computers, and distributed control systems. Within the network there are numerous information systems, two of which are vital for Eastman's continued competitive stance. First, Manufacturing Information Systems are in each of the major manufacturing divisions. There, data are collected from distributed control systems, operators, and from laboratory test results, then used for statistical process control, scheduling, inventory, quality assurance, process evaluation, and process improvement.

The second major information system is GLOBIIS, or Global Business Integrated Information System. When totally in place, GLOBIIS will process information in 11 different languages and integrate all Eastman's daily business functions into a single computer system.

Benchmarking has become routine at Eastman. Having learned early-on that performance indicators and goals have little use or credibility unless they are based on what the competition is doing, Eastman selected a core of 20 companies, 10 competitors and 10 customers, against which to compare performance data. All were chosen because of their market similarities to Eastman and for their track records of innovation and strategic and financial successes. Information gleaned from such benchmarking often has a direct, measurable effect. It was a benchmarking study that led to the company's Rapid Globalization goal that significantly increased sales and assets outside the United States.

To keep a constant check on the relevance of all this information, Eastman organized its customers and markets into more than 40 distinct businesses called "units of analysis." Based on the information coming from these units, Eastman makes significant business decisions: where to allocate capital, where to build relationships, and what kinds of services to provide. The company also does some 50 direct internal assessments yearly using the Malcolm Baldrige criteria. Results from these assessments help management determine whether the systems and processes are working in concert, and whether the company is achieving its vision, its goals.

At Ames, all information is collected and analyzed with the company goal and motto, "Survive, Grow and Prosper," in mind. Five major types of data and information contribute to the company's goal. *Customer-related data* are gathered in annual customer satisfaction surveys that measure performance in quality, cost, delivery, and service. Such survey data, when analyzed in a historical continuum, provide insight into the company's competitive position. Similarly, Ames considers its suppliers as partners and uses *supplier-related data* to recognize superior performance or to spot a need for additional training.

Product and service performance data come from nine different sources, including simulated functional product testing, sales, checks for parts-per-million defects, and cost of quality. *Business process data*, including information on internal operations, facilitate Ames' proactive approach to improving internal processes, providing training, and measuring Teammate satisfaction and involvement. The Executive Committee evaluates operating costs and overhead against the company's *cost and financial data*.

Ames began actively benchmarking in 1988. Since then, it has become a member of the International Benchmark Clearinghouse and has provided training for selected Teammates. Ames benchmarks in the areas of customers and suppliers, product and service quality, and internal operations, and is open to expanding its benchmarking efforts.

4. Strategic Quality Planning

Ames reviews and updates its Strategic Business Plan annually, fully integrating quality planning with goals to be achieved 5 years into the future. The plan, with a major section entitled "Total Quality," in addition to traditional components such as "Sales and Marketing" and "Finance and Human Resources," takes into account long- and short-term requirements of external and internal customers. Using the benefits of benchmarking even in planning, Ames adapted a concept from another Baldrige winner, The Wallace Company, to form seven Quality Strategic Objective teams that address various aspects of quality.

External customers' expectations are defined by means of surveys, quality audits, direct interviews, purchase contracts and market studies, while internal customers' needs generally include financial resources, workplace health and safety considerations, and Teammate recognition, empowerment, and training. A technology-oriented company, Ames also devotes a major section of the plan to research and development.

Eastman emphasizes that in its Strategic Quality Planning Process, "The planners are the doers." Another over-arching principle is that planning must involve each dimension of Eastman's organization: business organizations, functions, geographies, and core competencies.

The Strategic Quality Planning Process at Eastman is assessed annually to assure that the company plans and operates in a manner that provides greatest value for all stakeholders—suppliers, the public, investors, customers, and employees. Eastman divisions focus on key results areas for their organizational units and evaluate how performance in these areas contributes to overall company performance. At each level, teams own the planning process and are involved in and accountable for their plans and performances. They use a "Plan/Do/Check/Act" cycle for increased learning and standardizing to best practices. Eastman wants the company's initiatives translated into meaningful expectations in everyone's daily work. Management and employees have demonstrated a willingness to communicate, to be stakeholders, and a passion about the Eastman mission.

5. Human Resource Development and Management

Ames considers its Teammates its scarcest and most valuable resource, and places high priority on programs to train and retain them. Ames' high level of employee job satisfaction is due, in part, to a Labor Requirements Quality Improvement Plan, developed by a team of hourly and salaried employees. The company provides various opportunities for employee involvement and feedback: teammate involvement groups, quality improvement process and problem-solving process teams, a suggestion system, a direct line to the president, plant walk-arounds, social gatherings, cafeteria meetings, bulletin boards, and publications.

Employees are recruited based on Ames' business plan. Each new Teammate receives 24 hours of basic "Excellence Through Total Quality" training and is assigned a coach. Understudy programs are available for technical professionals, as are programs in basic literacy. Ames also supports an off-site tuition assistance program for technical course work, undergraduate and graduate degree programs and personal development and enrichment.

Performance recognition ranges from a simple "Atta boy" to gifts of up to thousands of dollars. The quarterly company magazine, *The Echo*, lists at least two full pages in every issue of Teammates who have been honored. Press releases also are sent to local newspapers.

Employee health, safety, and security are foremost in company priorities. In addition to health and life insurance, retirement savings, and a pension plan, Ames provides influenza vaccines for employees and contracts with an industrial health physician who visits several times each year.

Eastman approaches all human resource objectives—empowerment, teamwork, diversity, well-being—through a structure of interlocking teams. The teams enable employees to develop goals and measures that are compatible and integrated with the company's Major Improvement Opportunities. Eastman has found that such teams, interlocking up and down the supervisory chain, promote information sharing and feedback, innovation and ownership in managing work areas.

The company has removed traditional barriers to empowerment, modifying standard operating procedures, equalizing employee benefits, eliminating clock cards, and revising dress codes. Training needs are identified for each employee, placing emphasis on personal growth that is consistent with current job expectations and anticipated future requirements. Eastman's performance assessment system removes employee labels and encourages involvement and ownership.

6. Management of Process Quality/ Quality and Operational Results

For both Ames and Eastman, process quality and operational results begin with innovative product design and companywide communications networks taking into account the potential customer and market needs. At Eastman, multifunctional teams coordinate and integrate the subprocesses. The team members are given a Quality Management Facilitator, or coach, trained in statistical process control, and apply to their project an Eastman-developed quality implementation procedure called PECI, or Process Evaluation, Control, Improvement.

Process quality and operational results are assessed against the Baldrige criteria, the core of Eastman's evaluative process over the past four years. In addition, the company uses ISO 9000 quality standards, and now has seven manufacturing units registered to ISO 9000.

Eastman has shown three dramatic and measurable results after having applied the tools of quality to their manufacturing operations. The first is superior return on assets; compared to the companies against which Eastman benchmarks, Eastman has had the best profit margin since 1990. The next result, aggressive sales revenue growth, is particularly impressive; Eastman's annual sales have grown 40 percent since 1988. Last, Eastman has actively sought rapid globalization and succeeded, doubling sales outside the United States since 1984.

Eastman credits use of total quality management for much of its success. The company is obviously proud of its involved, committed, continually improving employees, but is also quick to say its quality journey is just that—a journey—not a destination.

Ames translates its strong commitment of leadership and teamwork into management of process quality for several hundred different products being manufactured in numerous ways. It sees the key element in a successful customer relationship as an exchange of information through continuous customer and supplier involvement, from prototype design to pilot plant to full-scale production and delivery. Throughout the process, built-in controls—systems checks, supplier audits, visual inspections and laboratory testing—ensure that Ames and the customer are satisfied with the product. Avoiding problems is the goal. "Prevention," Ames says, "not correction, is our policy."

The caution pays off. Ames has increased price reductions to its customers from $200,000 in 1990, to $5,300,000 in 1993. Its on-time delivery improved from 81 percent in 1989, to 98.6 percent in 1993. Corporate quality, as measured by defective parts per million, improved exponentially; Ames reduced its defective parts from 33,841 per million in 1989 to 11 in 1993. At the same time, as a planned consequence of the conscious commitment to quality process, operational quality, efficiency and workplace safety improved.

6. Customer Focus and Satisfaction

Based on the criteria which includes product quality and uniformity, supplier integrity, correct delivery, and reliability, over 70 percent of Eastman's customers rate the company "Number One." Eastman's high customer ratings reflect the company's ability to anticipate, understand, and meet customer needs.

Eastman forges strong relationships with customers through technically trained field sales and technical service representatives, sales support specialists, customer service specialists, and others. The contact frequently is made face-to-face. Also, a toll-free number for sales or service is available to customers and potential customers 7 days a week, 24 hours a day. A Strategic Intent Vision (Making Eastman the "World's Preferred Chemical Company") drives the organization to go beyond meeting customer needs to exceeding them. In contrast to the practice of many manufacturers, Eastman's sales force is not the only customer contact, but the first of many. Management, manufacturing units, quality assurance, health, safety and environment and supply and distribution departments are also in contact with customers in person or by phone (see Fig. 2).

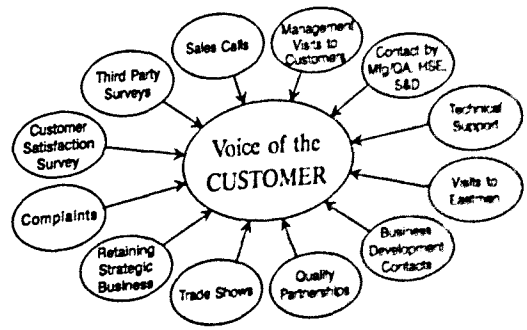

Fig. 2. Methods for collecting Eastman customer information.

The company provides customer-contact employees with important, tangible tools to maintain and improve Eastman's enviably high level of customer satisfaction. In addition to electronic data interchange with customers and advance notice of product changes, Eastman offers a simplified warranty on its Conditions of Sale and a no-fault return policy for plastics that is believed to be unique in the plastics industry.

Ames focuses on certain basic elements of its customers' perceptions of value: total quality of products and services, Ames' position as a technology leader, price, attention to customers, and ease of doing business. An annual survey, conducted by an outside, independent firm, asks customers to rate Ames in terms of total quality of such basic elements. Two additional surveys, a quarterly customer satisfaction survey and a monthly customer contact survey, both conducted by the sales department, give Ames an idea of how its doing in customers' eyes.

A customer service group collaborates with manufacturing management to set service standards through benchmarking and to incorporate changes into the Ames customer service manual. The company's performance in increasing its customer focus and satisfaction is reviewed monthly. As measured by a 60 percent decrease in occurrences of customer dissatisfaction, the system is effective, yet Ames states that it will constantly seek ways to improve.

8. Public Responsibility and Corporate Citizenship

Ames Rubber Corporation, located in rural Sussex County, New Jersey, is proud and protective of its home. Ames considers the surrounding communities its customers, and places its responsibility to the public's health, safety, and the environment first. Long before New Jersey became one of the most stringently environmentally regulated states, Ames formed a Department of Regulatory Affairs to address issues of waste disposal, water contamination, air emissions, and solvent usage. Even so, a company analysis showed that historically accepted practices could lead to substantial liability; thus, Ames adopted a proactive approach, preferring prevention to control, and spent over two million dollars in site evaluations and clean-up in 1992 alone.

Progress is evident in many processes. Ames has eliminated solvent-stripping processes, will soon implement solventless degreasing, and is testing aqueous-base adhesive systems. The company controls emissions from its manufacturing sites by thermal oxidation, has constructed a modern hazardous waste storage pad, and developed a program to recycle spent activated carbon from water.

Ames puts equal emphasis on protecting its Teammates. The company's safety record stands as almost twice as good as the industry average, and is a benchmark for Ames' insurance carriers.

Ames management encourages corporate and employee citizenship. Teammates donate time to many community outreach activities: local fire and rescue squads, Big Brothers, Big Sisters, United Way of Sussex County, March of Dimes, local athletic programs and holiday food drives. The company policy is that good corporate citizenship goes far beyond providing employment and paying taxes. As well as contributing financial resources to worthy causes in the community, Ames shares the total quality concept with other companies and with nearby colleges and universities, including Rochester Institute of Technology, New Jersey Institute of Technology, and Lehigh University.

Eastman is a highly visible participant in Responsible Care®, an initiative undertaken by the Chemical Manufacturers Association, with Eastman as a key contributor, to protect the environment and to meet or exceed the relevant regulations at local, state, and national levels. Eastman is recognized as an industry model for phasing out chlorofluorocarbons as coolants in refrigeration and air conditioning systems. The company also maintains its own wastewater and other waste treatment facilities.

Eastman strives to be a good neighbor, promoting a free flow of environmental information to the surrounding communities, opening its plants for tours and open houses, inviting interviews from the media, publishing newsletters, and sponsoring a special environmental hot line. The company takes an active lead in recycling plastics, forming a partnership with a waste management firm to provide recycling services in four southern states. The project was cited as best in the United States in 1991 by "Keep America Beautiful."

As with many organizations committed to the principles of quality, Eastman and its employees are active in community programs: Junior Achievement, recycling fairs, chambers of commerce, and other service organizations. In monetary contributions alone, Eastman gives over 2 million dollars each year to charitable and educational organizations. In addition, work schedules can be arranged, so that employees can speak to school classes,

deliver "Meals on Wheels" or spend time on the "Putting Children First" project, where employees in the Kingsport area and local educators have a partnership and long-term commitment to increase students' competence in math, science, and technology. Similarly, Eastman's Texas plant has entered into a business and education coalition called GLOBE, or Greater Longview Organization for Business in Education. More than 25,000 students have benefitted from this nationally recognized model of partnership in business and education.

8. Quality in Research and Development

With efforts in basic and applied research, including pilot plant operations, Eastman was one of the first to ask whether TQM could really work—especially in research. Beginning in 1987, Eastman included researchers on interlocking teams to identify processes and customers and to design experiments. However, after taking stock of their efforts in late 1989, Eastman saw that there was no significant improvement with its research initiatives. In fact, there was considerable griping about time spent in meetings and wasted money and effort.

In the final analysis, Eastman realized that the focus should have been on the main output of research: new and improved product and process concepts that were desirable in the marketplace. In 1990, the company instituted an annual fact-finding analysis system to evaluate opportunities for improvement. In 1991, it placed more emphasis on concept development teams. In 1992, new research liaison teams ensured better linkage with in-house business organizations, and in 1993, the research-customer interaction process was further refined. At each of these stages, Eastman realized an improvement in efficiency and an increase in output, while resource and people levels remained constant. Eastman emphasizes that it has changed its system, not the scientists, and the difference is measured in tens of millions of dollars per year savings to the company. The scientists themselves agree; in 1990, only 15 percent felt that they were contributing innovatively to research productivity. By 1993, after the shift in philosophy to research concepts, 90 percent thought of themselves as working to improve research productivity.

Like Eastman, Ames was sensitive to a common concern that TQM processes might inhibit the creative spirit inherent in research. Ames recognized that in its customer-driven world, the internal customers involved in research and development should receive just as much consideration as the external customers. Teammates in R&D interact regularly with their contacts in sales and marketing, the manufacturing divisions for factory service and for new products, and with the external customers.

Compared with like-sized manufacturers, Ames returns a high percentage of revenue to its R&D budget. Because the company sells in a very competitive market, it is committed to "cutting edge" materials and processes. By their measure of R&D performance, (taking into account material use, labor use, process capability, yield, total product cost, and cycle time), Ames is confident that it has fully integrated total quality management into its research and development process.

9. Conference Summary

Dr. Joseph M. Juran's reference literature, training courses, books, and video cassettes on quality management have been translated into 16 languages. His work has been formally honored by 12 countries with over 40 national, international, and foreign awards, including the Order of the Sacred Treasure, awarded by the Emperor of Japan and the National Medal of Technology, presented by the President of the United States. The following is a summary of highlights from his comments at the close of Quest for Excellence VI and his prognosis for quality in the future.

The two companies portrayed in depth both described wake-up calls as the impetus that started them on their quality journeys. As Eastman and Ames both learned, leadership has certain non-delegable roles: setting quality goals; personally presiding over a quality council; providing a vision statement, training and resources; establishing new performance goals; and being present for employee recognition. "No company has reached world-class quality status," Juran says, "without the personal involvement of senior management." Juran commended Ames and Eastman for getting "past the fog of buzzwords into the terrain of reality," defining values and establishing benchmarks.

Of the information and analysis systems developed by both companies, Juran observed that Ames and Eastman were provided with a broad array of measurements of quality of business, akin to the measurement means taken for granted by the technological world for centuries. In the 1980s, many U.S. companies had had no early warning of the foreign invasion. Juran says that now, through quality measurements, companies have useful market indicators.

Human relations, in Juran's estimation, have undergone irreversible change. At the beginning of the century, management was essentially by fiat, an approach that was in part responsible for U.S. ascendance to the height of industrial power. Although circumstances could be harsh and workers were largely unempowered, such a management style was warranted when educational levels and the literacy rate in English were low. Today, such a management philosophy is obsolete, and the consequence of that obsolescence is an underemployed workforce. The quality focus on involvement, training, accountability, communication, and empowerment has been, Juran says, "a watershed event" in human relations. Juran says of business, that it is a collection and series of processes, interdependent and synergistic, much like the parts and processes of the human body.

"Both companies assessed themselves against the Baldrige Award criteria and found no better standard," Juran observed. Noting that the Office of Quality Programs at the National Institute of Standards and Technology mails thousands of packets of information yearly, yet only around 100 companies apply, Juran is convinced that many other companies assess themselves privately against the Baldrige criteria and make changes.

"Where is the United States?" Juran asks. "In 1990," he recalls, "I declared that we had a break in the clouds; it was okay to be optimistic." He sees continued progress from his present 1994 perspective. He is not so optimistic for Europe, though, citing the continent's preoccupation with the ISO 9000 series. Juran allows that ISO 9000 has pluses as a documentation system, but it lacks emphasis on the need for senior leadership, training, empowerment, and continued improvement.

"Japan continues to improve, but," predicts Juran, "as the United States closes the quality gap, the force of patriotism takes over." "Now," he says, "the gap is not so large that it's undismissable." He concedes that perceptions are usually longer lasting than facts, but as perceptions change, customers will return to American goods. Juran says that if the twentieth century was marked by U.S. leadership in productivity, in the twenty-first century, quality will be the major area of world competition.

Dr. Curt Reimann, Director of the Office of Quality Programs at the National Institute of Standards and Technology, closed the Conference, encouraging participants to take to heart, and to take home, the examples of community involvement and dedication set by Ames and Eastman on their quality journeys.

11. General References

1994 Criteria for the Malcolm Baldrige National Quality Award.

Conference notebook, Quest for Excellence VI, February 7-9, 1994, Washington, DC.

Volume 99, Number 5, September–October 1994
Journal of Research of the National Institute of Standards and Technology

[J. Res. Natl. Inst. Stand. Technol. 99, 681 (1994)]

Conference Report

16th NATIONAL COMPUTER SECURITY CONFERENCE Baltimore, MD September 20–23, 1993

Report prepared by

Dennis Gilbert

Computer Security Division,
National Institute of Standards and Technology,
Gaithersburg, MD 20899-0001

1. Introduction

Each year the National Institute of Standards and Technology and the National Computer Security Center (NCSC) cosponsor the National Computer Security Conference. The conference provides a forum for technology interchange among system developers and a place where computer users can exchange ideas and learn new ways to apply current computer and information security technology. This major event on the computer security conference calendar provides an excellent opportunity for attendees to hear the leaders in the field report on their research and share experiences. A large, diverse national and international audience attends the conference. This past year, nearly 2000 attended from government, industry, and academe. One of the most important aspects of the conference is that its many activities provide an opportunity for contemporaries to network and gain new perspectives through the sharing of information and experiences.

2. Conference Program Highlights

In addition to a track on criteria and evaluation, there were also tracks on research and development, integration and applications, and management and administration. Each track provided 11 sessions, each of 1 1/2 hours, of peer-reviewed papers or panel sessions. The opening and closing plenary sessions presented subjects and issues of interest and importance to the community. An added highlight of the conference was a tutorial track for newcomers to the computer security field.

2.1 Criteria and Evaluation Track

A full track devoted to federal criteria, evaluation, and international harmonization efforts was featured at this 16th annual conference program. Collaborative efforts by NIST and the National Security Agency (NSA) to develop new criteria for trusted systems were presented. These criteria will be used to evaluate the ability of systems to protect confidentiality of data and provide other security controls. The evolutionary efforts of the Commission of European Communities (EC) are focused on producing a comprehensive set of security requirements for designing and developing trust technology for widespread international use. The work performed by the United States and the EC to develop a common basis for product evaluation will serve to reduce costs to users and vendors. Through tutorials, progress reports, and forums, the track placed in perspective the relationships among U.S. and European efforts and their short- and long-term significance.

2.2 Research and Development Track

Papers and panels in this track typically address technical R&D efforts related to security models. As in the past, a major interest in this track was the various aspects of the subject of access control, i.e., the rules, policies, and mechanisms that address which persons or which computer processes have access to a computer's data and resources, and under what circumstances. Access control-related papers covered: nonrepudiation in open teleco-operation; a mandatory denial of service model; issues and research directions in applying discretionary access control in object-oriented databases; new perspective on access control policies; regulating processing sequences through object state to achieve access control; and a proposed model and related security policy for a mechanism used to provide access to Internet protocol networks.

Two other papers addressed referential integrity and query acceleration in multilevel secure database systems. Still another presented an improved method of checking for "bad passwords" (See Sec. 4).

To share the learnings of other forums, Hilary Hosmer, Data Security, Inc., chaired *Best of New Security Paradigms II Workshop Panel*. This panel examined: the relationship of responsibility modeling and security requirements, a paradigm for flexible and adaptable access control in distributed applications, and identification and authentication when users have multiple accounts. The *Enterprise Security Solutions Panel*, chaired by Paul Lambert, Motorola, looked at security from an "enterprise" perspective, covering such areas as business issues and information security, securing the world's largest private internet, security with token-based access controls, and secure distributed computing for heterogeneous operating system environments. Three other panels presented research or concepts concerned with trusted applications. These included *Strategies for Integrating Evaluated Products*, chaired by Dr. James G. Williams, The Mitre Corp.; *Multilevel Information System Security Initiative (MISSI)*, chaired by Gary Secrest, NSA; and *Trusted Applications*, chaired by Janet Cugini, NIST.

2.3 Integration and Applications Track

This track focuses on how security technology is being applied and how security products are being evaluated and integrated into secure systems. One of the themes in this track was that of certification and accreditation (C&A), i.e., the evaluation of the technical and nontechnical security controls to: determine whether a specified set of security requirements are met; and support an official authorization by an appropriate management approving authority to place a system employing a prescribed set of safeguards into operational use. Papers in this area covered such subjects as C&A in a military communications network and in an Army multilevel secure (MLS) management information systems environment. Two other papers presented an approach and comprehensive methodology to C&A. Also, a panel in this track presented an update on INFOSEC design and certification initiatives at NSA.

In addition to the papers and panel described, another focus area in this track was network security. Panels in this area included *Network Security Management—The Harder Problem*, chaired by Ronda Henning, Harris Corporation, and *Application of INFOSEC Products on Wide-Area-Networks*, chaired by Joyce Capell, Lockheed Missiles & Space Company, Inc.

Still another set of papers explored the subjects of access control policy needs among federal and private sector organizations and the administration of access rights in a multi-vendor system. The use of commercial-off-the-shelf products for automated information systems (AIS) security, choosing a standard for security protocols, and performing product and system evaluations were also featured in this track, as were such topics as distributed auditing, an approach to risk assessment, designing secure MLS database systems, system testing, and integration of trusted products.

A panel presenting a *Debate of Critical Player Perspectives on MLS System Solution Acquisition Topics*, chaired by Joel E. Sachs, Arca Systems, Inc., and one on *Security Issues for the Securities Industry*, chaired by Sally Meglathery, New York Stock Exchange provided the benefit of practical experience to track attendees.

2.4 Management and Administration Track

This track presented a variety of papers and panel discussions on issues of concern in the management and administration of automated information systems and the security function.

A particularly interesting and thought-provoking paper in this track explored the applicability of social psychology to information security (See Sec. 4).

Two other panels—*On a Better Understanding of Risk Management Techniques*, chaired by Stuart W. Katzke, NIST; and "*How Much Security is*

Enough?" The Accreditor's Perspective, chaired by James P. Litchko, Trusted Information Systems, Inc. presented management considerations regarding risk management and accreditation. A related paper, *Trusted Systems: Applying the Theory in a Commercial Firm*, by Ernest C. Charles, Donna A. Diodati, and Walter J. Mozdzierz, Aetna Life & Casualty, showed an application of trusted systems in a commercial environment.

A particularly lively panel in this track, *Protection of Intellectual Property*, chaired by Gerald S. Lang, Harrison Ave. Corp., explored the technical, privacy, ethical, legal, political, and piracy issues involved in defining and protecting intellectual property. Another set of panels looked at planning for and responding to emergency situations. *Terror at the World Trade Center*, chaired by Sally Meglathery, New York Stock Exchange, discussed the security issues raised by the World Trade Center bombing. *Contingency Planning in the 90s*, chaired by Irene Gilbert, NIST, examined new technologies and innovative approaches to the subject from an organizational, service provider, and user perspective—with emphasis on the planning process and need to focus senior management attention.

Still another series of panels examined a related set of subjects. These included: *The Privacy Impact of Technology in the 90s*, chaired by Wayne Madsen, Computer Sciences Corporation; *Electronic Crime Prevention*, chaired by Robert Lau, National Security Agency; *Virus Attacks and Counterattacks: Real-World Experiences*, chaired by James P. Litchko, Trusted Information Systems, Inc.; and *Security and Auditability of Electronic Vote Tabulation Systems*, chaired by Rebecca Mercuri, University of Pennsylvania.

Security Awareness, Training, and Professionalization: Status Report, chaired by Dennis Gilbert, NIST presented a report by representatives of key organizations with a stake in promoting security training and professional development in the Federal government and the private sector. A related paper that addressed how to raise awareness about security issues was *How to Market the Information Systems Security Program*, by David Eakin, CISSP, Naval Ships Parts Control Center.

Another interesting panel, *The OECD Guidelines for the Security of Information Systems: A Look to the Future*, chaired by Christine Axsmith, Esq., ManTech Strategic Associates, Ltd., reported on the efforts of the Organization for Economic Cooperation and Development to establish a common international framework for computer security. The goal of the guidelines is to develop a common set of principals from which many nations can begin to develop their computer security awareness and practices. It is expected that the guidelines will foster the proliferation of international trade.

2.5 Tutorials and Presentations Track

A feature of each conference is a tutorial track. It provides those new to the field, those new to a particular subject, and those who are experienced practitioners wanting a "refresh," an opportunity to get a basic review of a given security subject. This year's conference provided a tutorial series on trusted systems, which covered a threats and security overview, trusted systems concepts, trusted networks, trusted database systems, and trusted integration. The tutorial portion of the track also included a session on viruses. In addition, the track offered a panel session on *Getting Your Work Published*, chaired by Jack Holleran, National Security Agency, and another on *Information Systems Security Standards, The DISA Process*, chaired by Bill Smith, CISSP, DISA. The former presented insights and "tips" by successful authors of security-related publications. The latter described the role of the Defense Information Systems Agency in the DoD INFOSEC standardization process. A final panel in this track, *Security Requirements for Cryptographic Modules*, chaired by Lisa Carnahan, NIST, gave information on the applicable NIST standards and validation program.

2.6 Closing Plenary

Of particular interest was the closing plenary session in which Thomas R. Malarkey, Department of Defense, presented a paper entitled *Seven Strategies for Information Technology Protection in the 1990s*, which attempted to lay out several useful strategies for improving the U.S. posture in information technology (IT) security. The first section of the paper presented the author's view of the success and failures of IT security in the 1980s. The second section identified IT trends and the IT infrastructure that needs to be protected over the next decade. The third section described seven suggested directions for government and industry. These include: 1) establishing a national IT protection policy; 2) promulgating a national policy on minimum IT protection requirements; 3) unifying the current security and safety communities into one protection community; 4) improved emphasis on system security management; 5) examining alternatives to current traditional in-depth evaluation

for product quality control; 6) improving accountability features of IT products; and 7) increasing our investment in security interoperability. The presentation of the paper was followed by a lively discussion by the previous recipients of the conference award for outstanding contributions to the field. (See Sec. 3). Chairing the session was award recipient, Stephen Walker, and fellow recipients, James P. Anderson, Dr. Roger Schell, and Dr. Willis Ware.

3. Outstanding Contributions to the Field

Each year the conference presents an award to an individual who has made significant contributions to the computer security community over a period of years. This year's recipient was Mr. Robert C. Courtney, of RCI, Inc. He was IBM's first Director of Data Security, Privacy, and Integrity. At IBM he launched a number of far-reaching research and development programs. Since 1981 he has been an independent security consultant and has testified frequently before Congress on data security-related matters.

4. Outstanding Papers

Also presented this year were two outstanding paper awards. One went to Michel E. Kabay, Ph.D., of the National Computer Security Association for his paper "Social Psychology and INFOSEC: Psycho-Social Factors in the Implementation of Information Security Policy." Significantly, the paper extends to computer security the learnings of another discipline—that of social psychology. By tapping into advice from the so-called "soft sciences," the paper argues that improving security depends on changing beliefs, attitudes, and behaviors of individuals and organizations. It shows how social psychology can help us to best work with human predilections and predispositions to achieve computer security goals. The other outstanding paper award went to Chris Davies and Ravi Ganesan of Bell Atlantic for their submission "BApasswd: A New Proactive Password Checker." This paper describes a process that can help people choose passwords that are less likely to be vulnerable to dictionary attack. Some people point to poorly chosen passwords as the single largest cause of security incidents. Of significance is that the authors present an approach that minimizes storage and time to examine chosen passwords.

5. Awards Ceremony

This year, as in past years, the conference held a joint awards ceremony in which NIST and NCSC honored the vendors who had successfully developed products meeting the standards of their respective organizations. In the case of NIST, its Computer Security Division provides validation services for vendors to use in testing devices for conformance to security standards defined in three Federal Information Processing Standards (FIPS): Data Encryption Standard (DES), Computer Data Authentication, and Key Management Using ANSI X9.17. In the case of NCSC, vendors are recognized who contribute to the availability of trusted products and who thereby expand the range of solutions customers can use to secure their data. The products are placed on the Evaluated Products List (EPL) following a successful evaluation against the Trusted Computer Systems Evaluation Criteria and its interpretations. (For further information, contact 301-975-2920 regarding the NIST awards and 410-859-4371 regarding the NCSC awards.)

6. Other Activities of Interest

In addition to the main track sessions, a number of other activities were available to the conference attendees including:

- Booths featuring NIST publications and NSA information security (INFOSEC) awareness activities. The NIST booth highlighted the NIST Computer Systems Laboratory Bulletins, 4 to 12 page documents, each of which covers a security topic in depth. The NSA booth highlighted NSA technical security guidelines, known as the Rainbow Series, named for the variety of its brightly colored document covers.
- A book exhibit representing a selection of leading publishing firms and the latest selections in published books on computer security.
- Demonstrations of the NIST Computer Security Bulletin Board and NSA's Dockmaster provide a wide variety of computer security information to federal agencies and to the public. Information posted on the NIST BBS includes an events calendar, software, reviews, publications, bibliographies, list of organizations, and other government bulletin board numbers. Also featured is a set of advisories providing up-to-date information on computer security incidents and

how to respond to them. Dockmaster is the focal point for nationwide dissemination and exchange of INFOSEC data through electronic mail and BBSs. Over 2000 users from federal government organizations, private companies, and academic institutions participate in its forums and retrieve data on INFOSEC products, conferences, and training.

- An overview of Air Force systems security initiatives and the status of the initiatives covering incident response, online surveys, and trends in tool development, with emphasis on tools to enhance security on systems and in organizations. Also, demonstrations of tools on intrusion detection, risk management, and training.
- "Networking" rooms for informal and "spur of the moment" discussions away from the crowded hallways.
- An evening reception following the vendor awards ceremony and a banquet, at which a distinguished member of the community provided a light-hearted, but thoughtful view of the profession in an after dinner talk. This year's speaker was Cheryl Helsing of Sun Microsystems, who has had considerable experience in many aspects of information systems security.

7. Future Conferences

It is expected that the next several National Computer Security Conferences will be held in the fall of each year in Baltimore, Maryland.

8. To Obtain the Conference Proceedings

Single copies of the 542-page NCSC16 conference proceedings are available upon request. Please contact NIST CSL Publications at 301-975-2821.

Volume 99, Number 5, September–October 1994
Journal of Research of the National Institute of Standards and Technology

[J. Res. Natl. Inst. Stand. Technol. 99, 687 (1994)]

Conference Report

SYSTEMS INTEGRATION NEEDS OF U.S. MANUFACTURERS Gaithersburg, MD August 16–17, 1993

Report prepared by

S. L. Stewart

Factory Automation Division,
National Institute of Standards and Technology,
Gaithersburg, MD 20899-0001

and

Ginger Pinholster
Pinholster Communications,
Wilmington, DE 19802

1. Introduction

In August 1993, the National Institute of Standards and Technology held a workshop for industry leaders to address the question of their needs for systems integration. These leaders were invited at this time because the Institute was on the verge of the largest program expansion in its history. Although the FY 1994 budget had not passed Congress at the time of the meeting, the expansion of information technology for manufacturing was very high on the Administration's list of priorities. This high priority and visibility made early planning an important step in the success of any future program. Accordingly the Institute sought the best possible industrial advice at a time when that advice could have the most impact on program formulation.

Howard Bloom, Chief of the Factory Automation Systems Division and host for the workshop, welcomed everyone and introduced Arati Prabhakar, Director of the National Institute of Standards and Technology. Dr. Prabhakar noted in her opening remarks that the Institute is "entering an era when technology is at the fore of the Administration's agenda." Over the next 4 years, NIST may well double its current budget of $192.9 million for in-house, laboratory activities. For Fiscal Year 1994, the total NIST budget is expected to jump to about $535.2 million—up from $384 million in 1993.

"At NIST today," Dr. Prabhakar commented, "we're at the beginning of what I think is going to be one of the most exciting times in the history of the Institute."

In the opening session, Prof. Roger Nagel chaired presentations by five speakers to set the context for the workshop:

(1) *Overview of U.S. Needs* by Professor James J. Solberg,

(2) *Overview of Federal Studies* by Mr. John Meyer,

(3) *Agile Manufacturing* by Mr. Rick Dove,

(4) *Standards Development* by Ms. Suzanne Olsen, and

(5) *Technology Transfer* by Mr. John Leary.

In the panel session, conducted by Ms. S. Jeane Ford, the workshop was divided into groups to consider system integration from three perspectives:

technology transfer, standards, and technology development. The consensus was that technology transfer and standards were the most important roles for new program direction with a significant, but smaller, role for technology development in conjunction with industry.

When the new initiative did indeed pass, the value of the workshop became evident in specifics of the new program in Systems Integration for Manufacturing Applications (SIMA). Technology transfer was recognized in a major new project for Manufacturing Integration Technology Transfer. The work on the Standard for Exchange of Product Model Data (STEP) was greatly expanded to help meet the standards needs of industry. A new Advanced Manufacturing and Networks Testbed (AMSANT) will support both standards and technology transfer in the new program. Finally, an expanded project for integration will develop new standards for enterprise integration.

The three groups returned from their deliberations with the following specific recommendations and conclusions.

Technology Transfer Needs

To boost U.S. competitiveness by speeding technology deployment, this working group recommended launching four initiatives:

(1) Technology Utilization Self-Assessment Study for small- and medium-sized companies,

(2) Technology Transfer Science Study,

(3) Technology Transfer Sharing Mechanisms, and

(4) Evaluation of the Impact of Government Policies on Technology Transfer.

Standards-Related Needs

This group felt that current standards-development process needs four critical repairs:

(1) A new perspective on the standards-setting process.

(2) Better metrics,

(3) improved communications between U.S. standards-making groups, and

(4) a more effective funding mechanism for standards development.

Technology-Related Needs

Scalable approaches to systems integration and better metrics for defining success are among the most critical technology-related needs of U.S. manufacturers, according to the third group, which suggested that NIST should:

(1) Expand the scope of metrics and lessons learned, providing manufacturers with new tools for rating themselves and setting targets,

(2) prepare better metrics for learning and retention, establishing a consistent model of Computer Integrated Manufacturing (CIM) to teach integration technologies,

(3) develop a demonstration Virtual Enterprise Testbed at NIST which would allow manufacturers and vendors to plug into the system, to test potential machine tools, software and other technologies, and

(4) establish a collaborative program, possibly involving a particular university or a group of universities, to form a Virtual Research and Development Center, thus speeding collaborative developments to market.

2. Setting the Context

In the United States, manufacturing generates significant revenue, representing 22 percent of the Gross National Product, and employing 21 million people, or 17 percent of the nation's total workforce. Noting the new White House Administration's commitment to a national economic strategy and increased support for U.S. manufacturing, NIST invited top industry experts to discuss their systems integration needs during a workshop on August 16 and 17, 1993. Prof. Roger N. Nagel, Operations Director, Iacocca Institute, and Harvey Wagner Professor of Manufacturing Systems Engineering, Lehigh University, chaired the first session with five speakers to set the context by addressing the question, "Where are we now?"

Overview of U.S. Needs

"Manufacturing systems," as defined by Professor James J. Solberg, include every technical, human, and organizational element associated with bringing classes of products into existence, and then disposing of them. Whether it involves linking

computer networks or motivating an engineering department to work productively with the accounting department, integrating various systems within a manufacturing setting presents many challenges—which have been addressed by countless studies and management concepts.

Improved systems integration today means "designing and operating manufacturing systems in a coordinated manner, avoiding the consequences of subsystems operating at cross purposes, and avoiding excess cost, lost time, lost quality, and lost opportunity," according to Professor Solberg. Achieving this goal will require developing new technologies, getting research results into practice faster, and using standards to improve efficiency, he added.

In the past, Professor Solberg said, a relatively stable market made it possible to develop manufacturing processes based on experience, by trial and error. But the current global marketplace demands new models for encapsulating state-of-the-art manufacturing knowledge, as well as sophisticated design tools. More and more often, he added, integration barriers involve human, rather than technical obstacles.

Overview of Federal Studies

According to Mr. John Meyer, Director of NIST's Office of Manufacturing Systems, the recent revitalization of the Federal Coordinating Council for Science, Engineering and Technology (FCCSET) reflects "the start of a major transformation of policy related to manufacturing." (Note: FCCSET was replaced by a cabinet-level National Science and Technology Council (NSTC) after the workshop was held, but the initiatives related to manufacturing are continuing under the NSTC.)

Currently, six Presidential initiatives established under FCCSET address: Advanced Manufacturing Technology (AMT); High Performance Computing and Communications (HPCC); Global Monitoring of the Environment for Environmental Change; Advanced Materials and Processing; Biotechnology; and Science, Mathematics, Engineering and Technology Education. But Mr. Meyer predicted that this list will soon be reorganized to focus primarily on two super-initiatives: AMT and HPCC.

Before setting up the AMT initiative, FCCSET determined that all U.S. federal agencies in 1994 will spend a total of $1.4 billion on advanced manufacturing technologies representing four general categories: (1) product and process design, (2) manufacturing processes, (3) supporting technologies, and (4) manufacturing infrastructure. Because of FCCSET efforts, an additional $70 million to $80 million worth of funding has been made available for research to support other high-priority technologies that could improve customer satisfaction and help U.S. manufacturers compete more effectively with foreign companies. These technologies include: Intelligent manufacturing cells, integrated design tools, and advanced technology infrastructures.

With a base budget of several billion dollars, the AMT should be launched in 1994 or 1995, Mr. Meyer said, and it is likely to include support for a Clean Car Initiative to develop environmentally benign vehicles.

Until now, the HPCC has focused primarily on scientific and educational applications for high performance computing and networking, but Mr. Meyer said that the initiative will be expanded in 1994 to address many additional areas. Included among the new HPCC applications will be computer-intensive manufacturing problems, such as integrated product and process design through modeling and simulation.

The Department of Defense Manufacturing Systems Strategic Research and Development Plan was prepared to assess the high *manufacturing support* costs associated with purchasing weapons systems. Noting the high pay-back potential of research, the Plan recommended support for the development of new: Integration methodologies, simulation and modeling, and manufacturing engineering support tools.

Collectively, Mr. Meyer noted, all recent studies suggest a need for research and development in five or six key areas, including: Integration methodologies and tools, standards and frameworks, networking and communications, integration of legacy systems, and industry demonstrations of promising concepts such as "agile manufacturing."

Agile Manufacturing

According to Mr. Rick Dove, President of Paradigm Shift International, the principles of "agile manufacturing" evolved in response to three driving forces in today's manufacturing environment: Continuous change, the need for rapid response, and an evolving definition of quality.

In an environment rife with constant change and increased foreign competition, Mr. Dove explained, U.S. manufacturers must become ever-more responsive and flexible. This quality—agility—may be described as "the ability to thrive

in an environment of unpredictable and constant change," he said.

As increasing globalism changes the U.S. marketplace, he said, the traditional rules of the game (or the "enterprise equation") have changed. Today, U.S. manufacturers are far more likely to be surprised by a competitor. Thus, they must strive constantly to reduce innovation cycle times, while also fighting the urge to add layers of management, which can make an enterprise more rigid and less responsive to market demands.

Born in chaos theory, which suggests that all events are inherently unpredictable, "agility" is often mistaken for the older concept of "lean manufacturing," an approach based on efficient practices. But, Mr. Dove said, a truly agile enterprise requires "reconfigurable architecture as a foundation for investments"—whether the systems in question are machine tools, organizational structures, or software integration programs. Today, central planning and hierarchical control no longer work. "I need to be able to reconfigure systems, instead of throwing them out and rebuilding them," Mr. Dove said.

Technology is important for achieving agility, he added, but people are the real key, since people make decisions, and rapid decision-making is critical in a global marketplace.

Standards Development

Faced with the rapid proliferation of hardware and software, many major corporations such as General Motors (GM) are trying to build a consistent set of bridges between automation islands by pushing for international standards, explained Ms. Suzanne Olsen. Specifically, GM is focusing on the Standard for Exchange of Product Model Data (STEP) as its "strategic direction for product data sharing," said Ms. Olsen, a Staff Project Manager for GM's Technical Center.

While participation in standards development may have been considered a civic duty at one point in time, Ms. Olsen noted, U.S. manufacturers today take part in the standards-setting process because standards clearly help reduce costs over the long-term.

Yet, she said, NIST and industry need to look at the current standards-development process "with a very hard, critical eye." Standards developed through traditional organizations such as the International Organization for Standardization (ISO) and the American National Standards Institute (ANSI) simply take too long to reach the marketplace, she said.

Ms. Olsen concurs with the advice of Ford's Keith Termaat, who has suggested that manufacturers need to know their customers and deliver a product that achieves better than 95 percent customer satisfaction—while also reducing standards-development time by at least 25 percent.

A proponent of international, rather than *de facto* standards, Ms. Olsen urged NIST to take a leadership role in improving the standards-development process. The U.S. voluntary standards process should not be allowed to stifle efficiency, she said.

Technology Transfer

In the United States, it takes many years to move new technology into general use, noted Mr. John Leary, citing a study completed by the National Center for Manufacturing Sciences (NCMS). That's too long, since "it's only when you ring the cash register that your ideas finally have value and social worth," said Mr. Leary, Engineering Director for AT&T's Standards and Global Manufacturing Planning Center.

To maintain a viable middle-class, Mr. Leary said, the United States must embrace advanced manufacturing technologies to achieve faster deployment of new products. Without improvement in manufacturing, he added, "We might end up with a nation where a few smart people will be creating software and designing products, while the rest of us will be flipping hamburgers."

Various collaborative research initiatives now hold promise for speeding U.S. technology deployment. The NCMS Strategy, for example, provides a framework for joint U.S./Canadian research supported by government and industry. Another collaborative strategy, NIST's Advanced Technology Program, has been highly effective in cutting technology lag-time. Collaborative ventures invariably increase the amount of market intelligence or know-how around the table, he said, and they reduce financial risks, offering greater leverage for smaller companies.

The key to successful collaboration, Mr. Leary noted, is to bring users and suppliers together—a challenge which has become less complicated since the 1984 Cooperative Research and Development Act eased anti-trust restrictions.

As more and more collaborative ventures are established, Mr. Leary said, NIST should support industry in dealing with intellectual property issues and cultural or "human" obstacles. New technologies, including electronically interfaced information

networks, will also be needed to support collaborative ventures.

3. Panel Summary: Where Do We Go?

During the NIST workshop, three working groups identified the systems integration needs of U.S. manufacturers in three areas: technology transfer, standards, and technology development. Ms. S. Jeane Ford, the Program Manager of the National PDES Testbed at NIST, led the panel discussion at which the results of the three working groups were presented.

Throughout discussions, participants repeatedly voiced dismay over the nation's slow technology-transfer process. Not surprisingly, a large number of industry leaders urged NIST to focus most of its resources on support for faster deployment of new technologies. For example, Mr. Michael Kennedy of Texas Instruments echoed the sentiments of other participants when he said: "There are many ways to develop technology quite effectively outside of NIST. NIST should focus instead on technology transfer and standards. The Institute has got to carry the ball in those areas."

NIST should also lead the charge in reengineering the standards-development process, workshop participants said. It would be appropriate now for NIST to take the lead in pushing for better standards to support U.S. manufacturing.

Among the new technologies seen as critical for U.S. manufacturers, participants identified numerous integration methodologies such as scalable approaches to systems integration, as well as improved metrics.

The participants' recommendations are summarized in the following sections.

Technology Transfer Needs

To boost U.S. competitiveness by speeding technology deployment, Mr. Peter N. Butenhoff reported, NIST should launch four initiatives:

(1) Technology Utilization Self-Assessment Study for small- and medium-sized companies,

(2) Technology Transfer Science Study,

(3) Technology Transfer Sharing Mechanisms, and

(4) Evaluation of the Impact of Government Policies on Technology Transfer.

Designed to help smaller companies determine their technology transfer needs in the face of increasingly fierce competition, the Technology Utilization Self-Assessment Study would include a "self-evaluation checklist" as well as a collection of "failure stories" illustrating the consequences of technological neglect, said Mr. Butenhoff, President of the Textile/Clothing Technology Corp. (TC2). Examples of "best practices," training laboratories for schools, and other manufacturing extension services could also be a part of the Self-Assessment Study.

Noting that "technology transfer" is a poorly defined process, Mr. Ronald Dick and others proposed a "Technology Transfer Science Study" to clarify the issue. Among other objectives, the Study would identify companies achieving technology transfer, develop a set of business cases related to technology deployment, and establish a process for applying new technology to commercial products, said Mr. Dick, Technical Director for IMAR.

Workshop participants also called for additional Technology Transfer Sharing Mechanisms. Specifically, the group urged NIST to establish a computer support system featuring: Electronic networking to industry and universities, an on-line database of abstracts describing technology, and user-friendly search techniques. By accepting a leadership role in commercialization endeavors, and by organizing national symposia on successful transfer cases, NIST could provide additional support for rapid technology deployment.

Finally, Mr. Butenhoff said, NIST's charter should be broadened to include research of business practices and cultures. A broader mission statement would allow the Institute to conduct an Evaluation of Government Policies on Technology Transfer, to determine which small manufacturing environments are critical to the entire U.S. economy, and to evaluate tax incentives for promoting technological advances.

Standards-Related Needs

According to Mr. Jack White, new standards succeed for three reasons: they are demanded by major users, they are driven by clear business needs, and they are supported by many vendors, or at least by a few market leaders. Whether they bubble up from a grassroots movement, or fall from a top-down development program, both *de facto* and proprietary standards must be clearly needed to be successful, said Mr. White of the Industrial Technology Institute.

Unfortunately, he said, the United States' current standards-development process is broken, and it will require four critical repairs: (1) a new perspective on the standards-setting process, (2) better metrics, (3) improved communications between U.S. standards-making groups, and (4) a more effective funding mechanism for standards development.

"NIST should lead the charge to re-engineer the critical processes involved in developing standards," Mr. White said. This effort should involve many different groups, including industry leaders, vendors, and consortia directors. Ultimately, the re-engineering effort should result in a set of "best practices" for standards-making. To sell the new approach to potential users, NIST could parlay its reputation for excellence in manufacturing support, said Mr. Michael Kennedy of Texas Instruments.

Improved metrics are essential for measuring the progress and quality of NIST's re-engineered standards-development process, Mr. White added. At the same time, NIST will need to maintain new electronic repositories for information on U.S. and global standards efforts. Funding could be provided through a new Standards Development Program, which would focus part of the efforts of the Advanced Technology Program (ATP) and the Advanced Manufacturing Systems and Networking Testbed (AMSANT) on standards and implementation. ATP may be contacted for more information by telephone at 1-800-287-3863 or by email at atp@micf.nist.gov or by fax at 1-301-926-9524. For more information about AMSANT or any other FASD programs, please see contact information at the end of this article.

Like Suzanne Olsen, the standards-related needs group suggested that NIST adopt the guidelines established by Ford Motor Company, which strives to reduce standards deployment time by at least 25 percent, while reducing internal expenses by 20 percent.

"Our group is urging NIST to become pro-active about reengineering standards development in this country," Mr. White said. "We're also strongly in favor of eliminating redundancy in the standards-making process—including redundant organizations. In the standards game, less is definitely best."

Technology-Related Needs

Scalable approaches to systems integration and better metrics for defining success are among the most critical technology-related needs of U.S. manufacturers, according to a group led by Dr. Michael C. Smith of Science Applications International Corp.

To support manufacturing in the 21st Century, Dr. Smith's group identified these and 37 other specific technology requirements, representing six general categories:

(1) Integration Methodologies,
(2) Business Models,
(3) Interoperable Tools,
(4) Active Learning and Feedback,
(5) Human Interfaces, and
(6) Education and Training.

Meeting industry's future technology needs will require NIST to undertake four basic development activities, said Mr. Gary K. Conkol of Cleveland Advanced Manufacturing Program. Specifically, Mr. Conkol and others suggested that NIST should:

(1) Expand the scope of metrics and lessons learned, providing manufacturers with new tools for rating themselves and setting targets;

(2) Prepare better metrics for learning and retention, establishing a consistent model of CIM to teach integration technologies;

(3) Develop a demonstration Virtual Enterprise Testbed at NIST which would allow manufacturers and vendors to *plug into* the system, to test potential machine tools, software and other technologies; and

(4) Establish a collaborative program, possibly involving a particular university or a group of universities, to form a Virtual Research and Development Center, thus speeding collaborative developments to market.

After the workshop, Tom Rhyne, a workshop participant, took the extra time to write and contribute his personal summary of what NIST should do in both the shorter- and longer-term. Here are his comments with special emphasis on standards. From a tactical (shorter-term) point of view:

- Provide full-time technical experts to participate in support of volunteer participants in key standards activities.
- Serve as a neutral site for demonstration projects involving proposed standards. Such demonstrations can identify strengths or weakness in the proposals. For U.S. proposals, the

fact that functionality has been proven by demonstration will strengthen the likelihood of adoption. For non-U.S. proposals, the demonstrations will help decide the appropriate U.S. position on the proposal as well as serve as an initial start to the technology transfer and commercialization of the new standard, if it is adopted.

- Support the continued presence of U.S. experts in leadership positions within critically important standards activities (travel support, part-time support for labor).
- Enhance awareness within U.S. industries of current and emerging standards activities which may have impact on their industrial activities and competitiveness.
- Assure commercial vendors within the U.S. that emerging standards are worthy of their investment, thereby helping to "jump-start" them into making those investments. (Committing limited development resources to an emerging standard is always a very risky decision.)

From strategic point of view:

- Review international standards activities to rank their importance to current and future U.S. industrial competitiveness, and become proactive in the high-priority areas, as for example, by proposing new STEP application protocols (AP's).
- Make certain that U.S. participation in those standards activities marked as critical to U.S. interests is effective and solid. (I believe that the United States can no longer accept a volunteer, catch-as-catch-can approach to participation in key standards activities. Instead, we need a well selected, properly supported team of participants, and NIST, in the Department of Commerce, needs to assume a clear leadership position in recruiting, training, guiding, and supporting those individuals.)
- Expand the demonstration and proof-of-concept laboratory proposed above to involve pilot projects which unite potential vendors and users of proposed standards in activities which (a) provide technical backing to U.S. standards proposals and (b) serve as accelerators to commercial deployment of emerging standards within the United States.
- Seek ways to deploy advanced technologies in support of critical standards processes. (Using semi-automated information modeling technology to help accelerate the STEP AP interpretation process is an example.)
- Seek opportunities to move *de facto* standards activities into the formal international standards pipeline.
- Provide assurance that draft international standards and even drafts for comment are properly evaluated by appropriate experts within the United States, considering both technical merit and potential impact on U.S. industry. Thereafter, provide assurance that appropriate U.S. positions are produced and forwarded to the adopting body.

For more information, please contact the Factory Automation Systems Division, Building 220, Room A-127, NIST, Gaithersburg, MD 20899-0001. This report and additional material about the work of the division are available electronically at http://elib.cme.nist.gov/fasd/fasdhome.html or ftp://ftp.cme.nist.gov/pub. The division office can be reached by telephone at 1-301-975-3508 or fax at 1-301-258-9749.

3. Appendix A. Agenda

Welcome and Introduction

Dr. Arati Prabhakar, Director, NIST
Mr. Howard M. Bloom, Chief, FASD

Session 1: Invited Presentations

Chair: Prof. Roger N. Nagel
Operations Director, Iacocca Institute
Harvey Wagner Professor of Manufacturing Systems, Lehigh University

Overview of U.S. Needs

Prof. James J. Solberg
Director, Engineering Research Center, Purdue University

Overview of Federal Studies

Mr. John Meyer
Director, Office of Manufacturing Programs, NIST

Agile Manufacturing

Mr. Rick Dove
President, Paradigm Shift International

Standards Development Needs of U.S. Industry

Ms. Suzanne Olsen
Staff Project Engineer, General Motors Technical Center

Technology Transfer Needs of U.S. Industry

Mr. John Leary
AT&T Technologies, Inc. and ANSI CIM Standards Board

Session 2: Discussion Groups

Group 1: Technology-Related Needs

Discussion Leader: Michael C. Smith, Science Applications Intl. Corp.
Reporter: Gary K. Conkol, Cleveland Advanced Manufacturing Program

Group 2: Standards-Related Needs

Discussion Leader: Jack White, Industrial Technology Institute
Reporter: Michael Kennedy, Texas Instruments

Group 3: Technology Transfer Needs

Discussion Leader: Peter N. Butenhoff, President, Textile/Clothing Technology Corp.
Reporter: Ronald L. Dick, Technical Director, IMAR

Session 3: Discussion Group Results

Chair: S. Jeane Ford, Program Manager, National PDES Testbed, NIST

Reports of Small Group Discussions

Presented by reporters

Panel Discussion/Clarification of Industry Needs

Panel of discussion leaders and reporters from each small group.

Wrapup and Agreement on Time Table for Subsequent Steps

S. Jeane Ford

Closing

Howard M. Bloom

4. Appendix B. Participants

Mr. Arlan Andrews, Sandia National Laboratory
Mr. Ali Bahroloomi, NAO Manufacturing Information Systems, General Motors
Mr. Howard Bloom, Chief, Factory Automation Systems Division, NIST
Mr. Randolph L. Burnette, Director, Merchandise Planning and Quick Response, Mercantile Stores Company, Inc.
Mr. Peter N. Butenhoff, President, Textile/Clothing Technology Corp. (TC2)
Mr. Gary K. Conkol, Cleveland Advanced Manufacturing Program
Mr. John Decaire, Acting Director of Technology, National Center for Manufacturing Sciences
Mr. Ronald L. Dick, Technical Director, IMAR
Mr. Rick Dove, President, Paradigm Shift International
Mr. Bob Finkelstein, President, Robotic Technology, Inc.
Ms. S. Jeane Ford, Program Manager, National PDES Testbed, NIST
Mr. Glenn Hollowell, SEMATECH
Mr. Joe Iseman, Innovative Technologies
Mr. Michael Kennedy, Texas Instruments
Mr. Robert Kiggans, General Manager, PDES, Inc.
Mr. Tim Lacoss, Mechanical Engineer Advanced Technologies Design Division, Watervliet Arsenal
Mr. John Leary, Engineering Director, Standards and Global Manufacturing Planning Center, AT&T Technologies, Inc.
Mr. Tom Mahoney, Manufacturing Studies Board, National Research Council
Mr. John Meyer, Director, Office of Manufacturing Systems, NIST
Prof. Roger N. Nagel, Operations Director, Iacocca Institute, Harvey Wagner Professor of Manufacturing Systems Engineering, Lehigh University
Ms. Suzanne Olsen, Staff Project Engineer, General Motors Technical Center
Dr. Arati Prabhakar, Director, NIST
Mr. Tom Rhyne, MCC/Atlas Standards Laboratories
Mr. Simon Schurr, Lehigh University
Dr. Michael C. Smith, Science Applications Intl. Corp.
Mr. Neil Snodgrass, DACOM
Prof. James J. Solberg, Director, Engineering Research Center for Intelligent Manufacturing Systems, Purdue University
Dr. Selden Stewart, Factory Automation Systems Division, NIST
Mr. Art Sullivan, Draper Laboratory